Mobile Information Systems

Smart Spectrum Technologies for Mobile Information Systems

Guest Editors: Miguel López-Benítez, Janne Lehtomäki, Kenta Umebayashi, and Fernando Casadevall

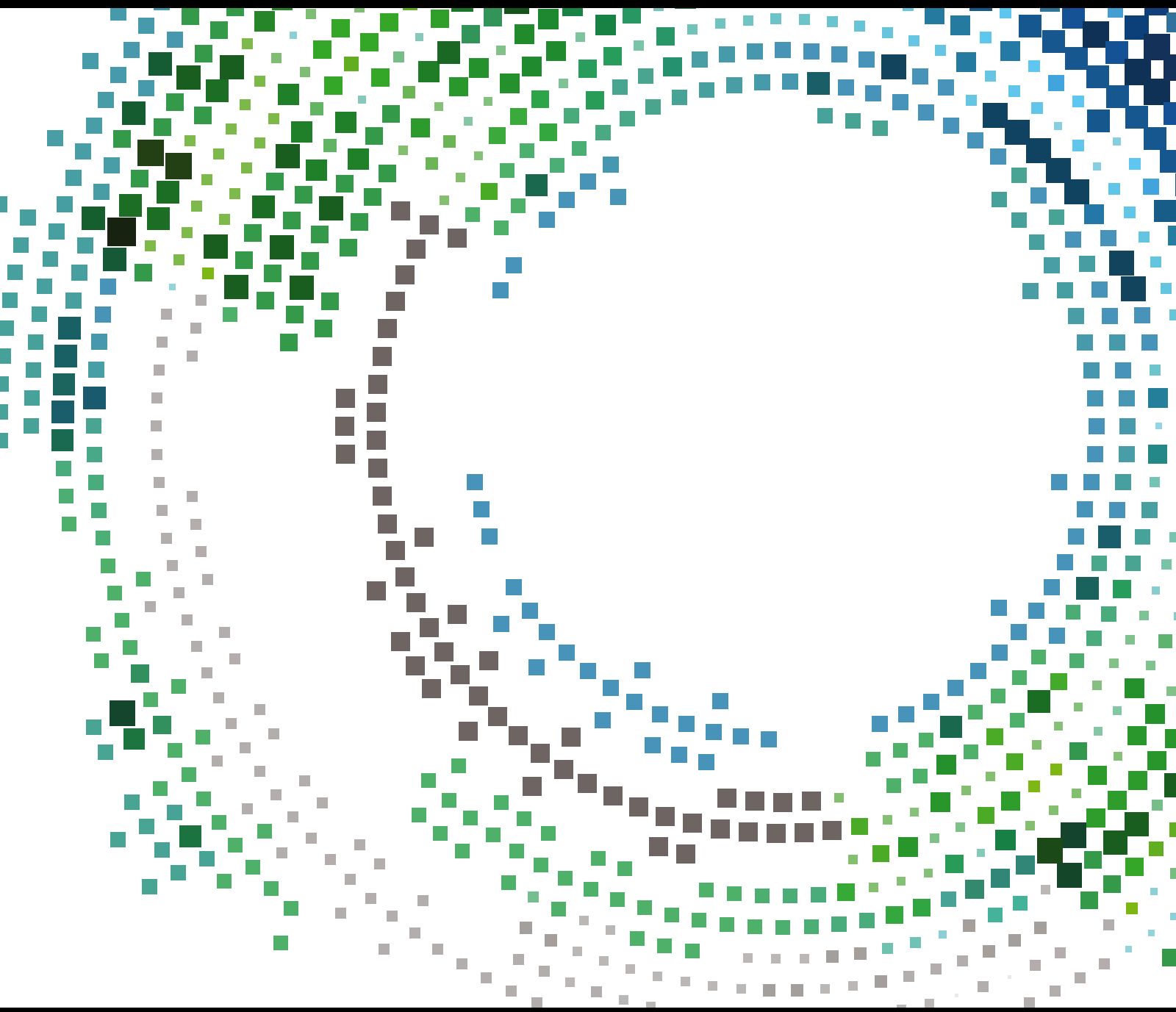

Smart Spectrum Technologies for Mobile Information Systems

Mobile Information Systems

Smart Spectrum Technologies for Mobile Information Systems

Guest Editors: Miguel López-Benítez, Janne Lehtomäki, Kenta Umebayashi, and Fernando Casadevall

Contents

Hindawi Publishing Corporation
Mobile Information Systems
Volume 2016, Article ID 3402450, 2 pages
http://dx.doi.org/10.1155/2016/3402450

Editorial
Smart Spectrum Technologies for Mobile Information Systems

Miguel López-Benítez,[1] Janne Lehtomäki,[2] Kenta Umebayashi,[3] and Fernando Casadevall[4]

[1]*Department of Electrical Engineering and Electronics, University of Liverpool, Liverpool L69 3GJ, UK*
[2]*Centre for Wireless Communications, University of Oulu, 90014 Oulu, Finland*
[3]*Department of Electrical and Electronic Engineering, Tokyo University of Agriculture and Technology, Fuchu 184-8588, Japan*
[4]*Department of Signal Theory and Communications, Technical University of Catalonia, 08034 Barcelona, Spain*

Correspondence should be addressed to Miguel López-Benítez; m.lopez-benitez@liverpool.ac.uk

Received 28 July 2016; Accepted 31 July 2016

Despite being one of the most important resources of mobile information systems, the radio frequency spectrum has usually been sparsely exploited as a result of the static spectrum allocation policies traditionally enforced by spectrum regulators. This situation has recently led to the development of novel smart technologies to improve the efficiency of spectrum utilization. Relying on the principles of dynamic spectrum access and sharing and addressing all layers of the communication protocol stack, smart spectrum technologies enable the coexistence of multiple mobile wireless systems within the same spectrum band and therefore offer the potential for a smarter and more efficient exploitation of the radio spectrum in a wide range of scenarios. The research community has been working over the last years to overcome many of the technical challenges posed by the development of smart spectrum technologies. This issue compiles some of the latest advances in the field.

In response to the open call for papers, we received regular papers as well as extended versions of outstanding papers presented at the 2nd IEEE Intentional Workshop on Smart Spectrum (IWSS 2016), held in conjunction with the IEEE Wireless Communications and Networking Conference (WCNC 2016) in Doha, Qatar, on April 3, 2016. All submissions have undergone a rigorous review process and as a result six high-quality papers have been selected for publication in this special issue.

The paper titled "PSUN: An OFDM-Pulsed Radar Coexistence Technique with Application to 3.5 GHz LTE," by S. Kim et al. (an extended version of the paper receiving the IEEE IWSS 2016 Best Paper Award) analyzes the performance of Precoded SUbcarrier Nulling (PSUN) as a coexistence mechanism between 5G Long-Term Evolution (LTE) systems and federal military radars in the 3.5 GHz Citizens Broadband Radio Service (CBRS) band. The pulsed radar interference can be suppressed by introducing null tones in the transmitted OFDM signal (PSUN) in addition to setting to zero (pulse-blanking) the received time-domain samples affected by pulsed interference. In this context, S. Kim et al. analyze the impact of imperfect radar pulse prediction on the performance of a PSUN OFDM system and discuss the feasibility of 5G applications using 3.5 GHz LTE with PSUN.

The paper titled "CBRS Spectrum Sharing between LTE-U and WiFi: A Multi-Armed Bandit Approach," by I. Parvez et al., considers the spectral coexistence between LTE unlicensed (LTE-U) and WiFi systems in the 3.5 GHz CBRS band. Given the contention-based channel access mechanism of WiFi systems, an unconstrained operation of LTE systems in the same band may prevent WiFi systems from accessing the spectrum. To enable a fair coexistence, LTE systems can introduce transmission gaps to allow for WiFi operation. I. Parvez et al. propose a multiarmed bandit based adaptive LTE duty cycle selection method for the dynamic optimization of these transmission gaps, which is combined with a downlink power control technique for an improved aggregate capacity and energy efficiency.

The paper titled "Licensed Shared Access System Possibilities for Public Safety," by K. Lähetkangas et al., explores the possibilities of the Licensed Shared Access (LSA) concept as an approach for spectrum sharing between public safety and commercial radio systems, taking into account the particular

features of public safety systems, discussing the advantages and disadvantages of several spectrum sharing alternatives, and providing illustrative results on the potential benefits.

The paper titled "ETSI-Standard Reconfigurable Mobile Device for Supporting the Licensed Shared Access," by K. Kim et al., presents an implementation of a reconfigurable mobile device for LSA. The prototype implements a procedure to transfer control signals among the software entities of the device in compliance with the reference model of the ETSI standard reconfigurable architecture.

The paper titled "Spectrum Assignment Algorithm for Cognitive Machine-to-Machine Networks," by S. Rostami et al., proposes a novel aggregation-based spectrum assignment algorithm for cognitive machine-to-machine networks. S. Rostami et al. develop a genetic algorithm taking into account practical constraints such as cochannel interference and maximum aggregation span and analyze its benefits in terms of spectrum utilization and network capacity.

The paper titled "A Survey of the DVB-T Spectrum: Opportunities for Cognitive Mobile Users," by L. Csurgai-Horváth et al., presents an experimental study of the potential opportunities offered by the terrestrial Digital Video Broadcasting (DVB-T) TV band for mobile cognitive radio applications. L. Csurgai-Horváth et al. perform a wideband spectrum survey employing a mobile measurement platform in a urban environment, where the received signal power and its statistics are analyzed in order to identify potential opportunities for mobile cognitive radio systems.

Acknowledgments

We highly appreciate the effort of all the authors in preparing and submitting their papers to this special issue as well as the dedication of the anonymous reviewers whose voluntary and invaluable work has contributed to the overall quality of this issue.

Miguel López-Benítez
Janne Lehtomäki
Kenta Umebayashi
Fernando Casadevall

Hindawi Publishing Corporation
Mobile Information Systems
Volume 2016, Article ID 5909801, 12 pages
http://dx.doi.org/10.1155/2016/5909801

Research Article

CBRS Spectrum Sharing between LTE-U and WiFi: A Multiarmed Bandit Approach

Imtiaz Parvez,[1] M. G. S. Sriyananda,[1] İsmail Güvenç,[2] Mehdi Bennis,[3] and Arif Sarwat[1]

[1]*Department of Electrical & Computer Engineering, Florida International University, Miami, FL 33174, USA*
[2]*Department of Electrical & Computer Engineering, North Carolina State University, Raleigh, NC 27513, USA*
[3]*Department of Communications Engineering, University of Oulu, 90014 Oulu, Finland*

Correspondence should be addressed to Arif Sarwat; asarwat@fiu.edu

Received 31 March 2016; Revised 14 June 2016; Accepted 19 July 2016

Academic Editor: Miguel López-Benítez

The surge of mobile devices such as smartphone and tablets requires additional capacity. To achieve ubiquitous and high data rate Internet connectivity, effective spectrum sharing and utilization of the wireless spectrum carry critical importance. In this paper, we consider the use of unlicensed LTE (LTE-U) technology in the 3.5 GHz Citizens Broadband Radio Service (CBRS) band and develop a multiarmed bandit (MAB) based spectrum sharing technique for a smooth coexistence with WiFi. In particular, we consider LTE-U to operate as a General Authorized Access (GAA) user; hereby MAB is used to adaptively optimize the transmission duty cycle of LTE-U transmissions. Additionally, we incorporate downlink power control which yields a high energy efficiency and interference suppression. Simulation results demonstrate a significant improvement in the aggregate capacity (approximately 33%) and cell-edge throughput of coexisting LTE-U and WiFi networks for different base station densities and user densities.

1. Introduction

Due to the proliferation of mobile devices and diverse mobile applications, the exponentially increasing mobile data is doubled approximately every year [1]. The 4G Long-Term Evolution (LTE) has recently emerged as a powerful technology to provide broadband data rates. On the other hand, to satisfy the throughput demand of broadband LTE networks in the upcoming years, larger bandwidth is needed [2, 3]. Since the licensed spectrum is expensive and limited, extending the operation of LTE in the underutilized unlicensed bands is recently getting significant attention, which requires effective coexistence with other technologies such as WiFi in these bands.

Recently, the Federal Communications Commission (FCC) in the United States has been working on opening a 150 MHz of spectrum in the 3.5 GHz band for sharing among multiple technologies, which is also commonly referred to as the Citizen Broadband Radio Service (CBRS). However, the use of this spectrum is subject to regularity requirements, where the incumbent military and meteorological radar systems have to be protected [4, 5]. In the CBRS band, there are three kinds of users with hierarchical priority: Incumbent Access (IA) users (tier-1), Prioritized Access License (PAL) users (tier-2), and General Authorized Access (GAA) users (tier-3) as illustrated in Figure 1. In the current scenario, the expansion of unlicensed LTE (LTE-U) as PAL or GAA user in the CBRS band is an enticing choice because of high penetration at 3.5 GHz, clean channel, and wide amount of spectrum [6]. The Third-Generation Partnership Project (3GPP) standardization group has been recently working on standardizing the licensed-assisted access (LAA) technology in the 5 GHz spectrum [7, 8]. The main goal is to develop a global single framework of LAA of LTE in the unlicensed bands, where operation of LTE will not critically affect the performance of WiFi networks in the same carrier. In the initial phase, only downlink (DL) operation LTE-A (LTE Advanced) Carrier Aggregation (CA) in the unlicensed band was considered, while deferring the simultaneous operation of DL and uplink (UL) to the next phase.

Another option for the operation of LTE in the unlicensed spectrum is through a prestandard approach, referred to

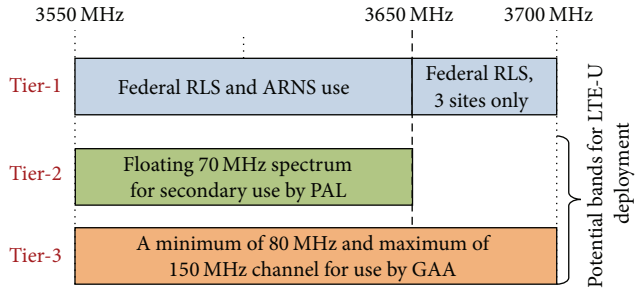

Figure 1: CBRS spectrum with 3 types of users.

LTE-U, where LTE base stations leave transmission gaps for facilitating coexistence with WiFi networks. Development of LTE-U technology is led by the industry consortium known as the LTE-U Forum. LTE-U mainly focuses on the operation of unlicensed LTE in the regions (e.g., USA, China) where listen before talk (LBT) is not mandatory. LTE-U defines the operation of primary cell in a licensed band with one or two secondary cells (SCells), each 20 MHz in the 5 GHz unlicensed band: U-NII-1 and/or U-NII-3 bands, spanning 5150–5250 MHz and 5725–5825 MHz, respectively. However, both the LTE-U and LAA need licensed band for control plane. Similar to the 5 GHz band, CBRS band can be utilized for LTE-U operation in the absence of IA users such as radar signal.

In our study, we consider the coexistence problem of LTE-U and WiFi networks in the CBRS bands. Since WiFi adopts a contention based medium access control with random back-off [9] for channel access and LTE uses dynamic scheduling for users, the unrestrained LTE operation in the same band will generate continuous interference on WiFi service. To operate LTE-U and WiFi simultaneously in the same unlicensed spectrum, fair and reasonable coexistence mechanism is indispensable. The adverse impact on DL and UL WiFi transmissions due to LTE deployment in the same band is analyzed in [10–12], emphasizing the need for rigorous studies. In this regard, discrete mechanisms such as dynamic channel selection, retaining transmission gaps, transmission duty cycle manipulation, and LBT have been proposed in the literature for harmonious coexistence with improved performance. To select resources dynamically, learn from the environment, and adaptively modify transmission parameters for performance improvement, various machine learning based techniques [13–16] have been introduced.

In this paper, we introduce a reinforcement learning (MAB) based adaptive duty cycle section for the coexistence between LTE-U and WiFi. Multiarmed Bandit (MAB) is a machine learning technique designed to maximize the long-term rewards through learning provided that each agent is rewarded after pulling an arm. Basically MAB [17, 18] problem resembles a gambler (agent) with a finite number of slot machines in which the gambler wants to maximum his rewards over a time horizon. Upon pulling an arm, a reward is attained with prior unknown distribution. The goal is to pull arms sequentially so that the accumulated rewards over the gambling period are maximized. However, the problem involves the exploration versus exploitation trade-off, that is, taking actions to yield immediate higher reward on the one hand and taking actions that would give rewards in the future, on the other hand.

In our technique, we use a multiarm bandit (MAB) algorithm for selecting appropriate duty cycle. Using a 3GPP compliant Time Division Duplex- (TDD-) LTE and Beacon enabled IEEE 802 systems in the 3.5 GHz band, we simulate and evaluate the coexistence performance for different percentage of transmission gaps. We found a significant throughput improvement for both systems ensuring harmonious coexistence. The objectives, subsequently the gains, of this study are not limited to throughput enhancements. The benefits that are achieved in different dimensions with the aid of MAB scheme and the other supporting techniques like PC can be summarized as follows:

(1) Proper coexistence is achieved due to the dynamic exploring and exploitation by MAB. So our technique is adaptive.

(2) The aggregate capacity is improved. Due to the application of MAB algorithm, optimal or suboptimal solutions are achieved.

(3) Using DL PC higher capacity values are achieved under dense UE and STA configurations.

(4) Higher energy efficiency is also achieved with PC, which always attempts to reduce the transmission power while increasing the energy efficiency.

(5) With the use of learning algorithm, a high degree of efficiency is achieved.

To the best of our knowledge, our work is the first study that introduces MAB for improving the coexistence of LTE and WiFi in the unlicensed bands.

The rest of the paper is organized as follows. Section 2 provides a literature review of coexistence of LTE-U and WiFi. In Section 3, we provide our system model and problem formulation for LTE and WiFi coexistence. Section 4 introduces the proposed MAB based dynamic duty cycle selection approach. Simulation results with various parameter configurations are presented in Section 5. Finally, Section 6 provides concluding remarks.

2. Related Works

2.1. Coexistence among Unlicensed LTE and WiFi. In the literature, several studies can be found that investigate the performance of LTE and WiFi coexistence in the unlicensed bands. In [19], coexistence performance of LTE and WiFi has been investigated in 900 MHz considering single floor and multifloor indoor office scenarios. It is shown that the performance of WiFi is heavily affected when WiFi and LTE operate simultaneously in the unlicensed spectrum.

To facilitate harmonious coexistence between LTE-U and WiFi in the same band, mainly three techniques have been proposed in the literature: (1) listen before talk (LBT), (2) dynamic channel selection, and (3) coexistence gaps. In Europe and Japan, LBT is mandatory for data offloading in

unlicensed band. The usage of LBT has been justified in [20] with different choice of LBT schemes. In [21], LBT is presented considering interradio access technology (RAT) and intra-RAT. In this technique, energy detection based LBT is proposed to handle inter-RAT interference whereas cross correlation based LBT is used to handle intra-RAT interference. However, LBT is not mandatory in USA and China, where alternative coexistence techniques can be explored.

In [22], Qualcomm presents an effective channel selection policy based on interference level. If the interference of the occupied channel exceeds a certain level, LTE-U changes the channel, provided that the interference is measured before and during the operation, and both at the user equipment (UE) and the network side. On the other hand, in [6] adaptive bandwidth channel allocation offered by LTE and Least Congested Channel Search (LCCS) has been suggested for channel selection. Dynamic channel selection requires free or low-interference channel to utilize. Since same band will be shared by other cellular service providers as well as different technologies such as WiFi, finding of clean channel may not be practical.

In [23], blank subframe allocation by LTE has been proposed where LTE is restrained from transmitting, and WiFi keeps on transmission. A similar technique has been proposed in [24] where certain subframes of LTE-U are reserved for WiFi transmission. Qualcomm has proposed Carrier Sensing Adaptive Transmission (CSAT) [22] for LTE-U MAC scheduling in which a fraction of TDD duty cycle is used for LTE-U transmission and the rest is used for other technologies. The cyclic ON/OFF ratio can be adaptively adjusted based on the activity of WiFi during the OFF period. In this paper, we focus on the dynamic optimization of coexistence gap/transmission time along with DL power control.

Uplink (UL) power control has been investigated on the performance of LTE-WiFi coexistence in [25, 26]. However, DL power control in coexistence problem has not been explored yet considering uncoordinated LTE and WiFi systems. The DL power control enhances performance by reducing interferences, which is demonstrated in [27–29]. In our study, we optimize both the transmission time and DL power using machine learning technique.

Reinforcement algorithm such as Q-learning, multiarm bandit, and value iteration is effective variant of machine learning which has been applied for optimization problems of cellular systems such as channel selection, mobility management, resource allocation, and rate adoption. In [13], Q-learning based duty cycle adjustment is presented to facilitate the sharing of the channel and to increase the overall throughput. In [30], a MAB based distributed channel selection is proposed to use vacant cellular channels in device to device (D2D) communication. To enhance handover process and increase throughput, MAB techniques based context-aware mobility management scheme is studied in [31]. In [32], dynamic rate adaptation and channel selection from free primary users have been proposed in cognitive radio systems using MAB, which yields extensive throughput improvements.

In our study, we propose a MAB based dynamic duty cycle selection for unlicensed LTE systems. In particular, LTE base stations (BSs) measure the utilization of the channel based on channel status information (CSI), learn the channel utilization of WiFi (current and previous), select the optimum duty cycle and transmission power, and perform transmission under this duty cycle, which results in effective sharing of wireless spectrum with WiFi networks. Due to this dynamic learning, our technique is adaptive and it improves aggregate capacity and energy efficiency. This is the first time we are applying MAB for coexisting operation of LTE and WiFi.

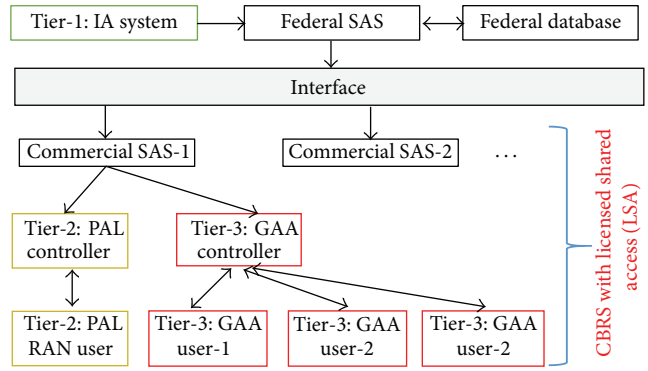

Figure 2: Users access priority.

2.2. CBRS Spectrum Sharing. The CBRS spectrum is composed of 150 MHz bandwidth divided into two chunks: 80 MHz and 70 MHz. Based on the architecture of CBRS band, the spectrum users are prioritized into three groups with decreasing interference protection requirements as illustrated in Figure 2.

The IA users in tier-1, such as military radars, have the most protection, mainly through geographical *exclusion zones* [33] that averts other users from transmiting in the vicinity of IA users. While the NTIA in April 2015 [5, 34] shrunk the earlier exclusion zones in [33] by 77%, they still cover several of the Nation's largest cities [35]. The main challenge of PAL users in tier-2 have is to protect the IA users and other PAL users from interference. To facilitate this, a spectrum access system (SAS) [36] is utilized, which grants spectrum access to users based on their locations. The network providers can purchase PAL licenses in given geographical areas, which consist of census tracts. Up to a 70 MHz of PAL spectrum will be available, with chunks of 10 MHz channels, which will be auctioned if there is more demand from providers than the available spectrum. Finally, tier-3 users are GAA users which are allowed to operate in the spectrum that are not used by IA and PAL tiers. In areas with no IA and PAL activity, GAA users may have access to whole 150 MHz, while in areas with PAL activity but outside of IA exclusion zones, at least 80 MHz of bandwidth will always be available for GAA use.

Since spectrum is limited and expensive, wireless service provider (LTE, WiFi) will be interested to operate in CBRS band as GAA users. In the GAA band, LTE needs to coexist with other cellular operators as well as other technologies such as WiFi. Besides that, Licensed Shared Access (LSA) concept [37, 38] allows an incumbent spectrum user to share

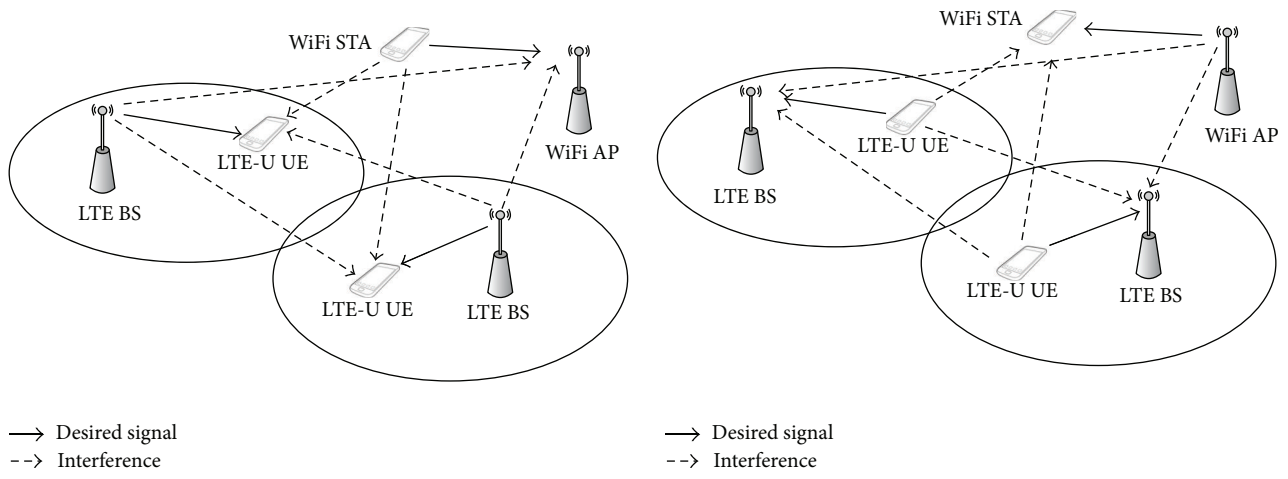

(a) Interference on LTE-U DL and WiFi UL

(b) Interference on LTE-U UL and WiFi DL

Figure 3: DL and UL interference scenarios for LTE-U/WiFi transmissions.

spectrum with licensed users with defined rights to access a portion of spectrum at a given location and time. This also requires to develop coexistence mechanism between mobile network operators (MNOs) and other technologists (licensed/unlicensed) such as WiFi. In this study, we focus on the coexistence of LTE and WiFi in the 3.5 GHz CBRS spectrum. For this study, for simplicity, we assume that the coexistence with IA and PAL users are already maintained through a SAS database, and we only consider coexistence among LTE-U and WiFi users in the GAA bands.

3. System Model and Problem Formulation

To evaluate the coexistence performance of LTE-U with WiFi in the unlicensed band, a collocated LTE-U and WiFi network scenario is considered. The sets of LTE-U BSs, WiFi APs, LTE-U UEs for BS i, and WiFi STAs for AP w are given by $\mathcal{B}_L$, $\mathcal{B}_W$, $\mathcal{Q}_L^i$, and $\mathcal{Q}_W^w$, respectively. $\mathcal{Q}_L = \{\mathcal{Q}_L^1, \mathcal{Q}_L^2, \ldots, \mathcal{Q}_L^i, \ldots, \mathcal{Q}_L^{|\mathcal{B}_L|}\}$ and $\mathcal{Q}_W = \{\mathcal{Q}_W^1, \mathcal{Q}_W^2, \ldots, \mathcal{Q}_W^w, \ldots, \mathcal{Q}_W^{|\mathcal{B}_W|}\}$ represent the sets of all UEs and STAs. For LTE-U, TDD-LTE is considered. For synchronization of WiFi STAs with the corresponding APs, a periodic beacon transmission is used as in [13].

3.1. Interference on DL and UL Transmissions. Interference caused to LTE-U UE and LTE-U BS during DL and UL transmissions is shown in Figure 3. A TDD frame structure similar to that in [39, Figure 6.2] is considered for all the BSs and UEs with synchronous operation. As shown in Figure 3(a), in the simultaneous operation of an LTE-U within a WiFi coverage area, the DL LTE-U radio link experiences interference from other LTE-U DL and WiFi UL transmissions. As the same time, WiFi UL suffers from near LTE-U transmission. During an UL transmission subframe, shown in Figure 3(b), LTE-U BS is interfered by the UL transmission of LTE-U UEs, as well as the DL transmissions of WiFi. Similarly, WiFi DL transmission is interfered by other LTE-U ULs where the DL received signal of a WiFi STA is interfered by other LTE-U UL transmissions. In the coexistence scenarios with high density of WiFi users, WiFi transmissions get delayed degrading their capacity performance due to the use of carrier sense multiple access with collision avoidance (CSMA/CA) mechanism [40]. This is an additional degradation other than the performance reduction experienced due to LTE-U transmissions operated on the same spectrum and this is valid only for WiFi APs and STAs.

3.2. Duty Cycle of LTE-U. In the case of designing a duty cycle for LTE-U, multiple LTE TDD frames are considered. For that purpose, five consecutive LTE frames [39, Figure 6.2(a)] are used to construct a duty cycle. Similar to [13], the LTE-U transmission ON/OFF condition is used to define a duty cycle which is shown in Figure 4 (e.g., 40% duty cycle: during the first two consecutive LTE-U frames, transmission is turned on and it is turned off during the following three frames). One out of these two configurations is used by the UEs and BS in an LTE cell during a duty cycle period. According to this structure, a constant UL:DL duty cycle value is maintained.

3.3. Capacity Calculation and Power Control. For any BS $i \in \mathcal{Q}_L$, there are $\mathcal{N}^i$ resource blocks (RBs) for the DL. For a given UE u associated with BS i, n_u^i RBs are allocated, where $\mathcal{N}^i = \sum_{u=1}^{|\mathcal{Q}_L^i|} n_u^i$. $p_{s,r}^i$, $p_{s,r}^b$, $p_{s,r}^a$, and $p_{s,r}^q$ are transmit power values associated with RB r and the transmit power index s from the LTE-U BS i, LTE-U BS b ($i \neq b$), WiFi AP a, and WiFi STA q. ith BS is considered as the desired BS where the BSs indexed by b are the interference generating BSs. For any AP, UE, or STA total transmit power is equally distributed among all RBs. However, in every BS, the total transmit power is dynamically changed for every duty cycle according to MAB algorithm. $h_{u,r}^i$, $h_{u,r}^b$, $h_{u,r}^a$, and $h_{u,r}^q$ are the channel gain values from BS i to UE u, from BS b to UE u, from AP a to UE u, and from WiFi STA q to UE u, respectively. All channel gain values are calculated considering path losses and shadowing. In that case, interference generated to UE u from BSs, APs, and STAs are given by I_{BS}^u, I_{AP}^u, and I_{STA}^u, respectively. Since a synchronized transmission is considered,

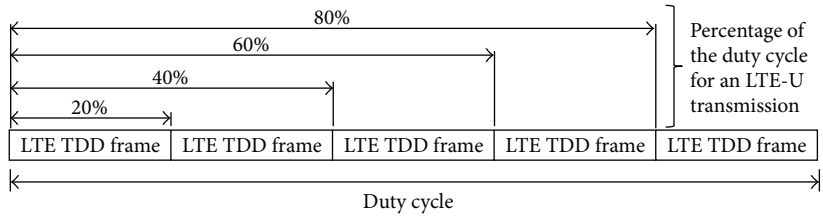

Figure 4: Structure of the duty cycle for LTE-U transmissions.

there is no interference from the UL transmission of LTE-U UEs. Noise variance is denoted by σ^2. The Signal-to-Interference-plus-Noise Ratio (SINR) expression for UE u served by BS i on RB r at time interval k is given as

$$\mathrm{SINR}_{u,r}^{i}[k] = \frac{p_s^i h_{u,r}^i}{\underbrace{\sum_{b\in\mathscr{B}_L\setminus i} p_s^b h_{u,r}^b}_{I_{\mathrm{BS}}^u} + \underbrace{\sum_{a\in\mathscr{B}_W} p_s^a h_{u,r}^a}_{I_{\mathrm{AP}}^u} + \underbrace{\sum_{q\in\mathbb{Q}_W} p_s^q h_{u,r}^q}_{I_{\mathrm{STA}}^u} + \sigma^2}, \quad (1)$$

where $b, i \in \mathscr{B}_L$.

The amount of successfully transmitted data bits N_B from ith LTE-U BS during T_{OFDM} time interval k within an active DL subframe/s of a duty cycle is given by

$$N_B^i = \sum_{k}^{\mathscr{K}^i} \sum_{u\in\mathbb{Q}_L^i} \sum_{r}^{R_u} W_{u,r}^i \log_2\left(1 + \mathrm{SINR}_{u,r}^i[k]\right) T_{\mathrm{OFDM}}, \quad (2)$$

where T_{OFDM} is the orthogonal frequency division multiplexing (OFDM) symbol duration, $T_{\mathrm{Tx}}^i = \mathscr{K}^i T_{\mathrm{OFDM}}$, and $\mathscr{K}^i$ is the total number of transmit T_{OFDM} time intervals for the considered duty cycle. The total allocated bandwidth for RB r for UE u served by BS i is $W_{u,r}^i$. The average capacity over a duty cycle period is used as a performance measure in this study as in [13]. The DL capacity C_i of LTE-U BS i is given as

$$C_i = \frac{N_B^i}{T_{\mathrm{Tx}}^i + T_{\mathrm{Wait}}^i}, \quad (3)$$

where T_{Wait}^i is the waiting time due to silent subframe allocation.

The capacity C_i in (3) is used as a performance measure for each LTE-U BS. Since the transmit power of one BS contributes to the interference power of the other BS, neighboring BSs are coupled in terms of interference. The goal of every BS is to maximize C_i while minimizing the DL transmit power p_s^i, $\forall i \in \mathscr{B}_L$. By minimizing the transmit power values p_s^i and p_s^b, the goal is to achieve a comparatively higher energy efficiency than the case of constant DL transmit power. In the same time a reduction in interference is also expected while guaranteeing a minimum capacity. Moreover, $P_{\min} \le p_s^b \le P_{\max}$, where $P_{\min}$ and $P_{\max}$ are the minimum and maximum transmit power constraints, respectively. The minimum capacity corresponding to a given action is denoted by $C_j^{\min}$. The objective is to maximize the average capacity while minimizing the transmit power, which can be written as

$$\text{maximize} \quad \frac{\sum_{i=1}^{|\mathscr{B}_L|} C_i}{|\mathscr{B}_L|} \quad (4)$$

$$\text{minimize} \quad p_s^i \quad \forall i \in \mathscr{B}_L \quad (5)$$

$$\text{subject to} \quad \left\{p_s^i, p_s^b\right\} \le P_{\max}, \quad \forall i, b \in \mathscr{B}_L,\ i \ne b,\ s \in S \quad (6)$$

$$\left\{p_s^i, p_s^b\right\} \ge P_{\min}, \quad \forall i, b \in \mathscr{B}_L,\ i \ne b,\ s \in S \quad (7)$$

$$C_i > C_j^{\min}, \quad \forall i \in \mathscr{B}_L,\ \forall j \in J. \quad (8)$$

In the case of energy efficiency, several parameter configurations are considered for (8) as

$$\frac{C_i}{p_s^i} > \frac{C_j^{\min}}{p_s^i}, \quad \text{or} \quad \frac{C_i}{p_s^i} > \frac{C_j^{\min}}{P_{\min}}, \quad \text{or} \quad \frac{C_i}{p_s^i} > \frac{C_j^{\min}}{P_{\max}}. \quad (9)$$

Due to the same denominator, $C_i/p_s^i > C_j^{\min}/p_s^i$ is simplified to (8), which can be used as a proportional measure of energy efficiency. The problem is reformulated defining a new objective to maximize energy efficiency as follows:

$$\text{maximize} \quad \frac{\sum_{i=1}^{|\mathscr{B}_L|}\left(C_i/p_s^i\right)}{|\mathscr{B}_L|} \quad \text{subject to} \quad (6), (7) \text{ and } (9). \quad (10)$$

4. MAB Techniques for LTE-U WiFi Coexistence

In a MAB problem, an agent selects an action (also known as arm) and observes the corresponding reward. The rewards for given action/arms are random variables with unknown distribution. The goal of MAB is to design action selection

(1) **Initialization**:
(2) Set the minimum capacity values $C_j^{\min}$, $\forall j \in J$, Exploration steps M, Beta (1, 1), α_j^i and β_j^i where $\forall j$: $j \in J$. Select d_j^i, $\forall j \in J$, update s, $n_{i,0}(d_j^i)$, $v_{i,0}(d_j^i)$ and accumulated hypothesis/reward $R_i(d_j^i)$ based on $C_i > C_j^{\min}$
(3) **if** $\alpha_j^i(m) = \beta_j^i(m), \forall (l, m) \in M$ **then**
(4) **Exploration**:
(5) **for** $m = 1, 2, 3, \ldots, M$ **do**
(6) Select d_j^i, $d_j^i \in \mathscr{D}_i$, $j \in \{\mathscr{U}(1, |\mathscr{D}_i|) \cap J\}$ and update s, (8)
(7) Execute $\{d_j^i, p_s^i\}$, observe C_i and update $n_{i,m}(d_j^i)$
(8) **if** $C_i > C_j^{\min}$ **then**
(9) Reward, $R_i(d_j^i) = R_i(d_j^i) + 1$
(10) Update s $(s \leftarrow s - 1)$ and $v_{i,m}(d_j^i)$, (11)
(11) Update $\alpha_j^i(m) = \alpha_j^i(m) + 1$
(12) **else**
(13) Reward, $R_i(d_j^i) = R_i(d_j^i) + 0$
(14) Update s $(s \leftarrow s + 1)$ and $v_{i,m}(d_j^i)$, (11)
(15) Update $\beta_j^i(m) = \beta_j^i(m) + 1$
(16) **end if**
(17) **if** $R_i(d_j^i) = R_i(d_a^i), d_j^i, d_a^i \in \mathscr{D}_i$, $j \neq a, \forall j, a \in J$ **then**
(18) Select $d_k^i, d_k^i \in \mathscr{D}_i, k \in \{\mathscr{U}(1, |\mathscr{D}_i|) \cap J\}$
(19) **else**
(20) Select d_k^i, (12)
(21) **end if**
(22) **Exploitation**:
(23) **for** $l = 1, 2, 3, \ldots, L$ **do**
(24) Execute the action $\mathscr{A}_i = \{d_k^i, p_s^i\}$
(25) **end for**
(26) **end for**
(27) **end if**

Algorithm 1: Multiarm bandit (Thomson sampling).

strategies to maximize accumulate rewards over a given time horizon. However, the strategies need to achieve a trade-off between exploration (selection of suboptimal actions to learn their average rewards) and exploitation (selection of actions which have provided maximum rewards so far).

In order to dynamically optimize LTE-U transmission parameters (i.e., duty cycle and transmit power), a variant of MAB learning techniques, called Thomson sampling [41, 42] algorithm, is applied. The scenario is formulated as a multiagent problem $\mathscr{G} = \{\mathscr{B}_L, \{\mathscr{A}_i\}_{\{i \in \mathscr{B}_L\}}, \{C_i\}_{\{i \in \mathscr{B}_L\}}\}$, considering the BSs as players, where $\mathscr{A}_i$ is the action set for player i. During the entire process, each BS needs to strike a balance between exploration and exploitation, where there are M exploration and L exploitation steps, indexed with m, $1 \leq m \leq M$, and l, $1 \leq l \leq L$, respectively.

(i) *Agents.* LTE-U BSs, $\mathscr{B}_L$.

(ii) *Action.* The action set of agent i, $\mathscr{A}_i$ is defined as $\mathscr{A}_i = \{d_j^i, p_s^i\}_{j \in J, s \in S}$. $\{d_j^i, p_s^i\}$ is the pair of duty cycle and transmit power elements. Configurations of duty cycles are used as part of the action space $\mathscr{D}$, where $\mathscr{D}$ is common for all players. A given BS i selects $d_j^i, d_j^i \in \mathscr{D}$ according to Algorithm 1 where $J = \{1, 2, \ldots, |\mathscr{D}|\}$, $j \in J$ and $J \in \mathbb{Z}^+$. Probability spaces of positive integers are denoted by $\mathbb{Z}^+$. The set of first elements of the action vector $\mathscr{D}_i = \{d_1^i, d_2^i, \ldots, d_{|\mathscr{D}|}^i\}$ of BS i is associated with the duty cycles as $\{20\%, 40\%, \ldots, 80\%\}$, respectively. The transmit power values set $\mathscr{P}$ is represented as $S = \{1, 2, \ldots, |\mathscr{P}|\}$, $s \in S$, and $S \in \mathbb{Z}^+$. p_s^i is the transmit power of player i, where $\mathscr{P}_i = \{p_1^i, p_2^i, \ldots, p_{|\mathscr{P}|}^i\}$. For each action $\mathscr{A}_i$, there is a distribution Beta (α_j^i, β_j^i), $\forall j \in J$, where α_j^i and β_j^i are the shape parameter. However, in the case of power control (PC), if $C_i > C_j^{\min}$, s is decreased by one $(s \leftarrow s-1)$ reducing the transmit power p_s^i by one level for the next step $m + 1$ and vice versa. Further, when $C_i > C_j^{\min}$ a reward is achieved. And, for $C_i > C_j^{\min}$, α_j^i is incremented; otherwise, β_j^i is incremented.

(iii) *Decision Function.* The DL capacity of a BS i, C_i is used as the utility function. In order to select a duty cycle, a decision function based on the policy UCB1 [43] is used where the accumulated rewards achieved due to values given by C_i are exploited. The decision value for the duty cycle d_j^i related to the exploration

step m of BS i, $v_{i,m}(d_j^i)$, is given in (11) while d_k^i based on the decision is given in (12):

$$v_{i,m}\left(d_j^i\right) = \overline{x}_{i,m}\left(d_j^i\right) + \sqrt{\frac{2\ln\left(m + \left|\mathscr{D}_i\right|\right)}{n_{i,m}\left(d_j^i\right)}}, \tag{11}$$

$$d_k^i = \underset{d_j^i \in \mathscr{D}_i}{\arg\max}\left(v_{i,m}\left(d_j^i\right)\right), \tag{12}$$

where $\overline{x}_{i,m}(d_j^i) = R_i(d_j^i)/n_{i,m}(d_j^i)$. The argument of the maximum value is given by arg max$(\cdot)$. $\overline{x}_{i,m}(d_j^i)$, $R_i(d_j^i)$, and $n_{i,m}(d_j^i)$ are the average reward obtained from d_j^i during the exploration step m, total rewards gained form the same d_j^i, and the total number of times d_j^i has been played, respectively. Selection of s is totally independent of the decision function.

The multiagent learning problem is addressed using a MAB approach. In the contextual MAB problem handled by the Thomson sampling algorithm [41], current and previous information (i.e., history) is used for the selection of an arm or action. Initially d_j^i, $\forall j \in J$, are played once with $p_s^i = p_{|\mathscr{P}|}^i$. Based on the accumulated reward $R_i(d_j^i)$, the parameters s, $n_{i,0}(d_j^i)$, and $v_{i,0}(d_j^i)$ are updated. In the learning process, the accumulated reward is used to play the role of the accumulated hypothesis defined in [44]. Subsequently, agents balance between M exploration and L exploitations steps. During the exploration steps, d_j^i is selected randomly, where $d_j^i, d_j^i \in \mathscr{D}_i$, $j \in \{\mathscr{U}(1, |\mathscr{D}_i|) \cap J\}$, where a uniform distribution with the minimum and maximum values x_1 and x_2 is given by $\mathscr{U}(x_1, x_2)$. s is decided based on the last available values of (8). Subsequently the same set of parameters is updated. At the end of each exploration step, based on (8) and the accumulated rewards an action is selected. Then the same action is repeatedly played for all the L exploitation steps of that particular exploration step as explained in Algorithm 1.

5. Simulation Results

For LTE-U, TDD-LTE is considered and it is assumed that all LTE-U UEs are synchronized in both time and frequency domain as in [13] with the serving BSs. A beacon is transmitted periodically for the purpose of synchronization of WiFi STAs with the corresponding APs. To evaluate the performance, an architecture containing two independently operated layers of cellular deployments is considered as shown in Figure 5. Hexagonal cells with omnidirectional antennas are assumed. LTE-U layer encompasses $|\mathscr{B}_L| = 7$ BSs and $|\mathscr{Q}_L|$ UEs, where the WiFi layer includes $|\mathscr{B}_W| = 7$ APs and $|\mathscr{Q}_W|$ WiFi STAs. In each cell, for each AP/BS, STAs/UEs are dropped at random locations. All of them are assumed to be uniformly distributed within the cells of their serving BSs having a mobility speed of 3 km/h and a random walk mobility model. We consider a nonfull buffer traffic for both WiFi and LTE networks, where the packet arrivals at the transmitter queues follow a Poisson distribution. The traffic

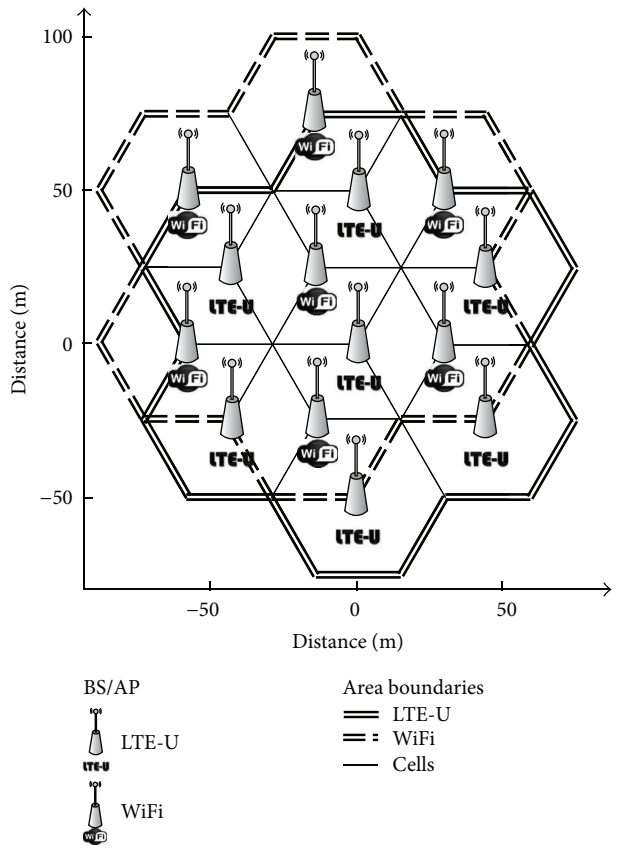

Figure 5: Cellular coverage layout used in LTE-U and WiFi coexistence simulations.

arrival rates for LTE-U and WiFi are $\lambda_{\text{LTE}} = \lambda_{\text{WiFi}} = 2.5$ packet/second.

The LTE and WiFi IEEE 802.11n medium access control (MAC) and physical (PHY) layers are modeled in which a PHY layer abstraction is used for Shannon capacity calculations of WiFi and LTE-U. The time granularity of each WiFi OFDM symbol duration is 4 μs, which we use to periodically capture the number of successfully received bits [13]. For both technologies wireless channel is modeled according to [45], when the systems are operated in the 3.5 GHz band. Indoor Hotspot (InH) scenario is considered with path loss and shadowing parameters. FTP Traffic Model-2 [45] is employed for either WiFi or LTE-U with a noise spectral power density of −95 dBm/Hz.

In each transmission time interval (TTI), DL SINR is reported to the corresponding BS. Based on the number of LTE-U UEs waiting and requesting UL transmission during one subframe, bandwidth is equally shared among themselves. The simulation parameters for LTE-U transmissions are summarized in Table 1. TDD configuration 1 [39, Figure 6.2(a)] is used for the LTE-U frames having a 50 ms total duty cycle period. Minimum required capacity level $C_j^{\min}$ is 10 Mbps and the set of power levels is $\mathscr{P}_i = \{p_1^i, p_2^i, \ldots, p_{|\mathscr{P}|}^i\} = \{8, 13, 18, 23\}$ dBm.

For WiFi, CSMA/CA with enhanced distributed channel access (EDCA) and clear channel assessment (CCA) has been

Table 1: LTE MAC/PHY parameters.

Parameter	Value
Frequency	3.5 GHz
Transmission scheme	OFDM
Bandwidth	20 MHz
DL Tx power	23 dBm
UL Tx power	PL Based TPC
Frame duration	10 ms
Scheduling	Round Robin
UL base power level P_0	−106 dBm
TTI	1 ms

Table 2: WiFi MAC/PHY parameters.

Parameter	Value
Frequency	3.5 GHz
Transmission scheme	OFDM
Bandwidth	20 MHz
DL/UL Tx power	23 dBm
Access category	Best effort
MAC protocol	EDCA
CCA channel sensing threshold	−82 dBm
CCA energy detection threshold	−62 dBm
No of service bits in PPDU	16 bits
No of tail bits in PPDU	12 bits
Backoff type	Fixed contention window
Contention window size	$\mathcal{U}(0, 31)$
Noise figure	6 [39]
Beacon interval	100 ms
Beacon OFDM symbol detection threshold	10 dB
Beacon error ratio threshold	15

implemented. All WiFi STAs with traffic in their queue will compete for channel access after receiving a beacon transmission. Without reception of a signal beacon, transmission or reception will not be initiated. The WiFi STA will sense the channel and will transmit if it is idle. Otherwise, transmission will be backed off and the next transmission will be initiated after a backoff time. Random backoff time mechanism is used for this study. All the parameters for the WiFi transmission are summarized in Table 2.

5.1. Aggregate Capacity with MAB. Aggregate capacity of stand-alone WiFi, coexisting LTE-U (80% duty cycle) and WiFi (with no MAB algorithm), and MAB based coexistence of LTE-U and WiFi are presented in Figure 7. The aggregate numbers of WiFi APs and LTE BSs in all scenarios are kept constant. For the WiFi only deployment, we replace all the LTE BSs in Figure 5 with WiFi APs. It is notable that, with the use of MAB, the overall capacity is increased significantly from stand-alone WiFi operation and simultaneous operation of LTE-U and WiFi (without MAB). Also we found that with the increase of intersite distance (ISD) in Figure 5, the

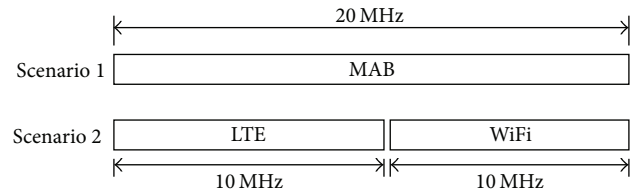

Figure 6: Scenario with two cases.

capacity deceases. This is because of higher serving area per APs/STA within the ISDs.

The WiFi throughput performance with and without MAB algorithm is shown in Figure 8, where it is noted that MAB algorithm improves the WiFi throughput over the two other scenarios. Moreover, with the increase of ISD, capacity degrades for all cases. The effect of LTE packet arrival rate on aggregate capacity is shown in Figure 9. We found that the aggregate throughput of coexisting LTE and WiFi networks is maximized for $\lambda_L = 2.5$, but then it decreases for larger values of λ_L due to increased interference levels. Also for full buffer LTE traffic ($\lambda_L = 0$), the coexisting system with MAB has degraded performance compared to coexisting system without MAB.

Impact of energy detection threshold on aggregate capacity is shown in Figure 10. It is observed that −62 dBm threshold provides best performance for all scenarios. Sensing threshold less than −62 dBm makes WiFi back off from transmission in the presence of LTE transmission and results in lower aggregate capacity. On the other hand, sensing threshold more than −62 dBm allows WiFi to transmit in the presence of LTE operation, which reduces aggregate capacity due to higher interference.

For Figure 11, we consider a scenario with two cases as described in Figure 6. In scenario 1, we consider simultaneous operation of LTE-U and WiFi using MAB on 20 MHz bandwidth. On the other hand, in scenario 2, stand-alone LTE (i.e., 100% duty cycle) and WiFi are operating on separate 10 MHz bandwidth. We find that the overall capacity using MAB is improved significantly when compared with the aggregate capacity of two stand-alone systems. This reflects how the spectral efficiency can be improved using MAB and motivates sharing of wireless spectrum among LTE and WiFi networks, rather than deploying them separately.

The impact of LTE-U UEs and WiFi STAs density on aggregate capacity is given in Figure 12. We find that the aggregate capacity improves for the reductions of users in both services. Comparatively high sensitivity could be seen when the density of STAs is changed. When the densities are reduced, particularly the STAs, a significant increase in capacity is achieved under reduced interference conditions. However, this reduction is further contributed by the CSMA/CA mechanism as well. Also it is notable that capacity decreases with the increase of ISD.

5.2. Cell-Edge Performance. In Figure 13, 5th percentile LTE throughput for different user densities of STAs is represented. We found that with the increase of STAs, 5th percentile UE throughput reduces due to more interference caused by STAs.

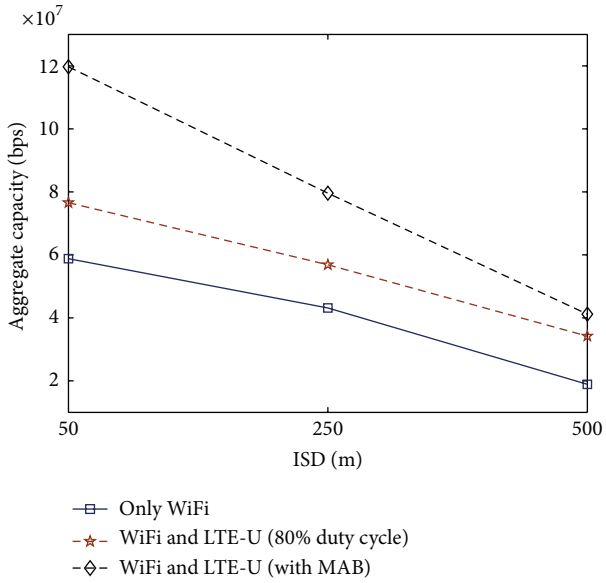

Figure 7: Aggregate capacity of coexisting WiFi and LTE-U (80% duty cycle), MAB based coexisting LTE-U and WiFi, and stand-alone WiFi system for different ISDs.

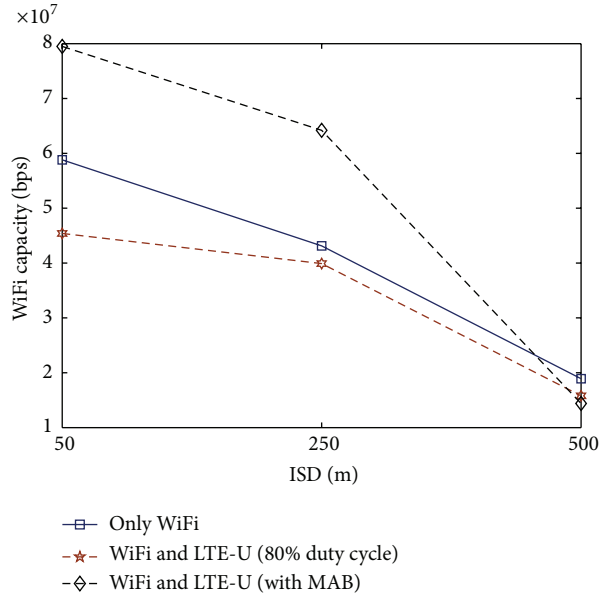

Figure 8: WiFi capacity of coexisting WiFi and LTE-U (80% duty cycle), MAB based coexisting LTE-U and WiFi, and stand-alone WiFi system for different ISDs.

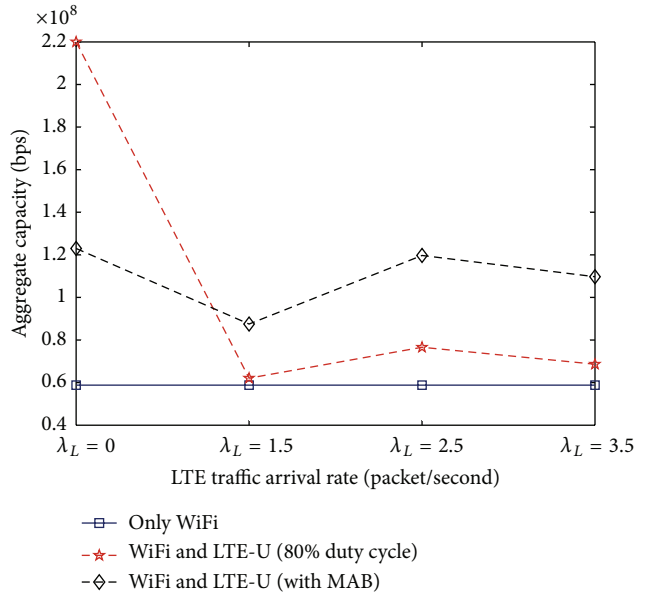

Figure 9: Aggregate capacity of coexisting WiFi and LTE-U (80% duty cycle), MAB based coexisting LTE-U and WiFi, and stand-alone WiFi system for different LTE traffic arrival rates.

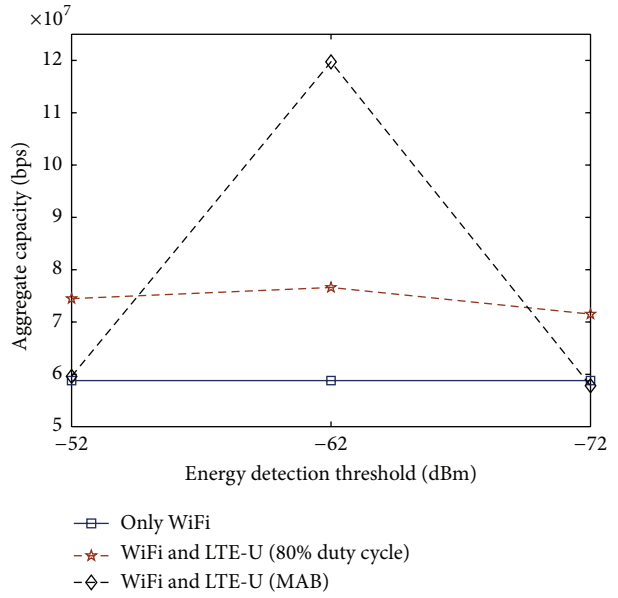

Figure 10: Aggregate capacity of coexisting sytem of WiFi and LTE-U (80% duty cycle), MAB based coexisting LTE-U and WiFi, and stand-alone WiFi system for various energy detection thresholds.

However, with the increment of UEs, the effect of STA density reduces. This means that, for higher density of UEs and STAs, fewer LTE users will experience higher capacity.

5.3. Energy Efficiency Performance. Aggregate capacity of $|\mathcal{Q}_L^i| = 10$ and $|\mathcal{Q}_W^w| = 10$ is presented in Figure 14 for different power control techniques. Four parameter settings are used for PC. In the first instance, no PC is considered. In the second case, PC is used by replacing the parameters in Step (7) of the Algorithm 1 with $C_i/p_s^i > C_j^{\min}/P_{\min}$, where $P_{\min} = 8$ dBm. For the third and forth cases, parameters are replaced with $C_i/p_s^i > C_j^{\min}/P_{\max}$ and $C_i > C_j^{\min}$, where $P_{\max} = 23$ dBm. The set of power levels is defined as $\mathcal{P}_i = \{p_1^i, p_2^i, \ldots, p_{|\mathcal{P}|}^i\} = \{8, 11, 14, 17, 20, 23\}$ dBm, where $P_{\min} = 8$ dBm and $P_{\max} = 23$ dBm. So, in the second and third cases a given level of energy efficiency is aimed at. In the last case, according to the explanation given for (9), the level is dynamically adjusted. It

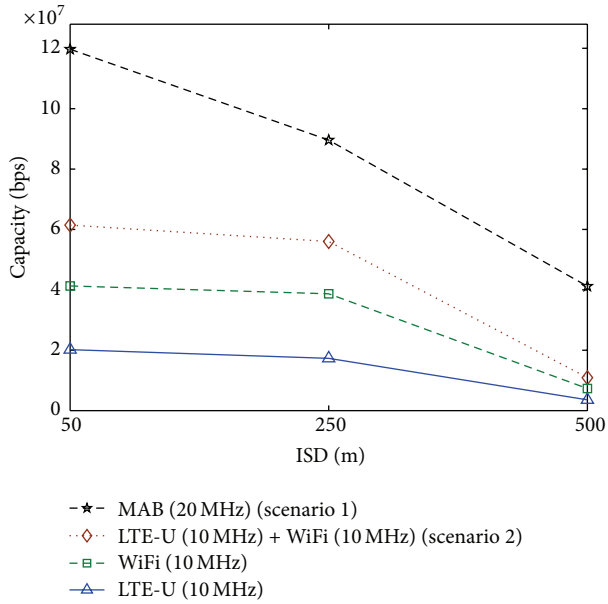

Figure 11: Capacity of 10 STAs or/and 10 UEs under stand-alone WiFi, stand-alone LTE, coexisting stand-alone WiFi, and LTE-U (scenario 1) and MAB based coexisting LTE-U and WiFi (scenario 2) for different bandwidths and ISDs.

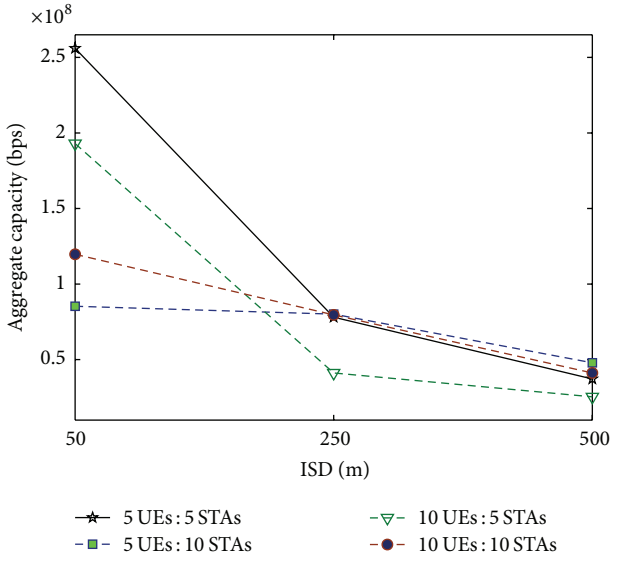

Figure 12: Capacity of MAB based coexistence for different UEs and STAs ratios and ISDs.

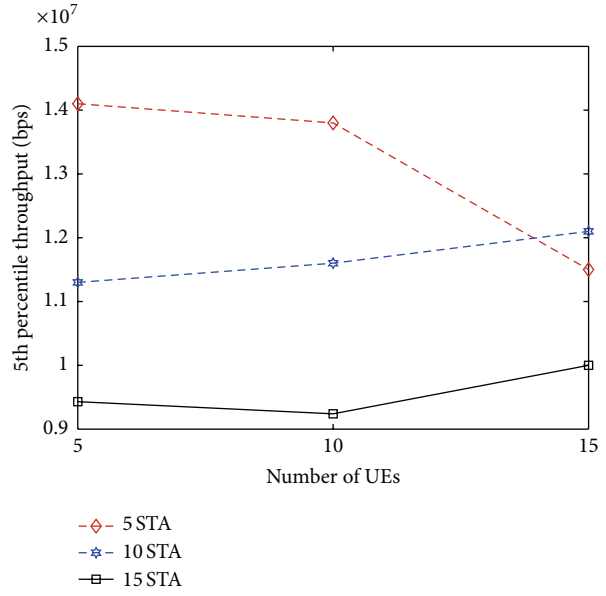

Figure 13: 5th percentile throughput of MAB based coexisting LTE-U and WiFi for different UEs and STAs ratios.

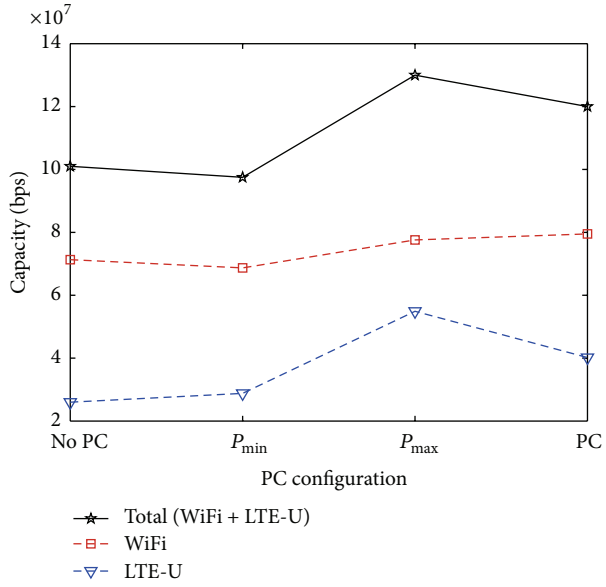

Figure 14: Capacity of 10 UEs and 10 STAs under different PC configurations.

is noted that the best and worst performances are found for P_{max} and P_{min}. For MAB with PC, optimum result is found.

In Figure 15, different numbers of UEs are considered to evaluate energy efficiency performance. For all the densities, the least efficiency is achieved with no PC. In the most dense scenario, the best efficiency can be observed under the second configuration, C_j^{min}/P_{min} [see (9)]. As it is expected with the reduction of densities, energy efficiency is increased. However, after a certain average energy efficiency level, no significant improvements could be observed.

6. Conclusion

In this paper, a MAB based dynamic duty cycle selection method was proposed to facilitate spectrum sharing between WiFi and LTE-U in the same unlicensed band. Performance of the proposed algorithm was further enhanced by using a DL PC technique. Subsequently, the proposed concept was extended to optimize energy efficiency. Considerable gains in overall throughputs could be achieved via the proposed MAB while ensuring a minimum capacity for LTE-U based services in the same band. Significant gains in terms of energy efficiency could be achieved where it is observed that the

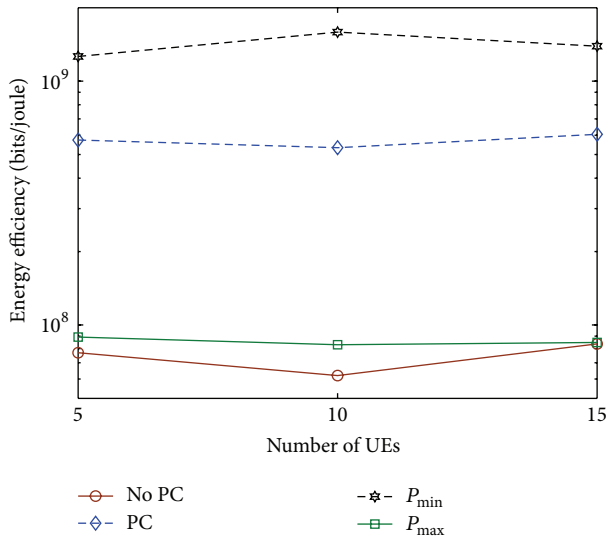

FIGURE 15: Energy efficiency under different PC configurations for various numbers of UEs (with 10 STAs).

gains under different parameter settings with PC are much higher than those with no PC. Our future work includes extending our framework to scenarios with IA and PAL users in the same spectrum.

Competing Interests

The authors declare that there is no conflict of interests regarding the publication of this paper.

Acknowledgments

The authors would like to thank Nadisanka Rupasinghe for developing an earlier version of the simulator used in this paper. This research was supported in part by the US National Science Foundation (NSF) under Grants nos. ACI-1541108 and AST-1443999 and Presidential Fellowship under Florida International University.

References

[1] NSN Whitepaper, "Enhance mobile networks to deliver 1000 times more capacity by 2020," Tech. Rep., 2013.

[2] M. Simsek, M. Bennis, and I. Güvenc, "Enhanced intercell interference coordination in HetNets: single vs. multiflow approach," in *Proceedings of the IEEE Globecom Workshops (GC Wkshps '13)*, pp. 725–729, Atlanta, Ga, USA, December 2013.

[3] M. Simsek, M. Bennis, and I. Guvenc, "Learning based frequency- and time-domain inter-cell interference coordination in HetNets," *IEEE Transactions on Vehicular Technology*, vol. 64, no. 10, pp. 4589–4602, 2015.

[4] FCC, "Amendment of the commissions rules with regard to commercial operations in the 3550–3650 MHz band," Notice of Proposed Rulemaking and Order, 2012, https://apps.fcc.gov/edocs_public/attachmatch/DA-15-955A1_Rcd.pdf.

[5] FCC, "Amendment of the commissions rules with regard to commercial operations in the 3550–3650 MHz band," Report and Order and Second Further Notice of Proposed Rulemaking 12-354, 2015, https://apps.fcc.gov/edocs_public/attachmatch/FCC-15-47A1.pdf.

[6] R. Zhang, M. Wang, L. X. Cai, Z. Zheng, X. S. Shen, and L.-L. Xie, "LTE-unlicensed: the future of spectrum aggregation for cellular networks," *IEEE Wireless Communications*, vol. 22, no. 3, pp. 150–159, 2015.

[7] "Study on licensed-assisted access using LTE," Tech. Rep. RP-141397, 3GPP Study Item, Edinburgh, Scotland, 2014.

[8] 3GPP, "Study on licensed-assisted access to unlicensed spectrum," Tech. Rep. TR 36.899, 3GPP, Athens, Greece, 2015.

[9] L. Cai, X. Shen, J. W. Mark, and Y. Xiao, "Voice capacity analysis of WLAN with unbalanced traffic," in *Proceedings of the 2nd International Conference on Quality of Service in Heterogeneous Wired/Wireless Networks (QSHINE '05)*, pp. 8–9, Lake Vista, Fla, USA, August 2005.

[10] F. M. Abinader, E. P. L. Almeida, F. S. Chaves et al., "Enabling the coexistence of LTE and Wi-Fi in unlicensed bands," *IEEE Communications Magazine*, vol. 52, no. 11, pp. 54–61, 2014.

[11] I. Parvez, N. Islam, N. Rupasinghe, A. I. Sarwat, and I. Güvenç, "LAA-based LTE and ZigBee coexistence for unlicensed-band smart grid communications," in *Proceedings of the SoutheastCon 2016*, pp. 1–6, Norfolk, Va, USA, March-April 2016.

[12] N. Rupasinghe and I. Guvenc, "Licensed-assisted access for WiFi-LTE coexistence in the unlicensed spectrum," in *Proceedings of the IEEE Globecom Workshops (GC Wkshps '14)*, pp. 894–899, Austin, Tex, USA, December 2014.

[13] N. Rupasinghe and I. Gülvenç, "Reinforcement learning for licensed-assisted access of LTE in the unlicensed spectrum," in *Proceedings of the IEEE Wireless Communications and Networking Conference (WCNC '15)*, pp. 1279–1284, New Orleans, La, USA, March 2015.

[14] M. G. S. Sriyananda, I. Parvez, I. Guvenc, M. Bennis, and A. I. Sarwat, "Multi-Armed Bandit for LTE-U and WiFi coexistence in unlicensed bands," in *Proceedings of the IEEE Wireless Communications and Networking Conference (WCNC '16)*, Doha, Qatar, April 2016.

[15] T. Ran, S. Sun, B. Rong, and M. Kadoch, "Game theory based multi-tier spectrum sharing for LTE-A heterogeneous networks," in *Proceedings of the IEEE International Conference on Communications (ICC '15)*, pp. 3033–3038, London, UK, June 2015.

[16] F. Shams, G. Bacci, and M. Luise, "A Q-learning game-theory-based algorithm to improve the energy efficiency of a multiple relay-aided network," in *Proceedings of the 31st General Assembly and Scientific Symposium of the International Union of Radio Science (URSI GASS '14)*, pp. 1–4, XXXIth URSI, August 2014.

[17] J. C. Gittins, "Bandit processes and dynamic allocation indices," *Journal of the Royal Statistical Society—Series B: Methodological*, vol. 41, no. 2, pp. 148–177, 1979.

[18] P. Auer, N. Cesa-Bianchi, and P. Fischer, "Finite-time analysis of the multiarmed bandit problem," *Machine Learning*, vol. 47, no. 2, pp. 235–256, 2002.

[19] A. M. Cavalcante, E. Almeida, R. D. Vieira et al., "Performance evaluation of LTE and Wi-Fi coexistence in unlicensed bands," in *Proceedings of the IEEE 77th Vehicular Technology Conference (VTC Spring '13)*, pp. 1–6, Dresden, Gramany, June 2013.

[20] R. Kwan, R. Pazhyannur, J. Seymour et al., "Fair co-existence of Licensed Assisted Access LTE (LAA-LTE) and Wi-Fi in unlicensed spectrum," in *Proceedings of the 7th Computer Science and Electronic Engineering (CEEC '15)*, pp. 13–18, Colchester, UK, September 2015.

[21] N. Whitepaper, "Views on LAA for unlicensed spectrum—scenarios and initial evaluation results," Tech. Rep. RWS-140026, 3GPP RAN1 Standard Contribution, Sophia Antipolis, France, 2014.

[22] Qualcomm, "Qualcomm research LTE in unlicensed spectrum: harmonious coexistence with WiFi," Tech. Rep., 3GPP RAN1 Standard Contribution, 2014.

[23] E. Almeida, A. M. Cavalcante, R. C. D. Paiva et al., "Enabling LTE/WiFi coexistence by LTE blank subframe allocation," in *Proceedings of the IEEE International Conference on Communications (ICC '13)*, pp. 5083–5088, IEEE, Budapest, Hungary, June 2013.

[24] T. Nihtila, V. Tykhomyrov, O. Alanen et al., "System performance of LTE and IEEE 802.11 coexisting on a shared frequency band," in *Proceedings of the IEEE Wireless Communications and Networking Conference (WCNC '13)*, pp. 1038–1043, Shanghai, China, April 2013.

[25] F. S. Chaves, E. P. L. Almeida, R. D. Vieira et al., "LTE UL power control for the improvement of LTE/Wi-Fi coexistence," in *Proceedings of the IEEE 78th Vehicular Technology Conference (VTC Fall '13)*, pp. 1–6, September 2013.

[26] N. Rupasinghe and I. Güvenç, "Licensed-assisted access for WiFi-LTE coexistence in the unlicensed spectrum," in *Proceedings of the IEEE Globecom Workshops (GC Wkshps '14)*, pp. 894–899, Austin, Tex, USA, December 2014.

[27] X. Xu, G. Kutrolli, and R. Mathar, "Dynamic downlink power control strategies for LTE femtocells," in *Proceedings of the 7th Next Generation Mobile Applications, Services and Technologies Conference*, pp. 181–186, September 2013.

[28] Z. Wang, W. Xiong, C. Dong, J. Wang, and S. Li, "A novel downlink power control scheme in LTE heterogeneous network," in *Proceedings of the International Conference on Computational Problem-Solving (ICCP '11)*, pp. 241–245, Chengdu, China, October 2011.

[29] T. Zahir, K. Arshad, Y. Ko, and K. Moessner, "A downlink power control scheme for interference avoidance in femtocells," in *Proceedings of the 7th International Wireless Communications and Mobile Computing Conference (IWCMC '11)*, pp. 1222–1226, July 2011.

[30] S. Maghsudi and S. Stanczak, "Channel selection for network-assisted D2D communication via no-regret bandit learning with calibrated forecasting," *IEEE Transactions on Wireless Communications*, vol. 14, no. 3, pp. 1309–1322, 2015.

[31] M. Simsek, M. Bennis, and I. Guvenc, "Mobility management in HetNets: a learning-based perspective," *EURASIP Journal on Wireless Communications and Networking*, vol. 2015, no. 1, article 26, pp. 1–13, 2015.

[32] R. Combes and A. Proutiere, "Dynamic rate and channel selection in cognitive radio systems," *IEEE Journal on Selected Areas in Communications*, vol. 33, no. 5, pp. 910–921, 2015.

[33] G. Locke and L. E. Strickling, "An assessment of the near-term viability of accommodating wireless broadband systems in the 1675–1710 MHz, 1755–1780 MHz, 3500–3650 MHz, and 4200–4220 MHz, 4380–4400 MHz bands," Report, 2010, https://www.ntia.doc.gov/files/ntia/publications/fasttrackevaluation_11152010.pdf.

[34] P. R. Atkins, "NTIA letter office of engineering and technology, FCC," GN Docket No. 12-354, 2015, http://www.ntia.doc.gov/files/ntia/publications/ntia_letter_docket_no_12-354.pdf.

[35] L. Stefani, "The FCC Raises the Curtain on the Citizens Broadband Radio Service," CommLawBlog Article, May 2015, http://www.commlawblog.com/2015/05/articles/unlicensed-operations-and-emer/the-fcc-raises-the-curtain-on-the-citizens-broadband-radio-service/.

[36] FCC, "3.5 GHz Spectrum Access System Workshop," Washington, DC, USA, 2014, https://www.fcc.gov/news-events/events/2014/01/35-ghz-spectrum-access-system-workshop.

[37] "RSPG opinion on licensed shared access," Tech. Rep. RSPG13-538, European Commission, Radio Spectrum Policy Group, 2013.

[38] ECC, "Licensed shared access," Tech. Rep. ECC 205, 2014.

[39] S. Sesia, I. Toufik, and M. Baker, *LTE—The UMTS Long Term Evolution: From Theory to Practice*, John Wiley & Sons, New York, NY, USA, 2009.

[40] E. Perahia and R. Stacey, *LTE: The UMTS Long Term Evolution, From Theory to Practice*, Cambridge University Press, New York, NY, USA, 2008.

[41] S. Agrawal and N. Goyal, "Analysis of thompson sampling for the multi-armed bandit problem," https://arxiv.org/abs/1111.1797.

[42] N. Gupta, O.-C. Granmo, and A. Agrawala, "Thompson sampling for dynamic multi-armed bandits," in *Proceedings of the 10th International Conference on Machine Learning and Applications (ICMLA '11)*, vol. 1, pp. 484–489, Honolulu, Hawaii, USA, December 2011.

[43] P. Auer, N. Cesa-Bianchi, and P. Fischer, "Finite-time analysis of the multiarmed bandit problem," *Machine Learning*, vol. 47, no. 2-3, pp. 235–256, 2002.

[44] J. Langford and T. Zhang, "The epoch-greedy algorithm for multiarmed bandits with side information," in *Advances in Neural Information Processing Systems*, J. C. Platt, D. Koller, Y. Singer, and S. T. Roweis, Eds., vol. 20, pp. 817–824, Curran Associates, 2008.

[45] 3GPP, "Evolved Universal Terrestrial Radio Access (E-UTRA); further advancements for E-UTRA physical layer aspects (release 9)," Tech. Rep. TR36.814, V9.0.0, 3GPP, 2010.

Hindawi Publishing Corporation
Mobile Information Systems
Volume 2016, Article ID 3282505, 8 pages
http://dx.doi.org/10.1155/2016/3282505

Research Article

Spectrum Assignment Algorithm for Cognitive Machine-to-Machine Networks

Soheil Rostami,[1] Sajad Alabadi,[1] Soheir Noori,[2] Hayder Ahmed Shihab,[3] Kamran Arshad,[4] and Predrag Rapajic[1]

[1]*Department of Engineering Science, University of Greenwich, London, UK*
[2]*Department of Computer Science, University of Karbala, Karbala, Iraq*
[3]*School of Engineering and Informatics, University of Sussex, Brighton, UK*
[4]*Department of Electrical Engineering, Ajman University of Science & Technology, Ajman, UAE*

Correspondence should be addressed to Soheil Rostami; s.rostami@gre.ac.uk

Received 18 March 2016; Revised 15 June 2016; Accepted 10 July 2016

Academic Editor: Fernando Casadevall

A novel aggregation-based spectrum assignment algorithm for Cognitive Machine-To-Machine (CM2M) networks is proposed. The introduced algorithm takes practical constraints including interference to the Licensed Users (LUs), co-channel interference (CCI) among CM2M devices, and Maximum Aggregation Span (MAS) into consideration. Simulation results show clearly that the proposed algorithm outperforms State-Of-The-Art (SOTA) algorithms in terms of spectrum utilisation and network capacity. Furthermore, the convergence analysis of the proposed algorithm verifies its high convergence rate.

1. Introduction

Today, there are around 4 billion M2M devices in the world, while in 2022, the number is expected to reach 50 billion [1]. According to Cisco systems, currently a single M2M device can generate as much traffic as 3 basic-feature phones; in addition, emerging applications and services of M2M networks are expected to increase average traffic per device from 70 MB per month in 2014 to 366 MB per month in 2018 [2]. Because of the growth rate of the number of devices and high demand of data traffic, future M2M networks will face many challenges, especially with the so-called spectrum scarcity problem.

Cognitive Radio (CR) is introduced as a promising solution to tackle spectrum scarcity problem in M2M networks. CR has become one of the most intensively studied paradigms in wireless communications. In CR, unlicensed users exploit CR technology to opportunistically access licensed spectrum as long as interference to LUs is kept at an acceptable level [3]. A number of M2M applications (such as smart grid, healthcare, and car parking) can benefit from the combination of CR and M2M communications [1]. CM2M networks can improve spectrum utilisation and energy efficiency in M2M networks [4]. The CM2M device can interact with the radio environment by either performing spectrum sensing or accessing spectrum databases or both of them to detect spectrum opportunities [4]. After sensing, CM2M device utilises the discovered unused spectrum according to the device requirements.

Furthermore, TV bands (VHF/UHF), which have highly favourable propagation characteristics, are traditionally reserved to broadcasters. But after the transition from the analogue broadcast television system to the digital one, a huge number of TV channels (also known as TV White Spaces (TVWS)) are freed up and unused. In September 2010, the Federal Communications Commission (FCC) released significant rule to enable unlicensed broadband wireless devices to use TVWS. Unfortunately, due to spectrum fragmentation and as a result of an inefficient command and control spectrum management approach, a continuous wide segment of TVWS is rare in many countries including the United Kingdom.

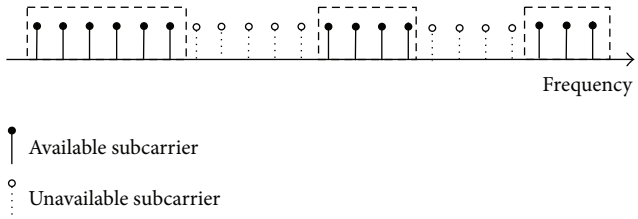

Figure 1: Subcarrier distribution over spectrum [7].

As CM2M network can sense and be aware of its radio environment, the aggregation of narrow spectrum opportunities becomes possible. Spectrum aggregation provides wider bandwidth and higher throughput for the CM2M devices. CM2M devices can access discontinuous portions of the TVWS simultaneously by means of Discontinuous Orthogonal Frequency Division Multiplexing (DOFDM) [5, 6].

DOFDM is a multicarrier modulation technique and is a variant of OFDM used to aggregate discontinuous segments of spectrum. The main difference between OFDM and DOFDM is ON/OFF subcarrier information block [7]. A multiple segments of spectrum can be occupied by other CM2M devices or LUs. As a result, these subcarriers are off-limits to the CM2M devices [6]. Thus, to avoid interfering with these other transmissions, the subcarrier within their vicinity is turned off and unusable for CM2M devices, as shown in Figure 1. Moreover, available (usable) subcarriers are located in the unoccupied segments of spectrum, which are determined by spectrum broker.

Spectrum aggregation is one of the most important LTE-advanced technologies from physical layer perspective and standardised in LTE Release 10 [8]. However, in spite of standardisation of spectrum aggregation, little effort has been made to optimise spectrum aggregation by exploiting CR technology in M2M networks. There is limited literature available on spectrum assignment among CM2M devices having spectrum aggregation capabilities.

In [9], an Aggregation-Aware Spectrum Assignment Algorithm (AASAA) is proposed to aggregate discrete spectrum fragments in a greedy manner. The algorithm in [9] utilises the first available aggregation range from the low frequency side and assumes that all users have the same bandwidth requirement.

Huang et al. [10] proposed a prediction based spectrum aggregation scheme to increase the capacity and decrease the reallocation overhead. The proposed scheme is referred to as Maximum Satisfaction Algorithm (MSA) for spectrum assignment. The main idea is to assign spectrum for the user with larger bandwidth requirement first, leaving better spectrum bands for remaining users, while taking into consideration different bandwidth requirements of users and channel state statistics. However, MSA does not enhance spectrum utilisation by reusing spectrum within unlicensed network; that is, CCI is neglected in MSA.

Recently, genetic algorithm (GA) is used for spectrum allocation [11]. Ye et al. [11] introduced a GA based spectrum assignment in CR networks; but spectrum aggregation capability of users is not considered.

For CM2M networks, existing spectrum assignment and aggregation solutions are not applicable directly as practical issues such as Maximum Aggregation Span (MAS) must be taken into account. Furthermore, in aggregation-based spectrum assignment a major challenge is to manage CCI among CM2M devices which is not taken into account in the existing literature. The major contributions of this study are twofold.

(1) To prevent multiple CM2M devices from colliding in the overlapping portions of the spectrum, a centralised approach is applied. Furthermore, an integer optimisation problem to maximise cell throughput is formulated, considering CCI and MAS in an aggregation-aware CM2M network.

(2) As the spectrum assignment problem is inherently seen as an NP-hard optimisation problem, evolutionary approaches can be applied to solve this challenging problem. In this article, GA is used to solve the aggregation-aware spectrum assignment because of its simplicity, robustness, and fast convergence of the algorithm [12].

This article is organised as follows. In Section 2, the spectrum assignment and aggregation models are presented. The proposed algorithm is explained in Section 3. Simulation results are discussed in Section 4, followed by conclusions in Section 5.

2. System Model

2.1. Spectrum Assignment Model. We assume a CM2M network consisting of N CM2M devices defined as $\Phi = \{\phi_1, \phi_2, \ldots, \phi_N\}$ competing for M nonoverlapping orthogonal channels $\Gamma = \{\gamma_1, \gamma_2, \ldots, \gamma_M\}$ in uplink. All spectrum assignment and access procedures are controlled by a central entity called spectrum broker. We assume that distributed sensing mechanism and measurement conducted by each device is forwarded to the spectrum broker [13]. A spectrum occupancy map that is constructed at the spectrum broker and CCI among CM2M devices is determined. Furthermore, the spectrum broker can lease single or multiple channels for $\phi_n \in \Phi$ in a limited geographical region for a certain amount of time. Finally, a base station can transmit data to ϕ_n in the assigned channels. Figure 2 depicts system model used in this article.

We define the channel availability matrix $\mathbf{L} = \{l_{n,m} \mid l_{n,m} \in \{0, 1\}\}_{N \times M}$ as an $N \times M$ binary matrix representing channel availability, where $l_{n,m} = 1$ if and only if γ_m is available to ϕ_n and $l_{n,m} = 0$ otherwise. Each ϕ_n is associated with a set of available channels at its location defined as $\overline{\Gamma}_n \subset \Gamma$; that is, $\overline{\Gamma}_n = \{\gamma_m \mid l_{n,m} \neq 0\}$. Due to the different interference range of each LU (which depends on LU's transmit power and the physical distance) at the location of each CM2M device, $\overline{\Gamma}_n$ of different CM2M devices may be different [14]. According to the sharing agreement, any $\gamma_m \in \Gamma$ can be reused by a group of CM2M devices in the vicinity defined by $\overline{\Phi}_m$ such that $\overline{\Phi}_m \subset$

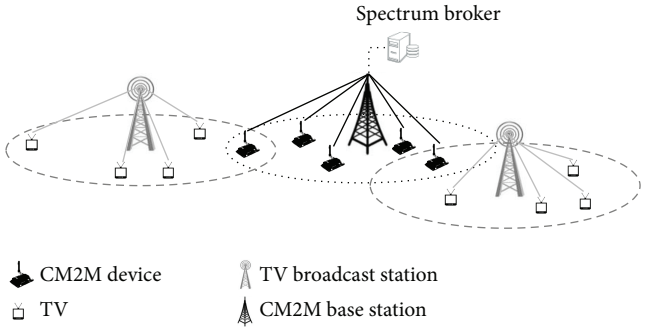

Figure 2: Architecture diagram of CM2M network operating in TVWS.

Φ, if CM2M devices are located outside the interference range of LUs; that is, $\overline{\Phi}_m = \{\phi_n \mid l_{n,m} \neq 0\}$.

The interference constraint matrix $\mathbf{C} = \{c_{n,k,m} \mid c_{n,k,m} \in \{0, 1\}\}_{N\times N\times M}$ is an $N \times N \times M$ binary matrix representing the interference constraint among CM2M devices, where $c_{n,k,m} = 1$ if ϕ_n and ϕ_k would interfere with each other on γ_m, and $c_{n,k,m} = 0$ otherwise. It should be noted that for $n = k$, $c_{n,n,m} = 1 - l_{n,m}$. Value of $c_{n,k,m}$ depends on the distance between ϕ_n and ϕ_k. Interference constraint also depends on γ_m as power and transmission rules vary greatly in different frequency bands. The bandwidth requirements of all CM2M devices are diverse because of different quality of service requirements for each device. We define $\mathscr{R} = \{r_n\}_{1\times N}$ as device requested bandwidth vector, where r_n represents bandwidth demand of ϕ_n.

In a dynamic environment, channels availability and interference constraint matrix both vary continually; in this study, we assume that spectrum availability is static or varies slowly in each scheduling time slot; that is, all matrices remain constant during the scheduling period. In our proposed solution, a subset of CM2M devices is scheduled during each time slot and the available spectrum is allocated among them without causing interference to LUs.

2.2. Spectrum Aggregation Model. In the traditional spectrum assignment, each channel is composed of a continuous spectrum fragment; thus it is not feasible for users to utilise small spectrum fragments which are smaller than the users bandwidth demand. For instance, assume a CM2M network where every machine requires 4 MHz channel bandwidth, and the available spectrum consists of two spectrum fragments of 4 MHz and four spectrum fragments of 2 MHz (Figure 3). For continuous spectrum allocation, the 2 MHz spectrum fragments cannot be utilised by any machine. Therefore, a continuous spectrum assignment mode can only support two devices for communication (2×4 MHz). However, spectrum aggregation-enabled device can exploit fragmented segments of the spectrum by using specialised air interface techniques, such as DOFDM. In Figure 3, if a number of small spectrum fragments are aggregated into a wider channel, then 16 MHz of unused spectrum is available to support four CM2M devices (4×4 MHz).

Due to the limited aggregation capabilities of the RF front-end, only channels that reside within a range of MAS can be aggregated. With this constraint, some spectrum fragments may not be aggregated because their span is larger than MAS. Our proposed algorithm takes MAS into consideration. For the sake of simplicity, we make following assumptions.

(1) All CM2M devices have the same aggregation capability (i.e., MAS for all devices is the same).

(2) Guard band between adjacent channels is neglected.

(3) Bandwidth requirement of each device and bandwidth of each channel are an integer multiple of subchannel bandwidth Δ, which is the smallest unit of bandwidth (in fact, the smaller fragments would demand excessive filtering to limit adjacent channel interference); that is,

$$\begin{aligned} r_n &= \omega_n \cdot \Delta, \quad \omega_n \in \mathbb{N},\ 1 \le n \le N, \\ \mathscr{BW}_m &= \kappa_m \cdot \Delta, \quad \kappa_m \in \mathbb{N},\ 1 \le m \le M, \end{aligned} \tag{1}$$

where $\mathbb{N}$ is the set of natural numbers, ω_n is the number of requested subchannels by ϕ_n, κ_m is the number of subchannels in γ_m, and $\mathscr{BW}_m$ is the bandwidth of γ_m.

The total available spectrum (i.e., M channels) is subdivided into multiple number of subchannels. If the available spectrum band consists of $\mathscr{C}$ subchannels (i.e., total available bandwidth is $\mathscr{C} \cdot \Delta$), then

$$\begin{aligned} \gamma_m &= \bigcup_{i=1}^{\kappa_m} \widetilde{\gamma}_{i,m}, \\ \kappa_m &= \frac{\mathscr{BW}_m}{\Delta}, \\ &\qquad \text{where } 1 \le m \le M, \\ \mathscr{C} &= \sum_{m=1}^{M} \kappa_m, \end{aligned} \tag{2}$$

where γ_m has κ_m subchannels and $\widetilde{\gamma}_{i,m}$ represents the ith subchannel of γ_m. Each $\widetilde{\gamma}_{i,m}$ can be represented in an interval defined as $[\mathscr{F}^L_{i,m}, \mathscr{F}^H_{i,m}]$, where $\mathscr{F}^L_{i,m}$ and $\mathscr{F}^H_{i,m}$ are the lowest and highest frequency of $\widetilde{\gamma}_{i,m}$:

$$\mathscr{F}^H_{i,m} - \mathscr{F}^L_{i,m} = \Delta, \quad \text{for } 1 \le i \le \kappa_m,\ 1 \le m \le M. \tag{3}$$

Based on this new subchannel indexing, matrices $\mathbf{L}$ and $\mathbf{C}$ can be rewritten as

$$\begin{aligned} \mathbf{L}^* &= \left\{ l^*_{n,\mathsf{c}} \mid l^*_{n,\mathsf{c}} = l_{n,m} \right\}_{N\times\mathscr{C}}, \\ \mathbf{C}^* &= \left\{ c^*_{n,k,\mathsf{c}} \mid c^*_{n,k,\mathsf{c}} = c_{n,k,m} \right\}_{N\times N\times\mathscr{C}} \end{aligned} \tag{4}$$

if

$$\begin{aligned} &1 \le \mathsf{c} \le \kappa_1 \quad \text{for } m = 1, \\ &\sum_{j=1}^{m-1} \kappa_j < \mathsf{c} \le \sum_{j=1}^{m} \kappa_j \quad \text{for } 1 < m \le M, \end{aligned} \tag{5}$$

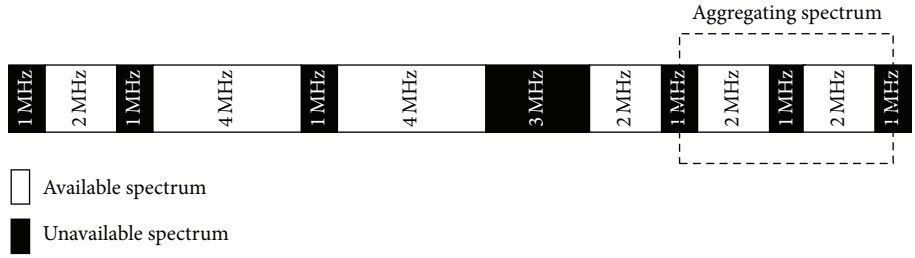

Figure 3: Aggregation of disjoint spectrum fragments.

where c represents index of each subchannel within the available spectrum.

The subchannel assignment matrix $\mathbf{A} = \{a_{n,\mathsf{c}} \mid a_{n,\mathsf{c}} \in \{0,1\}\}_{N\times\mathscr{C}}$ is an $N\times\mathscr{C}$ binary matrix representing subchannels assigned to CM2M devices for aggregation such that $a_{n,\mathsf{c}} = 1$ if and only if subchannel c is available to ϕ_n and 0 otherwise. We define the reward vector $\mathscr{B} = \{b_n = \Delta \cdot \sum_{\mathsf{c}}^{\mathscr{C}} a_{n,\mathsf{c}}\}_{N\times 1}$ to represent total bandwidth that is allocated to each CM2M device during scheduling time period for a given subchannel assignment.

3. Problem Formulation

3.1. Optimisation Problem. One of the key objectives of the deployment of CM2M network is to enhance the spectrum utilisation. To consider this crucial goal, we define network utilisation to maximise the total bandwidth that is assigned to CM2M devices and referred to as Maximising Sum of Reward (MSR):

$$\text{MSR} = \sum_{n=1}^{N} b_n. \tag{6}$$

To maximise MSR the spectrum aggregation problem can be defined as a constrained optimisation problem as follows:

$$\max_{a} \quad \sum_{n=1}^{N} b_n \tag{7}$$

$$\text{subject to} \quad b_n = \Delta \cdot \sum_{\mathsf{c}=1}^{\mathscr{C}} a_{n,\mathsf{c}} = \begin{cases} 0 & \text{if } \phi_n \text{ is rejected,} \\ r_n & \text{if } \phi_n \text{ is accepted.} \end{cases} \tag{8}$$

$$\text{for } 1 \le n \le N,$$

$$\mathscr{F}_{d,t}^{H} - \mathscr{F}_{e,f}^{L} \le \text{MAS}, \tag{9}$$

$$a_{n,\mathsf{c}} = 0 \quad \text{if } l_{n,\mathsf{c}}^{*} = 0, \text{ for } 1 \le n \le N,\ 1 \le \mathsf{c} \le \mathscr{C}, \tag{10}$$

$$a_{n,\mathsf{c}} \cdot a_{k,\mathsf{c}} = 0 \quad \text{if } c_{n,k,\mathsf{c}}^{*} = 1, \text{ for } 1 \le n,k \le N,\ 1 \le \mathsf{c} \le \mathscr{C}. \tag{11}$$

Expression (8) assures that rewarded bandwidth b_n to each accepted ϕ_n must be equal to ϕ_n's bandwidth demand r_n; if CM2M network cannot satisfy ϕ_n's bandwidth request, ϕ_n is rejected and $b_n = 0$. If $\mathscr{F}_{e,f}^{L}$ $(1 \le e \le \kappa_f$ and $1 \le f \le M)$ is the lowest frequency of an initial aggregated subchannel and $\mathscr{F}_{d,t}^{H}$ $(1 \le d \le \kappa_t$ and $1 \le \mathrm{t} \le M)$ is the highest frequency of a terminative subchannel, (9) guarantees that the range of allocated spectrum is equal to or less than MAS. **A** must satisfy the interference constraints (10) and (11); expressions (10) and (11) guarantee that there is no harmful interference to LUs and other CM2M devices, respectively.

3.2. Spectrum Aggregation Algorithm Based on Genetic Algorithm. Traditionally the spectrum assignment problem has been classified as an NP-hard problem [12]. Herein, GA is employed to solve the aggregation-based spectrum assignment problem in order to obtain faster convergence. GA is a stochastic search method that mimics the process of natural evolution. In addition, it is easy to encode solutions of spectrum assignment problem to chromosomes in GA and compare the fitness value of each solution. The specific operations of the proposed algorithm, referred to as MSR Algorithm (MSRA), can be described through the following steps.

(1) *Encoding.* In MSRA, a chromosome represents a possible conflict-free subchannel assignment. In order to decrease search space (by reducing redundancy in the data) and obtain faster solutions, similar approach as described in [12] is adopted in this article. We apply a mapping process between **A** and the chromosomes, based on the characteristics of $\mathbf{L}^*$ and $\mathbf{C}^*$. Only those elements of **A** are encoded whose corresponding elements in $\mathbf{L}^*$ take the value of 1; that is, $a_{n,\mathsf{c}} = 0$, where (n,c) satisfies $l_{n,\mathsf{c}}^{*} = 0$. As a result of this mapping, the chromosome length is equal to the number of nonzero elements of $\mathbf{L}^*$ and the search space is greatly reduced. Based on a given $\mathbf{L}^*$, length of the chromosome can be calculated as $\sum_{i=1}^{N}\sum_{j=1}^{\mathscr{C}} l_{i,j}^{*}$.

(2) *Initialisation.* During initialisation process, the initial population is randomly generated based on a binary coding mechanism as applied in [12]. The size of the population depends on $|\Phi|$ and $|\Gamma|$; for larger $|\Phi|$ and $|\Gamma|$, population size should be increased, where $|\cdot|$ indicates cardinality of a set.

(3) *Selection*. The fitness value of each individual of the current population according to MSRA criteria defined in (6) is computed. According to the individuals fitness value, excellent individuals are selected and remain in the next generation. The chromosome with largest fitness value replaces the one with a small fitness value by the selection process.

(4) *Genetic Operators*. To maintain high fitness values of all chromosomes in a successive population, the crossover and mutation operators are applied. Two randomly selected chromosomes are chosen in each iteration as the parents and the crossover of the parent chromosomes is carried out at probability of crossover rate. In addition to selection and crossover operations, mutation at certain mutation rate is performed to maintain genetic diversity.

(5) *Termination*. The stop criteria of GA are checked in each iteration. If they can not be satisfied, step (3) and step (4) are repeated. The number of maximum iterations and the difference of fitness value are used as the criteria to determine the termination of GA.

The population of chromosomes generated after initialisation, selection, crossover, and mutation may not satisfy the given constraints defined in (8)–(11). To find feasible chromosomes that satisfy all constraints, a constraint-free process is applied that has the following steps (in order).

(1) *Bandwidth Requirements*. The vector $\mathcal{B}$ as given in Section 2.2 is calculated. b_n should be equal to either r_n or zero; otherwise all genomes related to ϕ_n are changed to zero.

(2) *MAS*. To satisfy the hardware limitations of the transceiver, expression (9) should be satisfied; otherwise all genomes related to ϕ_n are changed to zero.

(3) *No Interference to LUs*. Expression (10) guarantees that CM2M devices transmissions do not interfere LUs transmissions, ensuring that CM2M network does not harm LUs performance. If expression (10) is not satisfied, all genomes related to ϕ_n are changed to zero.

(4) *CCI*. Expression (11) guarantees that there is no harmful interference to other CM2M devices. If expression (11) is not satisfied, one of two conflicted devices is chosen at random, and then all genomes of the selected device are changed to zero.

To achieve higher spectrum utilisation and faster convergence, after each generation, MSRA assigns all unassigned spectra to remaining CM2M devices randomly, whenever possible. At the same time, MSRA guarantees that all the constraints defined in (8)–(11) are satisfied at all time.

4. Simulation Results

In this section, a set of system-level performance results are presented in order to compare and show the efficiency of MSRA over MSA [10], AASAA [9], and RCAA. The simulation results demonstrate high potential of the proposed method in terms of spectrum utilisation and system capacity. To assess the performance of network, independent of each device's traffic distribution model, backlogged traffic model (known as full-buffer model) is used where packet queue length of every device is much longer than what can be scheduled during each scheduling time slot.

Table 1: Simulation parameters.

Parameter	Value
Δ	1 MHz
MAS	40 MHz
$\mathcal{BW}_m$	$\Delta \cdot U(1, 20)$
r_n	$\Delta \cdot U(1, 20)$
Total transmit power	26 dBm (400 mW)
Scheduling time slot	1 ms
Traffic model	Backlogged
Population size	20
Number of generations	10
Mutation rate	0.01
Crossover rate	0.8

Due to the random nature of the channel bandwidth and the devices bandwidth demand, Monte Carlo simulations are performed and each simulation scenario is repeated 100,000 times. The default parameters used in the simulations are listed in Table 1, where $U(1, 20)$ represents the discrete uniform random integer numbers between 1 and 20. Each of the channels is modeled as flat Rayleigh channel with path loss model of PL $= 128.1 + 37.6 \log_{10} R$ (R is in km) and penetration loss of 20 dB. The mean and standard deviation of log-normal fading are zero and 8 dB, respectively. In our simulation model, the CM2M devices located randomly without restrictions within a rectangular area of 2 km × 1 km. All channels are randomly selected between 54 MHz and 806 MHz television frequencies (channels 2–69). Typically, the number of M2M devices is very high in each cell, but in this study, because of high computational complexity of SOTA solutions, smaller number of M2M devices is considered for comparison purposes.

To investigate the simulation results effectively, the following terms are defined and used in our analysis.

(1) *Spectrum Utilisation*. It is referred to as $\mathcal{U}$ which is defined as the ratio of the sum of rewarded bandwidth to the sum of all available bandwidths; that is,

$$\mathcal{U} = \frac{\sum_{n=1}^{N} b_n}{\sum_{m=1}^{M} \mathcal{BW}_m}. \tag{12}$$

(2) *Network Load*. It is referred to as $\mathcal{L}$ which is defined as the ratio of the sum of all CM2M devices bandwidth requirements to the sum of all available bandwidths; that is,

$$\mathcal{L} = \frac{\sum_{n=1}^{N} r_n}{\sum_{m=1}^{M} \mathcal{BW}_m}. \tag{13}$$

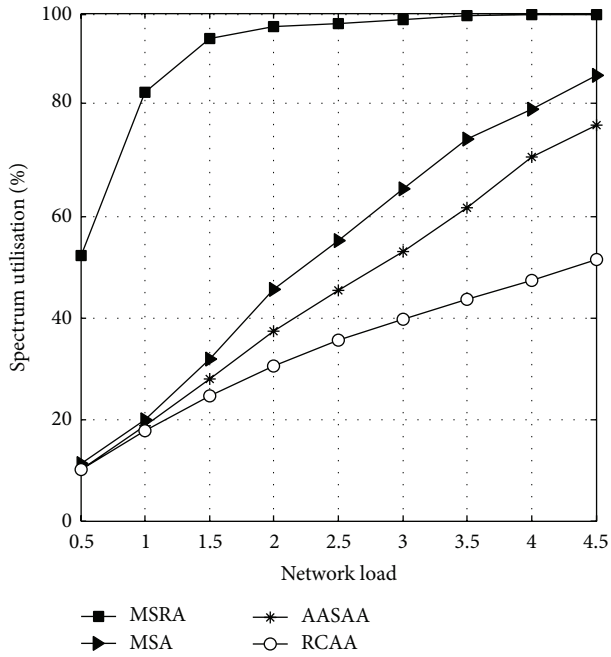

Figure 4: The impact of varying network load conditions on spectrum utilisation (scenario I: without CCI).

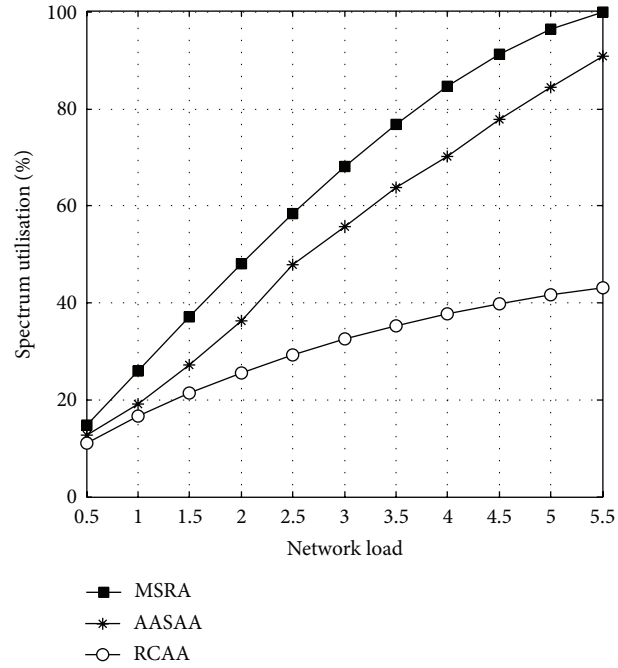

Figure 5: The impact of varying network load conditions on spectrum utilisation (scenario II: with CCI).

(3) *Number of Rejected Devices*. Rejected devices are those machines that are not assigned any spectrum in a certain scheduling time slot.

4.1. Scenario I: Without CCI. In this scenario, the performance of MSRA is compared with the SOTA algorithms including MSA [10], AASAA [9], and RCAA when CCI among CM2M devices is not considered. Therefore, we assume that CM2M devices transmissions do not overlap with the transmission of other CM2M devices using the same channel.

For $M = 30$, $\mathscr{L}$ increases by increasing the number of CM2M devices from 5 to 60. Figure 4 shows that when the number of CM2M devices increases, the spectrum utilisation also increases in all three methods, but MSRA utilises all available whitespaces in various network loading conditions more efficiently than MSA, AASAA, and RCAA. This can be explained by the fact that, in case of higher $\mathscr{L}$, network can allocate better segments of spectrum to users because of higher multiuser diversity. In addition, because of using stochastic search method, MSRA achieves near to optimum solution in comparison to other SOTA solutions which are based on approximate algorithms. For MSRA, when $\mathscr{L}$ is higher than 3, CM2M network becomes saturated due to the lack of available spectrum. However, for the rest of the methods, there are still unassigned spectrum slices.

4.2. Scenario II: With CCI. In this scenario, CCI exists among CM2M devices and we compare our algorithm, MSRA, with AASAA and RCAA. As MSA inherently does not consider CCI, for that reason, we do not include MSA for comparison. Figure 5 shows the spectrum utilisation, according to different network loads by increasing the number of CM2M devices from 5 to 55 when there are only seven available channels (i.e., $M = 7$). As shown in Figure 5, MSRA outperforms AASAA and RCAA for different network loads. Similar to Scenario I, MSRA utilises TVWS even better than previous scenario, because some CM2M devices in network may reuse spectrum that is used by other devices in CM2M network.

Figure 6 represents the number of rejected CM2M devices when the network load increases. The number of rejected CM2M devices increases with the network load; MSRA has fewer numbers of rejected CM2M devices (or more satisfied devices) than AASAA and RCAA of different network loads. MSRA optimises spectrum utilisation by admitting devices with better channel quality to the network and allocates the spectrum resources effectively. Furthermore, MSRA does not assign any spectrum resources to the devices that has least contribution to overall network throughput. Figure 6 implies that MSRA increases the capacity of network (which is very vital for M2M networks because of a very large number of devices). Our approach may starve some of devices which are located far from the base station; in our future work, we will optimise network performance based on proportional fairness objective function to guarantee the fairness among devices.

4.3. Convergence of MSRA. Because of the nature of genetic programming, it is arguably impossible to make formal guarantees about the number of fitness evaluations needed for an algorithm to find an optimal solution. However, herein, computer experiments are performed to show the impact of

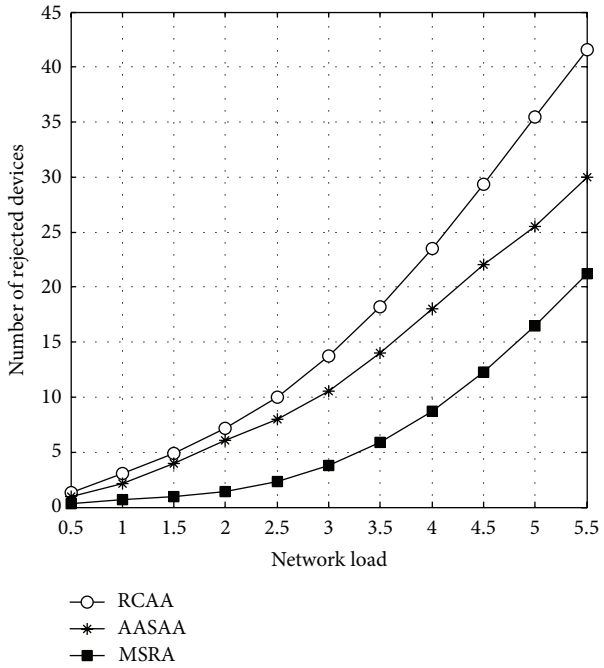

Figure 6: The impact of varying network load conditions on the number of rejected CM2M devices (scenario II: with CCI).

Table 2: System parameters.

Parameter	Value
M	10
N	200
Processor	Intel Core i7-3667U 2.00 GHz
Memory (RAM)	4 GB
OS	Windows 7 (64-bit)
Simulator	MATLAB R2011a (64-bit)

the number of generations on the performance of MSRA. The system parameters used in the section for simulation are listed in Table 2. For the purpose of convergence studies, we assume $N = 200$ and $M = 10$.

Figure 7 shows the best fitness value (MSRA) for a population in a different number of generations. As shown in Figure 7, the performance of algorithm is enhanced, when the number of generations increases; however this is at the cost of increased processing time. After roughly 34 generations, the fitness value saturates at optimal value which shows the effectiveness of using GA for spectrum assignment using spectrum aggregation.

Moreover, Figure 8 illustrates distribution of processing time for MSRA to find an optimal solution. As shown in Figure 8, at 85% of time, MSRA finds an optimum solution in less than scheduling time slot (1 ms) and 15% takes more than scheduling time slot. Additionally, MSRA can be optimised to use fewer processor resources, so that it can execute more rapidly.

Furthermore, Lobo et al. [15] provided a theoretical and empirical analysis of the time complexity of traditional

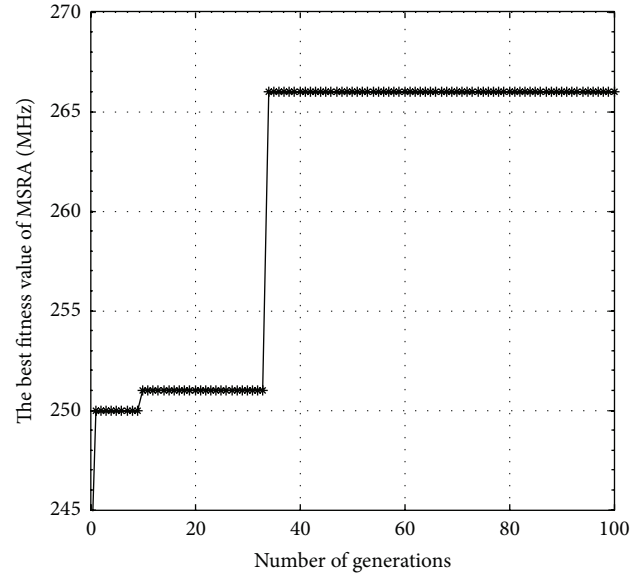

Figure 7: The impact of the number of generations on MSRA results.

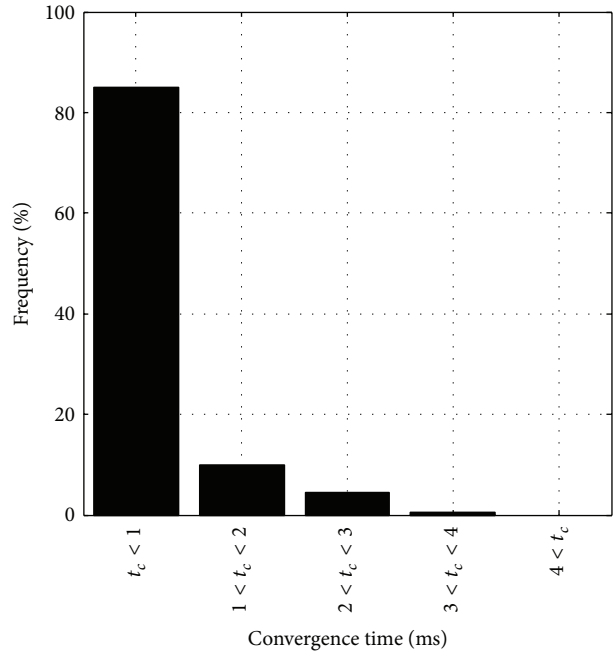

Figure 8: Distribution of processing time for MSRA to find an optimal solution.

simple GAs. According to [15], GA has time complexities of $\mathcal{O}(\sum_{i=1}^{N} \sum_{j=1}^{\mathscr{C}} l_{i,j}^{*})$ which is dependent on length of each chromosome. The linear time complexity for GA occurs because the population sizing grows with the square root of chromosome length. The time complexity presented herein is for the worst-case scenario when the population size is assumed to be fixed and maximum of rest of generations.

5. Conclusion

This article introduces an aggregation-aware spectrum assignment algorithm using genetic algorithm. The proposed algorithm maximises the spectrum utilisation to CM2M devices as a criterion to realise spectrum assignment. Moreover, the introduced algorithm takes into account the realistic constraints of co-channel interference and Maximum Aggregation Span. Performance of the proposed algorithm is validated by simulations and results are compared with algorithms available in the literature. The proposed algorithm decreases the number of rejected devices and improves the spectrum utilisation of CM2M network. Our algorithm increases the capacity of network which is very vital for M2M networks. For future work, we will investigate the impact of the various parameters used in genetic algorithm to solve the introduced utilisation function; in particular, population size, crossover rate, and mutation rate are the parameters that will be investigated in our study; in addition, we will further work on developing genetic algorithm based method to assign spectrum to CM2M devices in an energy-efficient manner.

Competing Interests

The authors declare that they have no competing interests.

References

[1] R. Lu, X. Li, X. Liang, X. Shen, and X. Lin, "GRS: the green, reliability, and security of emerging machine to machine communications," *IEEE Communications Magazine*, vol. 49, no. 4, pp. 28–35, 2011.

[2] "Cisco visual networking index: Global mobile data traffic forecast update 2014–2019 white paper," 2015, http://www.cisco.com/c/en/us/solutions/collateral/service-provider/visual-networking-index-vni/mobile-white-paper-c11-520862.html.

[3] S. Rostami, K. Arshad, and K. Moessner, "Order-statistic based spectrum sensing for cognitive radio," *IEEE Communications Letters*, vol. 16, no. 5, pp. 592–595, 2012.

[4] Y. Zhang, R. Yu, M. Nekovee, Y. Liu, S. Xie, and S. Gjessing, "Cognitive machine-to-machine communications: visions and potentials for the smart grid," *IEEE Network*, vol. 26, no. 3, pp. 6–13, 2012.

[5] M. Wylie-Green, "Dynamic spectrum sensing by multiband OFDM radio for interference mitigation," in *Proceedings of the 1st IEEE International Symposium on New Frontiers in Dynamic Spectrum Access Networks (DySPAN '05)*, pp. 619–625, IEEE, Baltimore, Md, USA, November 2005.

[6] J. D. Poston and W. D. Horne, "Discontiguous OFDM considerations for dynamic spectrum access in idle TV channels," in *Proceedings of the 1st IEEE International Symposium on New Frontiers in Dynamic Spectrum Access Networks (DySPAN '05)*, pp. 607–610, Baltimore, Md, USA, November 2005.

[7] R. Rajbanshi, A. M. Wyglinski, and G. J. Minden, "An efficient implementation of NC-OFDM transceivers for cognitive radios," in *Proceedings of the 1st International Conference on Cognitive Radio Oriented Wireless Networks and Communications (CROWNCOM '06)*, pp. 1–5, Mykonos Island, Greece, June 2006.

[8] 3GPP, "LTE; evolved universal terrestrial radio access (e-utra); physical layer procedures," Tech. Rep. 3GPP TS 36.213 version 10.1.0 Release 10, 3GPP, 2010, http://www.3gpp.org.

[9] D. Chen, Q. Zhang, and W. Jia, "Aggregation aware spectrum assignment in cognitive ad-hoc networks," in *Proceedings of the 3rd International Conference on Cognitive Radio Oriented Wireless Networks and Communications (CrownCom '08)*, pp. 1–6, May 2008.

[10] F. Huang, W. Wang, H. Luo, G. Yu, and Z. Zhang, "Prediction-based Spectrum aggregation with hardware limitation in cognitive radio networks," in *Proceedings of the IEEE 71st Vehicular Technology Conference (VTC '10)*, pp. 1–5, May 2010.

[11] F. Ye, R. Yang, and Y. Li, "Genetic algorithm based spectrum assignment model in cognitive radio networks," in *Proceedings of the 2nd International Conference on Information Engineering and Computer Science (ICIECS '10)*, pp. 1–4, Wuhan, China, December 2010.

[12] Z. Zhao, Z. Peng, S. Zheng, and J. Shang, "Cognitive radio spectrum allocation using evolutionary algorithms," *IEEE Transactions on Wireless Communications*, vol. 8, no. 9, pp. 4421–4425, 2009.

[13] K. Arshad, M. A. Imran, and K. Moessner, "Collaborative spectrum sensing optimisation algorithms for cognitive radio networks," *International Journal of Digital Multimedia Broadcasting*, vol. 2010, Article ID 424036, 20 pages, 2010.

[14] Y. Li, L. Zhao, C. Wang, A. Daneshmand, and Q. Hu, "Aggregation-based spectrum allocation algorithm in cognitive radio networks," in *Proceedings of the IEEE Network Operations and Management Symposium (NOMS '12)*, pp. 506–509, IEEE, Maui, Hawaii, USA, April 2012.

[15] F. G. Lobo, D. E. Goldberg, and M. Pelikan, "Time complexity of genetic algorithms on exponentially scaled problems," in *Proceedings of the Genetic and Evolutionary Computation Conference (GECCO '00)*, pp. 151–158, Morgan-Kaufmann, 2000.

Hindawi Publishing Corporation
Mobile Information Systems
Volume 2016, Article ID 3234618, 11 pages
http://dx.doi.org/10.1155/2016/3234618

Research Article

A Survey of the DVB-T Spectrum: Opportunities for Cognitive Mobile Users

László Csurgai-Horváth, István Rieger, and József Kertész

Department of Broadband Infocommunications and Electromagnetic Theory, Budapest University of Technology and Economics, Egry J. Street 18, Budapest 1111, Hungary

Correspondence should be addressed to László Csurgai-Horváth; csurgai@hvt.bme.hu

Received 18 February 2016; Revised 30 May 2016; Accepted 5 July 2016

Academic Editor: Janne Lehtomäki

Cognitive radio (CR) systems are designed to utilize the available radio spectrum in an efficient and intelligent manner. Terrestrial Digital Video Broadcasting (DVB-T) frequency bands are one of the future candidates for cognitive radio applications especially because after digital television transition the TV white spaces (TVWS) became available for radio communication. This paper deals with the survey of the DVB-T spectrum; wideband measurements were performed on mobile platform in order to study the variation of the radio signal power in city area aboard a moving vehicle. The measurement environment was a densely built-in region where the proper DVB-T receiving was guaranteed by three TV transmitters, utilizing three central channel frequencies using 610, 746, and 770 MHz. In our paper the methods, the applied antenna, and measurement devices will be presented together with simulated and measured fading statistics. The final result is an estimation of the cognitive DVB-T spectrum utilization opportunity; furthermore a scenario is also proposed for secondary channel usage.

1. Introduction

Cognitive radio is an emerging technology to utilize the radio spectrum with high efficiency. The main owners of the spectrum, the primary users (PUs), are not constrained during their operation, while the secondary users (SUs) can operate in the same frequency band if the spectrum is free [1]. It is very important to avoid the degrading of PU's quality of service (QoS) during the cognitive channel usage whereas an acceptable level of service should also be provided for the secondary users. Several technologies should be applied to guarantee these—sometimes contradictory—requirements [2]. Sensing of the spectrum and detecting the available channels are some of the main tasks of a CR system. The frequency range that can be utilized by the CR devices depends on the local frequency regulation and therefore it may vary in different countries. In the crowded radio spectrum it is not a simple task to find the appropriate radio bands for cognitive terrestrial devices [3, 4]. This paper concentrates on the terrestrial television bands and their secondary usage.

In the literature, numerous works are presented about spectrum measurements and on different technologies to support cognitive users in better utilization of the available bandwidth. TV white space is also of a great interest due to the digital TV transition that recently took place in several countries. In the following an overview of this research field will be given in order to put our research into context.

In [5], despite the actual theory that the capacity of the radio spectrum is already achieved, the underutilization of the spectrum is highlighted and the importance of cognitive radio techniques is shown. The paper is focusing on major technologies for opportunistic spectrum access through a hierarchical model approach that adopts the primary and secondary user structure. Spectrum sensing is the key technology to estimating the availability of the licensed spectrum for secondary usage. In [6], the various spectrum occupancy models used in different research campaigns worldwide were studied and compared. The authors evaluate the percentage of the whole spectrum occupied by different services. Long- and short-term statistics are presented, showing most of the commercial terrestrial frequency bands (GSM, TV broadcasting, 3G, etc.), utilizing the available spectrum almost below 20–40%. The experiments have been conducted in various locations such as US, Europe, New Zealand, South

Africa, China, Singapore, and Vietnam. A similar study was performed in Chicago, New York, Washington, DC, and a few rural locations in 2005 between 30 and 3000 MHz [7]. In a large business like Chicago, low spectrum occupancy was observed indicating that a DSS (Dynamic Spectrum Sharing) radio system could access a huge amount of prime spectrum as there are large, unoccupied, contiguous spectrum blocks. The paper [8] collects previous research work carried out worldwide and compares it with spectrum occupancy measurements at the University of Hull, UK. The collected historical measurements are covering also the 30–3000 MHz band and they confirmed the generally low occupancy of the investigated spectrum. The measurements in the UK were performed with a similar hardware configuration to what we also applied during our research work and will be detailed later (spectrum analyser and computer); the frequency range was 80–2700 MHz. For DVB-T spectrum measurements in [9], several results can be found especially for occupancy estimations serving as input for outdoor REM (Radio Environment Maps). The measurement setup was similar to the campaign performed in Budapest, but the latter research is focusing also on fade duration statistics and its consequences as it will be later demonstrated. The cellular and the UHF/VHF TV band were studied in [10] for Malaysia and actual spectrum utilization statistics are provided with static measurements. The low duty cycle of the spectrum occupancy was also proved by this study. A comparative spectrum occupancy study was carried out in Barcelona, Spain, and Poznan, Poland [11]. The measurement setups were harmonized to obtain comparable results by concentrating on the problem of the efficient noise floor estimation. As a result, differences have been obtained in the TETRA bands due to the different spectrum allocation regulations in these countries. This study highlights that efficient spectrum detection is always required in order to avoid the congestions due to different local regulatory rules. The change of the UHF TV band spectrum availability due to digital transition in Greece is studied in [12]. They proved that the spectrum availability was significantly increased after the analogue switch-off. Furthermore, the risk of LTE-4G interference to TV services and vice versa is also pointed out according to the spectrum measurements they carried out. A general and detailed discussion on different approaches to spectrum occupancy measurements is provided in the relating ITU report SM.2256 [13]. Unlicensed communication in the UHF band has also a great actuality. Measurements in Italy, Spain, and Romania are presented in [14, 15] in order to estimate practical parameters to ensure the feasible and harmless unlicensed communication in the UHF TV bands. Special devices like wireless microphones may also utilize this band under strict regulatory control [16], that is, also increasing the importance of accurate spectrum sensing methods.

In the present paper we demonstrate mobile measurements in the DVB-T spectrum by concentrating on the occupancy statistics that can be inferred from the channel fading dynamics. We significantly extended our former paper [17] with technical details and additional measurement route; furthermore results and conclusions are amended.

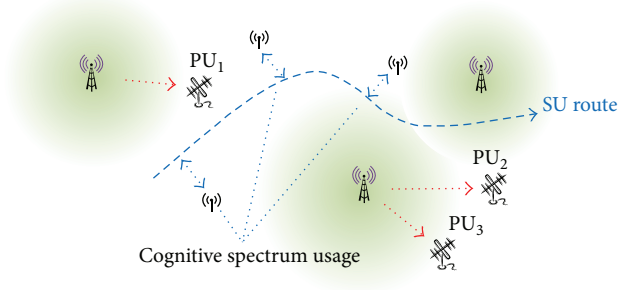

Figure 1: Fixed PUs and a moving SU for smart DVB-T spectrum utilization.

DVB-T users are the primary owners of the television receivers [18, 19]. In large cities, like Budapest, where we conducted our measurements, the sufficient service requires several multiplexed channels and usually more than one transmit station. DVB-T receivers are the primary users of this spectrum and the service provider takes care of the sufficient quality of service at the whole geographical region [20]. Nevertheless, in densely built-in areas and especially in case of hilly areas the received signal level could be locally insufficient to receive the DVB-T signal properly. In this case by applying smart spectrum sensing technologies a secondary, mobile user has an opportunity to utilize this spectrum for different kind of short-distance communications, like accessing locally transmitted traffic information and car-to-car communications, or for general type of data transfer. A hypothetical scenario is depicted in Figure 1.

Therefore our main goal during this survey was to investigate the frequency band of the terrestrial digital television broadcasting between 400 and 900 MHz to have an overview of the possibilities for mobile CR applications [21]. In order to achieve this goal the appropriate measurement devices had to be selected and also designed if off-the-shelf equipment was not available. The air interface was a custom designed wide band discone antenna. For sensing the radio spectrum, a handheld spectrum analyser was applied. As the measurement campaign was planned for mobile measurements aboard a vehicle, an appropriate and safe mechanical setup was needed. The route and the speed of movement were recorded by a GPS-based navigation system.

The main target of this research was twofold: primarily received power time series was recorded in a wide DVB-T band while a vehicle was moving in city area. Secondly, by processing the measured data, first- and second-order statistics were derived allowing inferring the CR opportunities in this band.

2. Measurement Location and Modelling

In the time of the measurements (12/2013 and 03/2014) in Budapest three DVB-T transmitters were operating. Each of them has multiplex channels with the standard 8 MHz bandwidth providing the sufficient receiving conditions over the whole city. It is worthy of note that in the majority of the

Table 1: DVB-T transmitters in Budapest.

	UHF channels [MHz]			Max. ERP [kW/dBm]		
CH	Starting	Centre	Ending	Széchenyi Hill [1]	Hármashatár Hill [2]	Száva Street [3]
38	606	610	614	100/80	9,5/69,8	6,2/67,9
55	742	746	750	39,8/76	9,8/70	7,1/68,5
58	766	770	774	100/80	7,4/68,7	5,6/67,5
	Location Lat./Lon./ASL			47°29′/18°58′/457 m	47°33′/19°00/443 m	47°28′/19°07′/120 m

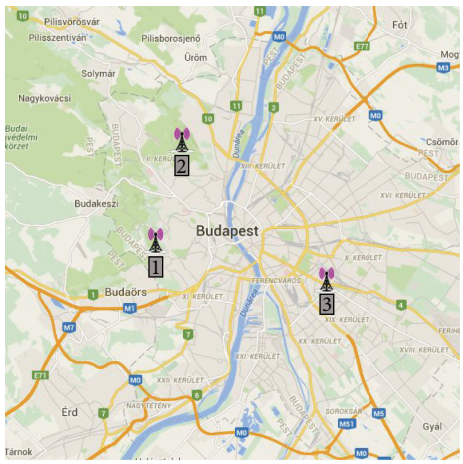

Figure 2: DVB-T transmitters in Budapest *(map source: Google)*.

European countries the transition from analogue to digital TV broadcasting technologies was finished (see, for example, [22]), and there are only a few countries where this is still an ongoing process.

In Table 1 the main transmitter parameters can be found for Budapest.

The transmitter locations are depicted in the map shown in Figure 2, denoted with [1], [2], and [3] signs. It is worth mentioning that the left side of the city is hilly while the right side is flat; however transmitter [3] can be found on elevated location. The arrangement of the transmitters and their power radiated ensure the location-independent receiving despite the geographical variability.

For a first and rough estimation of the received signal power at the different geographical positions the Okumura-Hata channel model [23] was selected to illustrate the capabilities and limitations of such calculations. This model is valid for 150–1500 MHz frequency range; therefore it is well applicable for DVB-T. It is an empirical model suitable to calculate the path loss L_U for different urban areas. The h_T height of the transmit antenna and the h_R receiver antenna height are also input parameters of the model:

$$L_U = 69.55 + 26.16 \log_{10} f^{[\mathrm{MHz}]} - 13.82 \log_{10} h_T - C_H + \left[44.9 - 6.55 \log_{10} h_T\right] \log_{10} D^{[\mathrm{km}]}. \quad (1)$$

C_H is the antenna height coefficient and it is for small and medium cities:

$$C_H = 0.8 + \left(1.1 \log_{10} f^{[\mathrm{MHz}]} - 0.7\right) h_R - 1.56 \log_{10} f^{[\mathrm{MHz}]}, \quad (2)$$

and for big cities,

$$C_H = \begin{cases} 8.29 \log_{10} \left(1.54 h_R\right)^2 - 1.1, & 150 \le f^{[\mathrm{MHz}]} \le 200 \\ 3.2 \log_{10} \left(11.75 h_R\right)^2 - 4.97, & 200 \le f^{[\mathrm{MHz}]} \le 1500. \end{cases} \quad (3)$$

The model has limitations in range (1–20 km) and transmitter antenna height (30–200 m). By taking into account that the sea level height of the city (river floor) is 90 m, the model could be applied for a rough estimation of the received signal level. In the following this calculation is presented, where we considered big city model coefficients and provide received signal power map for each transmitter frequency.

To calculate with the Okumura-Hata model, we positioned three transmitters into a hypothetical square of 20 ∗ 20 km; the origin of this area was N47°25′ and E18°54′. The positions of the transmitters are representing their real geographical places relatively to this origin. The gain of the transmitter antennas was selected uniformly 15 dB and the receiver location was 3 m, respectively. The result is depicted in Figure 3, where the transmitters are numbered according to Table 1.

The modelled signal level in the rectangular area visualizes the received power at different locations produced by the DVB-T transmitters. Besides the Okumura-Hata model, the Walfisch-Ikegami and the Lee models are compared and tested for different geographical areas in [24]. In this paper, the goal of the modelling was to get a quantitative overview of the received signal power field and therefore we selected for our calculations one of the best known models.

Nevertheless, the effect of the local variation of the environment, for example, shadowing of buildings, reflections, and local interferences, is not visible in Figure 3. In order to generate a more accurate power map, a detailed geolocation map would be required, containing an exact database of the object positions and dimensions across the city, but such a database was not available for the authors.

The lack of the fine structure and the variation of the signal level on a specific route require a different approach. The description of this method and its conclusions is the following subject of this paper.

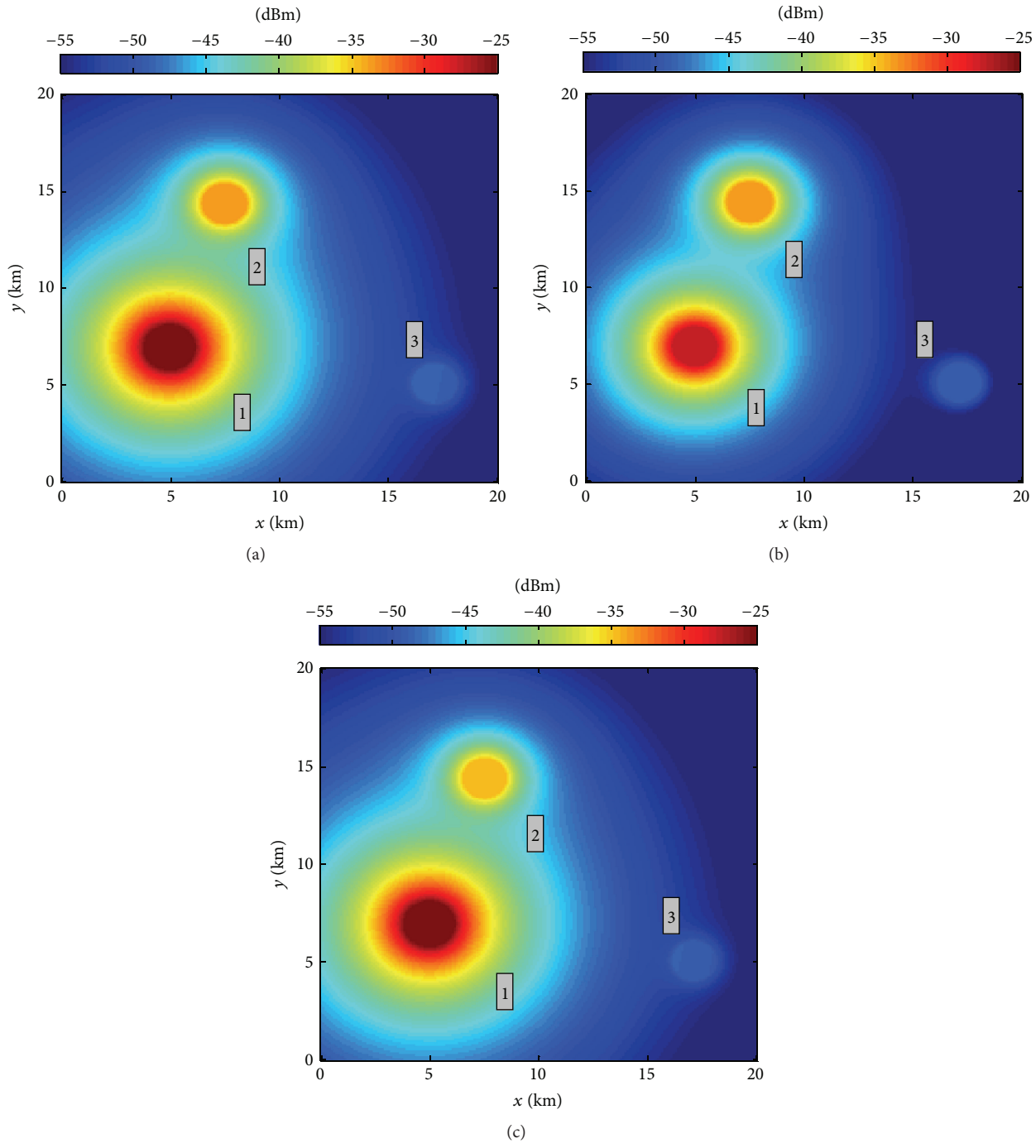

Figure 3: DVB-T signal power at 610 MHz (a), 746 MHz (b), and 770 MHz (c), calculated with Okumura-Hata model.

3. Receiver Antenna Design for Spectrum Sensing

Our goal was to build an all-purpose system that is capable of wide range spectral observations between 0.4 and 3 GHz. In [25] for a similar measurement a commercially available 25–1300 MHz antenna was proposed, but for our purposes we selected a customized antenna that has a broader bandwidth. Therefore a special wideband antenna was designed [26] at our department whose omnidirectional characteristic was one of the most important requests (see Figure 4).

The requirements are well fulfilled by a discone antenna that consists of a flat disc on the top of a conical part. Within this structure, the wideband operation is mainly determined by the conical structure. The drawing and final dimensions of the antenna can be found in Figure 4. Before antenna fabrication, computer simulations were done in order to prove the performance and check the main parameters.

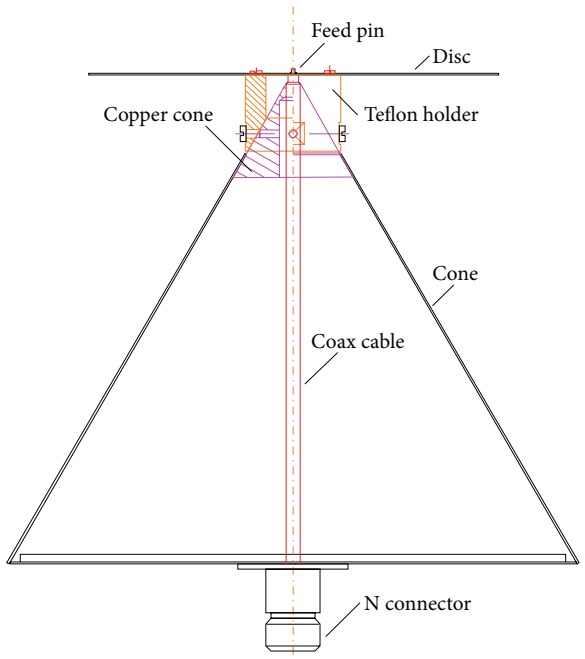

Main antenna dimensions:	
Cone max. diameter:	210 mm
Cone angle:	60°
Disc diameter:	150 mm
Total height (w/o connector):	180 mm

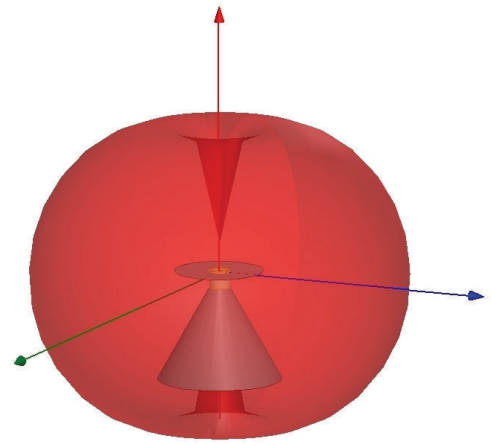

Figure 4: Antenna dimensions and simulated characteristics at 746 MHz.

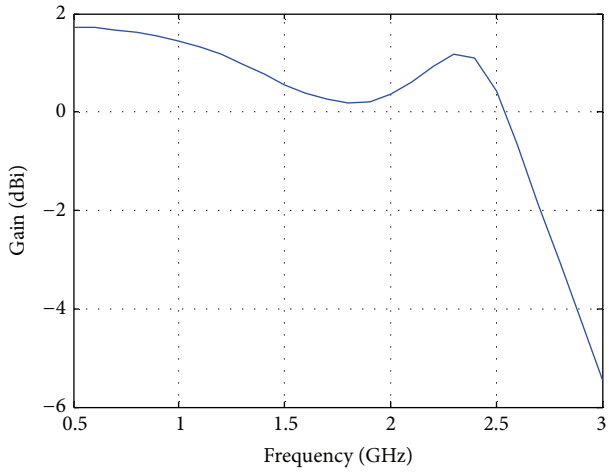

Figure 5: Simulated antenna gain and a two-channel measurement setup.

The simulated antenna of a characteristic at 746 MHz is depicted in Figure 4 while variation of the gain with frequency is depicted in Figure 5. The latter figure also illustrates a two-antenna system assembled on the top of a car, ready for mobile measurements. The gain of the antenna is slightly varying with the frequency and according to the simulation it is nearly 2 dB in the investigated DVB-T frequency band.

4. Mobile Sensing of the DVB-T Spectrum

Spectrum sensing is a secondary user's task when his operation is based on CR technology. SUs should discover usually a wide frequency band before they can utilize any spectra. This is an indispensable process, because the main owners of the spectrum, the Pus, cannot be disturbed or restricted in their operation. The air interface of this kind of sensing is usually a wideband and omnidirectional antenna. Wideband sensing requires intelligent, programmable received signal detection that allows scanning the selected frequency range and performing fast energy detection at the single frequencies. During our work we applied professional measurement devices for similar purposes in order to explore the DVB-T spectrum in a larger geographical area. The measurement could be a base to qualify the DVB-T spectrum for mobile cognitive radio applications.

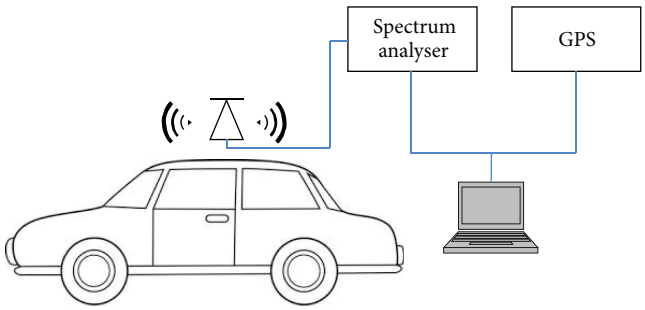

Figure 6: Mobile spectrum measurement setup.

This section provides the detailed measurement setup for our experiments, and then time series and different statistics will be presented.

In Section 2 we have seen that the modelled received signal map, especially in absence of a geolocation database of terrestrial objects, cannot provide sufficient information about the local variability of the signal level. In order to investigate the exact time series of the DVB-T signal power aboard a moving vehicle a measurement with location-tagging was designed and conducted. As spectrum sensing device, a type of Agilent N9340B Handheld RF spectrum analyser was utilized. For our research purposes, the flexibility and precision of such a measurement tool were an obvious solution. The investigated frequency band is supported by the applied device [27], and its built-in memory was able to store the measurement data through the whole route.

The measurement setup for the mobile system is depicted in Figure 6 and it has the following main blocks:

(i) A car equipped with a single discone antenna (see Section 3).

(ii) A GPS device to record the route and the moving speed (Mitac P560 PDA).

(iii) A portable spectrum analyser [27] with data storage capability (Agilent N9340B).

(iv) A notebook to archive measurement files.

To have a first look of the measured data, a waterfall diagram is a good opportunity (see Figure 8), depicting the received signal power in the complete frequency band for the total measurement period.

In order to survey the DVB-T frequency band during movement, two measurements were conducted in the city area of Budapest. The routes are depicted in Figure 7, also denoting their length and duration.

In order to cover the whole frequency band of the TV transmitters, the following spectrum analyser settings were applied:

(i) Starting frequency: 590 MHz.

(ii) Stop frequency: 800 MHz.

(iii) Span: 210 MHz.

(iv) Span time: 2 sec.

(v) Attenuation: 10 dB.

(vi) Bandwidth: 100 kHz.

(vii) Reference noise power: −109 dBm.

10 dB attenuation was required to keep the measured signal level within the analyser measurement range. The 590–800 MHz frequency band was sensed with 10/22 MHz steps; thus, for example, for a 8 MHz DVB-T channel, 17.6 samples were collected. The spectrum analyser stores the measured received power in floating point data type with two decimal places. The antenna was connected with RG-58 type cable of 3 m length; therefore the cable attenuation was 0.9 dB.

TV transmitters $\boxed{1}$ and $\boxed{3}$ were closed by the routes (their places are marked on the maps). The speed of the car was slightly varying, but it was kept during the route as stable as possible.

After processing the measurements, the spectrogram and the time series of the received power for three TV channels are providing the first overview of the investigated spectrum. In the spectrogram and even more clearly in the received power time series, the strong variations of the signal levels are well observable (Figures 8-9).

The results are indicating that the conditions of proper DVB-T receiving do not always exist. As the measurement was performed in densely built-in city area and we considered the movement of the car, different type of channel impairments may arise. The shadowing, interference, and multipath propagation could decrease the quality of service. However the Okumura-Hata propagation model is a well-known tool to calculate the received signal level in built-in areas [28, 29]; this is a general model and cannot substitute the real measurements like the present one, allowing deriving a more accurate characterization of the mobile propagation channel. For proper DVB-T, receiving primary users require 50 dBμV signal level, or considering a 50 Ω termination from (4), this level is −57 dBm [30]:

$$\begin{aligned} \mathrm{RP}_{\mathrm{min}}{}^{\mathrm{dBm}} &= \mathrm{RP}_{\mathrm{min}}{}^{\mathrm{dB}\mu\mathrm{V}} - 90 - 20\log\left(\sqrt{Z^{\Omega}}\right) \\ &= -57\ \mathrm{dBm}. \end{aligned} \tag{4}$$

More detailed discussion about the planning of DVB-T service area and the minimum field strength requirements can be found in [31].

We will apply this threshold as an opportunity indicator for secondary channel usage. On the other hand, it should be also considered that, in order to minimise the harmful interference caused by the cognitive secondary user devices, the TV signal sensing margin should be much lower than that of TV receivers required for high quality receiving [32]. The hidden node problem, when a primary user with good receiving conditions is interfered by a secondary transmitting device [33], is one of the reasons that cognitive devices are usually operating with lower sensing margin. Nevertheless, this kind of problem is beyond the scope of this paper; the abovementioned −57 dBm will be for us the measure of the local DVB-T signal quality. As the goal of this paper is a survey of the TVWS, the investigation of some statistical properties of the received signal time series will lead to the estimation of the secondary channel utilization

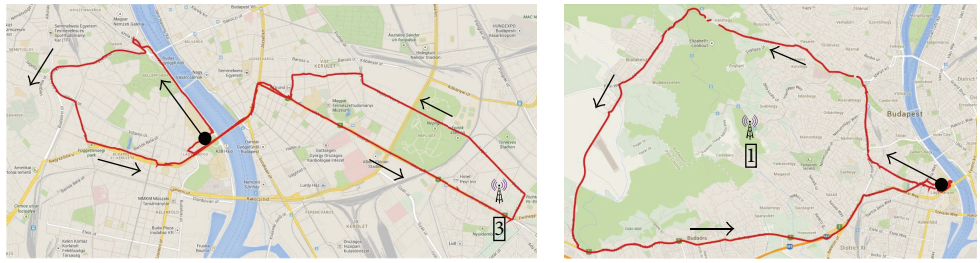

(a) (b)

Figure 7: (a) Route 1 (22.9 km, 58 min, 12/2013). (b) Route 2 (34.9 km, 58.8 min, 03/2014) *(map sources: Google).*

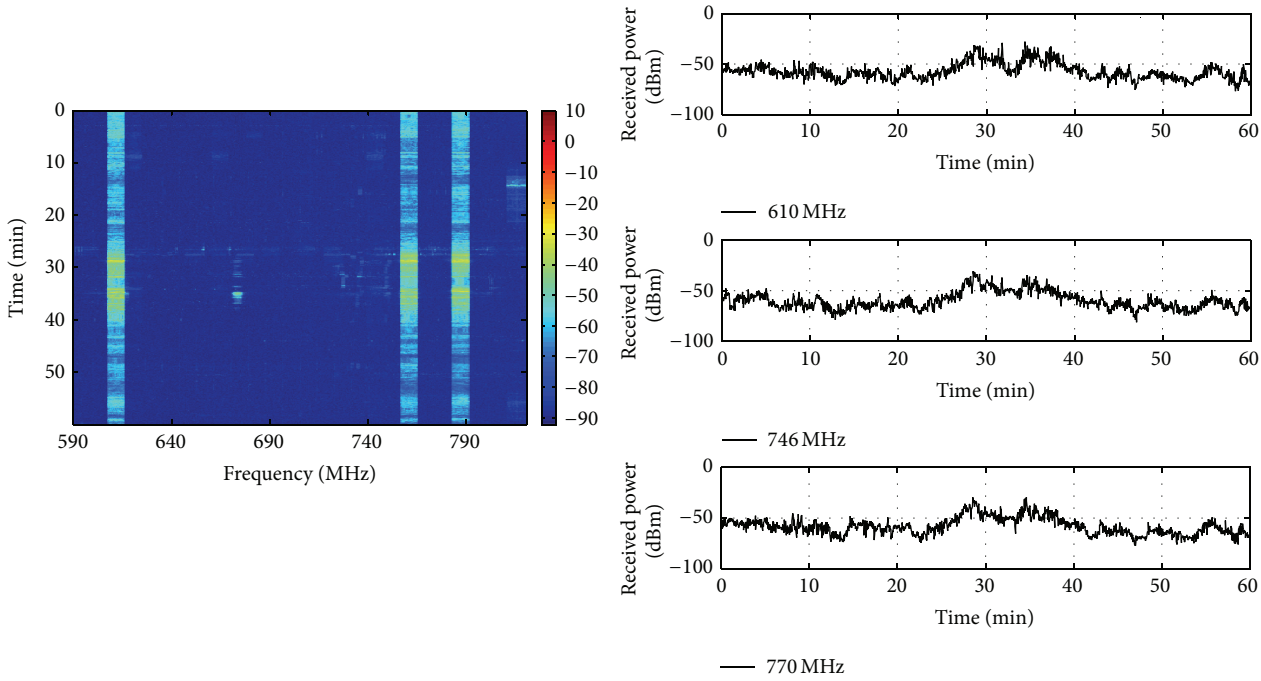

Figure 8: Spectrogram and received power time series at TV channel centre frequencies (Route 1).

opportunities. We emphasize that for an operational cognitive radio application a lower sensing margin should be required. Furthermore, especially to avoid the interference additional techniques would be also desirable, for example, pilot detection, cyclostationary feature detection, or cyclic prefix and autocorrelation detection [32].

To find the probability of the minimal received signal level, the Cumulative Distribution Function (CDF) of the attenuation could help. To estimate a realistic receiving condition, an increased antenna gain should be applied, because the discone antenna is only an experimental device and it does not represent correctly the antenna of a standard DVB-T receiver. The applied discone antenna has ~2 dB gain; nevertheless for real DVB-T receiving an antenna with 10–12 dB gain is recommended [34] and usually applied by PUs.

The CDF of the received power indicates the probability that the signal level is less than or equal to a certain value, as it is depicted in Figure 10 for the two different routes. If we take into account that a standard PU has a receiving antenna with an additional 10 dB gain compared to the discone antenna in the measurement, according to (4) the probability values at $-57 - 10 = -67$ dB are representing the thresholds of the improper receiving conditions.

One can see that the probability of insufficient DVB-T signal level is relatively high; in Figure 10 these values are indicated for each channel. Contrarily, in case of this condition the spectrum could be utilized by the secondary users for their own purposes by applying CR technologies.

Another aspect of the estimation of the channel impairment is the fade duration statistics [35]. While the attenuation statistics inform us about the probability that the fading depth exceeds a specified level, the length of the individual fade events and thus the possible outage periods could be determined only from the fade duration distribution. The duration of fades can be calculated from the attenuation time series; therefore the received power time series (see Figures 8

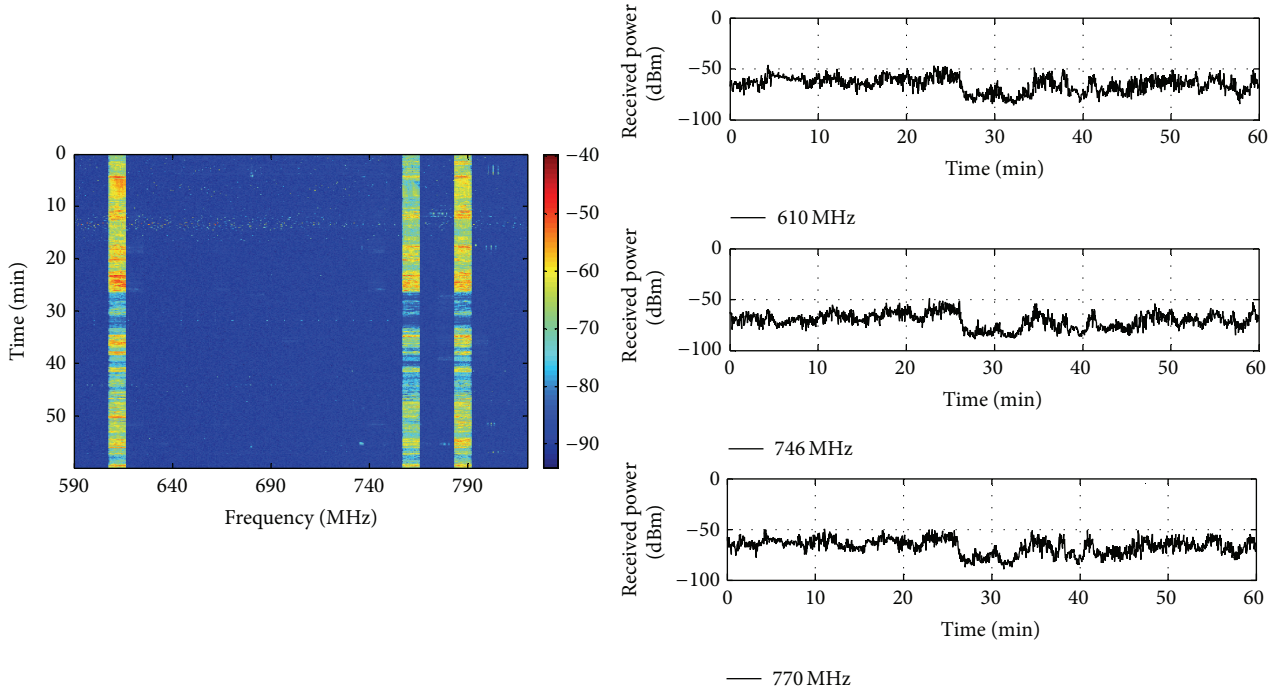

Figure 9: Spectrogram and received power time series at TV channel centre frequencies (Route 2).

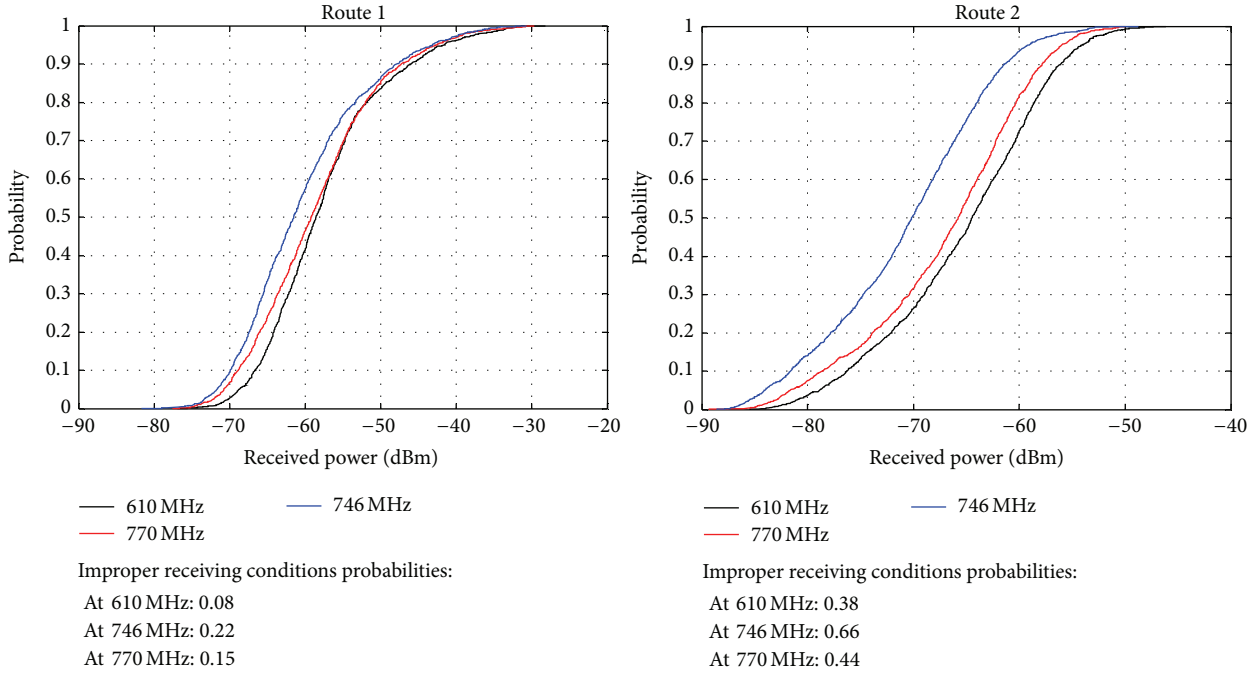

Figure 10: CDF of received power and probabilities of improper receiving conditions.

and 9) should be converted. For this conversion, the highest measured received power value in the DVB-T channel was considered as a reference (zero attenuation) level.

Besides the fade duration, in cognitive radio applications the level crossing rate as another dynamics aspect of the channel is studied in [36] for Rayleigh and Rician fast fading channels. The effect of imperfections in the radio environment map (REM) information on the performance of cognitive radio (CR) systems was investigated in [37]. In opportunistic channel allocation algorithms [38] the duration of fade event may play an important role. Therefore in our paper we propose fade duration statistics as a tool for opportunity length estimation.

Figure 11 indicates the probability of fade durations at 15 dB and 20 dB attenuation levels for 10 and 60 seconds, respectively. We proved with our measurements and with the

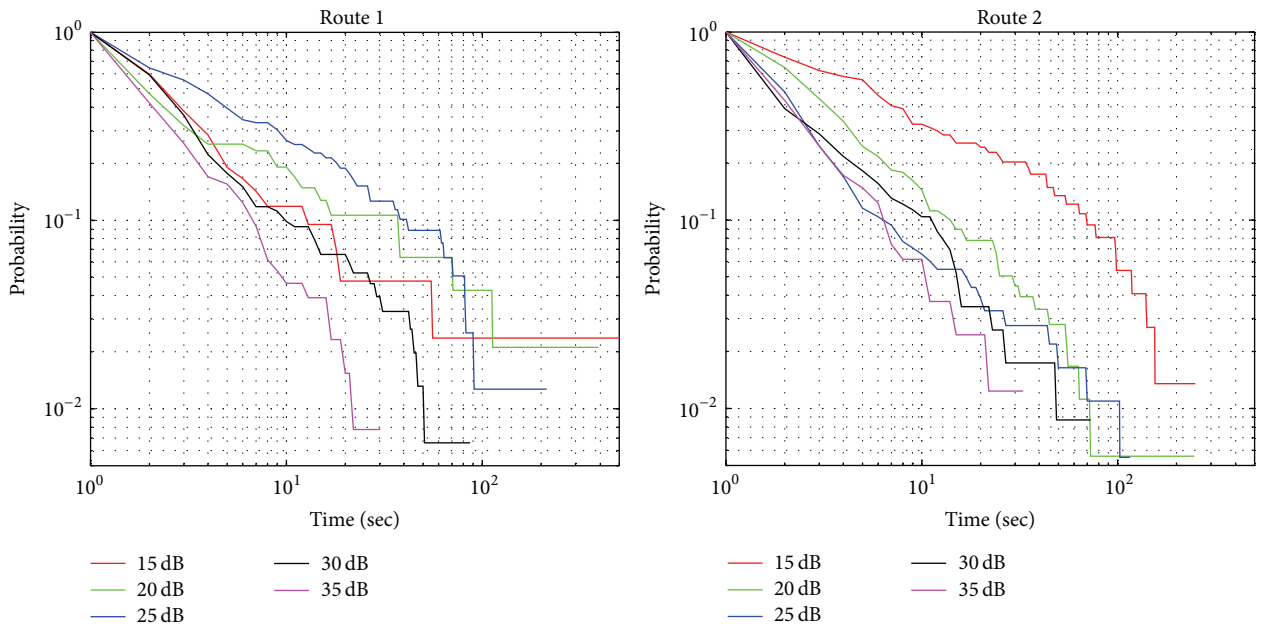

Frequency	$P(d > D)$ | Th = 15 dB	$P(d > D)$ | Th = 20 dB
610 MHz	0.12 (D = 10 sec) 0.02 (D = 60 sec)	0.19 (D = 10 sec) 0.06 (D = 60 sec)
746 MHz	0.17 (D = 10 sec) 0.03 (D = 60 sec)	0.20 (D = 10 sec) 0.09 (D = 60 sec)
770 MHz	0.17 (D = 10 sec) 0.03 (D = 60 sec)	0.13 (D = 10 sec) 0.09 (D = 60 sec)

Frequency	$P(d > D)$ | Th = 15 dB	$P(d > D)$ | Th = 20 dB
610 MHz	0.11 (D = 10 sec) 0.01 (D = 60 sec)	0.07 (D = 10 sec) 0.02 (D = 60 sec)
746 MHz	0.20 (D = 10 sec) 0.03 (D = 60 sec)	0.07 (D = 10 sec) 0.02 (D = 60 sec)
770 MHz	0.08 (D = 10 sec) 0.02 (D = 60 sec)	0.08 (D = 10 sec) 0.01 (D = 60 sec)

Figure 11: Fade duration distribution of the 610 MHz channel and probabilities of 10 and 60 sec fade events (all channels).

relating fade duration statistics that aboard a moving device in city area the DVB-T spectrum can be used for secondary purposes even for several seconds or for a minute duration. Calculating with one-hour travelling, the opportunity for secondary channel usage during this journey is several minutes in 10 s quanta and even some complete minutes. These are significant values that should be taken into account if secondary channel utilization of the DVB-T spectra is planned.

For the calculations above we applied −57 dBm threshold, that is, according to the literature, the signal level required for the error-free DVB-T reception. Our proposal is that the secondary usage of the spectrum is a reality when the service quality is insufficient for the primary users. Contrarily, for cognitive radio applications the protection of primary user's service quality is a key issue. The appearance of secondary users may cause significant interference in the TVWS; therefore an advanced spectrum sensing technique is essential. A study about this emerging technology [39] discusses that the sensing threshold is −112.8 dBm for 8 MHz wide channels, showing that high quality sensing technique is inevitable in a real CR application.

5. Conclusions

In this paper we presented wideband, mobile DVB-T spectrum measurements to study the variation of the received signal power in the TV channel frequencies. Our suggestion is that for cognitive radio applications the same frequency band is applicable if the service quality for the PUs is insufficient. It may happen in densely built-in city areas that, due to shadowing, reflections, or interference, the DVB-T signal quality is improper for primary usage. This fact has been proved by the measurements. In this case of short-distance communications, for example, for car-to-car data transfer or access local traffic information databases or even for self-driving vehicles, the DVB-T spectrum could be utilized. In the paper the antenna design for spectrum detection, the applied spectrum sensing hardware, measurement methods, and their statistics were shown. After the evaluation of the results it was proven that for mobile CR users it is possible to utilize the DVB-T band with intelligent devices for secondary purposes, even without decreasing the QoS of the primary users.

Competing Interests

The authors declare that they have no competing interests.

References

[1] I. F. Akyildiz, W.-Y. Lee, M. C. Vuran, and S. Mohanty, "NeXt generation/dynamic spectrum access/cognitive radio wireless networks: a survey," *Computer Networks*, vol. 50, no. 13, pp. 2127–2159, 2006.

[2] O. Simeone, J. Gambini, Y. Bar-Ness, and U. Spagnolini, "Cooperation and cognitive radio," in *Proceedings of the IEEE International Conference on Communications (ICC '07)*, pp. 6511–6515, Glasgow, UK, June 2007.

[3] E. Axell, G. Leus, and E. G. Larsson, "Overview of spectrum sensing for cognitive radio," in *Proceedings of the 2nd International Workshop on Cognitive Information Processing (CIP '10)*, pp. 322–327, Elba, Italy, June 2010.

[4] A. Garhwal and P. P. Bhattacharya, "A survey on spectrum sensing techniques in cognitive radio," *International Journal of Computer Science and Communication Networks*, vol. 1, no. 2, pp. 196–206, 2011.

[5] Q. Zhao and B. M. Sadler, "A survey of dynamic spectrum access," *IEEE Signal Processing Magazine*, vol. 24, no. 3, pp. 79–89, 2007.

[6] D. Das and S. Das, "A survey on spectrum occupancy measurement for cognitive radio," *Wireless Personal Communications*, vol. 85, no. 4, pp. 2581–2598, 2015.

[7] M. A. McHenry, P. A. Tenhula, D. McCloskey, D. A. Roberson, and C. S. Hood, "Chicago spectrum occupancy measurements & analysis and a long-term studies proposal," in *Proceedings of the 1st International Workshop on Technology and Policy for Accessing Spectrum (TAPAS '06)*, article 1, ACM, Boston, Mass, USA, 2006.

[8] M. Mehdawi, N. Riley, M. Ammar, and M. Zolfaghari, "Comparing historical and current spectrum occupancy measurements in the context of cognitive radio," in *Proceedings of the 20th Telecommunications Forum (TELFOR '12)*, pp. 623–626, Belgrade, Serbia, November 2012.

[9] A. Kliks, P. Kryszkiewicz, K. Cichoń, A. Umbert, J. Perez-Romero, and F. Casadevall, "DVB-T channels measurements for the deployment of outdoor REM databases," *Journal of Telecommunications and Information Technology*, no. 3, pp. 42–52, 2014.

[10] S. Jayavalan, H. Hafizal, N. M. Aripin et al., "Measurements and analysis of spectrum occupancy in the cellular and TV bands," *Lecture Notes on Software Engineering*, vol. 2, no. 2, pp. 133–138, 2014.

[11] A. Kliks, P. Kryszkiewicz, J. Perez-Romero, A. Umbert, and F. Casadevall, "Spectrum occupancy in big cities-comparative study. Measurement campaigns in Barcelona and Poznan," in *Proceedings of the 10th International Symposium on Wireless Communication Systems (ISWCS '13)*, pp. 1–5, Ilmenau, Germany, August 2013.

[12] P. I. Lazaridis, S. Kasampalis, Z. D. Zaharis et al., "UHF TV band spectrum and field-strength measurements before and after analogue switch-off," in *Proceedings of the 2014 4th International Conference on Wireless Communications, Vehicular Technology, Information Theory and Aerospace and Electronic Systems (VITAE '14)*, pp. 1–5, Aalborg, Denmark, May 2014.

[13] ITU-R, "Spectrum occupancy measurements and evaluation," Report ITU-R SM.2256, 2012.

[14] P. Angueira, M. Fadda, J. Morgade, M. Murroni, and V. Popescu, "Field measurements for practical unlicensed communication in the UHF band," *Telecommunication Systems*, vol. 61, no. 3, pp. 443–449, 2016.

[15] M. Fadda, V. Popescu, M. Murroni, P. Angueira, and J. Morgade, "On the feasibility of unlicensed communications in the TV white space: field measurements in the UHF band," *International Journal of Digital Multimedia Broadcasting*, vol. 2015, Article ID 319387, 8 pages, 2015.

[16] Federal Communications Commission, "Spectrum access for wireless microphone operations," FCC Record FCC-14-145, Federal Communications Commission, 2014.

[17] L. Csurgai-Horváth, I. Rieger, and J. Kertesz, "Mobile access of the DVB-T channel and the opportunity for cognitive spectrum utilization," in *Proceedings of the 17th International Conference on Transparent Optical Networks (ICTON '15)*, pp. 1–4, Budapest, Hungary, July 2015.

[18] W. Van den Broeck and J. Pierson, *Digital Television in Europe*, VUBpress, Brussels, Belgium, 2008.

[19] U. Reimers, *DVB: The Family of International Standards for Digital Video Broadcasting*, Springer, Berlin, Germany, 2004.

[20] D. Noguet, R. Datta, P. H. Lehne, M. Gautier, and G. Fettweis, "TVWS regulation and QoSMOS requirements," in *Proceedings of the 2nd International Conference on Wireless Communication, Vehicular Technology, Information Theory and Aerospace & Electronic Systems Technology (Wireless VITAE '11)*, pp. 1–5, Chennai, India, February 2011.

[21] B. Wild and K. Ramchandran, "Detecting primary receivers for cognitive radio applications," in *Proceedings of the 1st IEEE International Symposium on New Frontiers in Dynamic Spectrum Access Networks (DySPAN '05)*, pp. 124–130, IEEE, Baltimore, Md, USA, November 2005.

[22] R. A. Saeed and S. J. Shellhammer, Eds., *TV White Space Spectrum Technologies: Regulations, Standards, and Applications*, CRC Press, New York, NY, USA, 2012.

[23] M. Hata, "Empirical formula for propagation loss in land mobile radio services," *IEEE Transactions on Vehicular Technology*, vol. 29, no. 3, pp. 317–325, 1980.

[24] P. M. Ghosh, Md. A. Hossain, A. F. M. Zainul Abadin, and K. K. Karmakar, "Comparison among different large scale path loss models for high sites in urban, suburban and rural areas," *International Journal of Soft Computing and Engineering*, vol. 2, no. 2, 2012.

[25] A. Marţian, C. Vlădeanu, I. Marcu, and I. Marghescu, "Evaluation of spectrum occupancy in an urban environment in a cognitive radio context," *International Journal on Advances in Telecommunications*, vol. 3, no. 3-4, 2010.

[26] K.-H. Kim, J.-U. Kim, and S.-O. Park, "An ultrawide-band double discone antenna with the tapered cylindrical wires," *IEEE Transactions on Antennas and Propagation*, vol. 53, no. 10, pp. 3403–3406, 2005.

[27] Agilent N9340B Handheld RF Spectrum Analyzer (HSA), 3 GHz User Manual.

[28] ITU, "Prediction methods for the terrestrial land mobile service in the VHF and UHF bands," ITU-R Recommendation P. 529-2, ITU, Geneva, Switzerland, 1995.

[29] A. Medeisis and A. Kajackas, "On the use of the universal Okumura-Hata propagation prediction model in rural areas," in *Proceedings of the IEEE 51st Vehicular Technology Conference Proceedings*, vol. 3, pp. 1815–1818, Tokyo, Japan, May 2000.

[30] ROVER Laboratories SpA, "Understanding Digital TV," 2013, http://www.roverinstruments.com/.

[31] E. P. J. Tozer, *Broadcast Engineer's Reference Book*, Taylor & Francis, London, UK, 2012.

[32] M. Nekovee, "A survey of cognitive radio access to TV white spaces," *International Journal of Digital Multimedia Broadcasting*, vol. 2010, Article ID 236568, 11 pages, 2010.

[33] Ofcom, "Statement on Cognitive Access to Interleaved Spectrum," July 2009.

[34] ITU, "DVB-T coverage measurements and verification of planning criteria," ITU-R Recommendation SM.1875-2, ITU, 2014.

[35] ITU-R Rec. P.1623-1, Prediction method of fade dynamics on Earth-space paths, 2005.

[36] M. F. Hanif and P. J. Smith, "Level crossing rates of interference in cognitive radio networks," *IEEE Transactions on Wireless Communications*, vol. 9, no. 4, pp. 1283–1287, 2010.

[37] M. F. Hanif, P. J. Smith, and M. Shafi, "Performance of cognitive radio systems with imperfect radio environment map information," in *Proceedings of the Australian Communications Theory Workshop (AusCTW '09)*, pp. 61–66, IEEE, Sydney, Australia, February 2009.

[38] H. Shatila, M. Khedr, and J. H. Reed, "Opportunistic channel allocation decision making in cognitive radio communications," *International Journal of Communication Systems*, vol. 27, no. 2, pp. 216–232, 2014.

[39] C. Kocks, A. Viessmann, P. Jung, L. Chen, Q. Jing, and R. Q. Hu, "On spectrum sensing for TV white space in China," *Journal of Computer Networks and Communications*, vol. 2012, Article ID 837495, 8 pages, 2012.

Hindawi Publishing Corporation
Mobile Information Systems
Volume 2016, Article ID 8035876, 11 pages
http://dx.doi.org/10.1155/2016/8035876

Research Article

ETSI-Standard Reconfigurable Mobile Device for Supporting the Licensed Shared Access

Kyunghoon Kim,[1] Yong Jin,[1] Donghyun Kum,[1] Seungwon Choi,[1] Markus Mueck,[2] and Vladimir Ivanov[3]

[1]*School of Electrical and Computer Engineering, Hanyang University, Seoul 04763, Republic of Korea*
[2]*Intel Mobile Communications Group, 85579 Munich, Germany*
[3]*Mobile SoC Development Department, LG Electronics Inc., Seoul 06744, Republic of Korea*

Correspondence should be addressed to Seungwon Choi; choi@dsplab.hanyang.ac.kr

Received 4 March 2016; Revised 15 June 2016; Accepted 3 July 2016

Academic Editor: Miguel López-Benítez

In order for a Mobile Device (MD) to support the Licensed Shared Access (LSA), the MD should be reconfigurable, meaning that the configuration of a MD must be adaptively changed in accordance with the communication standard adopted in a given LSA system. Based on the standard architecture for reconfigurable MD defined in Working Group (WG) 2 of the Technical Committee (TC) Reconfigurable Radio System (RRS) of the European Telecommunications Standards Institute (ETSI), this paper presents a procedure to transfer control signals among the software entities of a reconfigurable MD required for implementing the LSA. This paper also presents an implementation of a reconfigurable MD prototype that realizes the proposed procedure. The modem and Radio Frequency (RF) part of the prototype MD are implemented with the NVIDIA GeForce GTX Titan Graphic Processing Unit (GPU) and the Universal Software Radio Peripheral (USRP) N210, respectively. With a preset scenario that consists of five time slots from different signal environments, we demonstrate superb performance of the reconfigurable MD in comparison to the conventional nonreconfigurable MD in terms of the data receiving rate available in the LSA band at 2.3–2.4 GHz.

1. Introduction

Global mobile data traffic is expected to grow up to 24.3 exabytes per month by 2019, which is nearly a tenfold increase compared to the traffic in 2014 [1]. To cope with this explosive increase in data traffic, various enabling technologies, such as full dimensional multiple-input multiple-output, device-to-device communication, and new waveform designs, such as nonorthogonal multiple access, have been actively researched [2, 3]. In particular, the World Radio Communication conference in 2015 (WRC-15) of the International Telecommunication Union-Radio (ITU-R) communication sector considers spectrum sharing technology to be a key methodology that is applicable in the 5th Generation (5G) mobile communications [4]. Among the various spectrum sharing techniques, Licensed Shared Access (LSA), which is a framework for sharing the spectrum among a limited number of users [5], has been the focus of research, especially in Europe. The Electronic Communications Committee (ECC) performed a comprehensive study of the regulatory aspect of LSA. They also released the results of their research on the applicability of the LSA concept in the 2.3–2.4 GHz band using Time-Division Duplexing (TDD) [6]. The Cognitive Radio Trial Environment (CORE) demonstrated an LSA live test in the LSA band at 2.3–2.4 GHz [7], while Mustonen et al. introduced a novel network architecture, namely, self-organizing networking features [8], to support LSA. During this time, Working Group (WG) 1 of the Technical Committee (TC) on the Reconfigurable Radio System (RRS) of the European Telecommunications Standards Institute (ETSI) has been developing LSA-related standards. In addition, [9–11] introduced an early-stage overview of the LSA system concept, LSA system requirements, and architecture for operation of mobile broadband systems, respectively. All the LSA-related developments introduced above, however, have only considered the LSA technology from the viewpoint of

network or infrastructure systems but not from the viewpoint of Mobile Device (MD). This is problematic because the previous work has not specified the functionalities required in MDs in order to operate using LSA. For example, if a MD does not support TDD Long Term Evolution (LTE) at the frequency band of 2.3–2.4 GHz, an additional spectral band for LSA, that is, 2.3–2.4 GHz [9], would provide very little advantage [12]. Consequently, in order to fully exploit spectrum sharing, MD must be able to adaptively change its configuration appropriately for the radio application (RA) defined in a given LSA band. Therefore, it seems that reconfigurability is a mandatory characteristic of MD in order to fully exploit the benefits of LSA-based spectrum sharing.

Recently, WG2 of TC-RRS of ETSI developed a standard architecture and related interfaces for reconfigurable MDs. In [13], WG2 released a standard reconfigurable MD architecture with its main effort focused on resolving the problem of portability between the RA code and the MD hardware platform. WG2 has also defined standard interfaces in accordance with the standard architecture for reconfigurable MDs in [14, 15].

The main contribution of this paper is to show how the reconfiguration of MDs should be achieved for realizing LSA demonstrated by WG1 of TC-RRS of ETSI in [9] where it is assumed that the target MD is compliant with the standard architecture released by WG2 of TC-RRS of ETSI [13]. If the target MD is reconfigurable, there is no restriction on the RA in an LSA region. For example, a MD is configured with TDD LTE in the frequency region at 2.3–2.4 GHz in order for the scenario in [9] to be valid because TDD LTE has been defined as the designated RA in the LSA region of the 2.3–2.4 GHz band [12]. Since we do not know in general which RA will be adopted in the LSA region, the LSA technology is not useful for nonreconfigurable MDs. In order to verify the reconfiguration of MDs for LSA, we specify in this paper which interactions should occur in what order among the software entities in the reconfigurable MDs using the ETSI-standard architecture. The systematic interactions among the software entities of the reconfigurable MD are referred to as a "procedure" in this paper. We also present implementation of the reconfigurable MD prototype that realizes the proposed procedures. The implemented test-bed using the MD prototype is compliant with the reference model of the standard architecture [13] released by WG2 of TC-RRS of ETSI. The modem and Radio Frequency (RF) of the prototype MD are implemented with the NVIDIA GeForce GTX Titan Graphic Processing Unit (GPU) and Universal Software Radio Peripheral (USRP) N210, respectively. Assuming the LSA region adopts TDD LTE, as shown in [12], we demonstrate superb performance of the reconfigurable MD compared to a conventional nonreconfigurable MD in terms of the data receiving rate available in the LSA band at 2.3–2.4 GHz. In addition to the experimental tests performed with the implemented test-bed, computer simulations have also been presented considering a scenario of multiple users in an LSA band. It was verified through the computer simulations that the reconfigurable MDs not only increase the total sum rate itself but also increase the number of users satisfying a given QoS.

The rest of this paper is organized as follows. Section 2 introduces the standard architecture for a reconfigurable MD developed by WG2 of TC-RRS, based on which the procedure is set up in the following section. Section 3 proposes the procedures that specify the interactions among the software entities of the ETSI-standard reconfigurable MD for realization of the LSA. Section 4 introduces the implemented reconfigurable MD, while Section 5 presents the experimental results obtained from the implemented MD and performance evaluations obtained from the computer simulations considering the scenario of multiple users. Finally, Section 6 concludes this paper.

2. Architectural Model for Reconfigurable MD

WG2 of TC-RRS of ETSI has developed a standard architecture for reconfigurable MDs and related interfaces with the intention that any desired Radio Access Technologies (RATs) can be realized in a reconfigurable MD by downloading the target RA code from the public domain, for example, the RadioApp Store [16], regardless of the hardware platform of the MD. This section introduces a brief summary of the standard architecture and related interfaces based on which a systematic procedure is developed in the following section in such a way that the software entities in the reconfigurable MD interact with one another for implementing the LSA.

2.1. Architecture for Reconfigurable MD. Figure 1 illustrates the reconfigurable MD architecture and related interfaces proposed by WG2 of TC-RRS of ETSI. As shown in the figure, the architecture consists of a Communication Services Layer (CSL), Radio Control Framework (RCF), Unified Radio Applications (URAs), and radio platform [13]. Although the four components are shown in the figure, the necessary part of the ETSI standard includes the four entities in CSL, that is, the Administrator, Mobile Policy Manager (MPM), networking stack, and monitor, as well as the five entities in RCF, that is, the Configuration Manager (CM), Radio Connection Manager (RCM), Flow Controller (FC), multiradio controller (MRC), and Resource Manager (RM). This means that the radio platform is vendor-specific and the URA is the downloaded RA code consisting of functional blocks, metadata, and other software needed for the processing of context information [13–15].

The functionality of each of the four entities in the CSL can be summarized as follows. Administrator entity requests (un)installation of URA and creates or deletes instances of URA. The MPM entity monitors the radio environments and MD capabilities, requests (de)activation of URA, and provides information about the URA list. The networking stack entity sends and receives the user data. The monitor entity transfers the context information from the URA to the users or the proper destination entity in a MD.

The functionality of each of the five entities in the RCF can be summarized as follows. The CM entity (un)installs, creates, or deletes instances of URA and manages access to the radio parameters of the URA. The RCM entity (de)activates URA according to user requests and manages user data flows. The FC entity sends and receives user data packets and controls

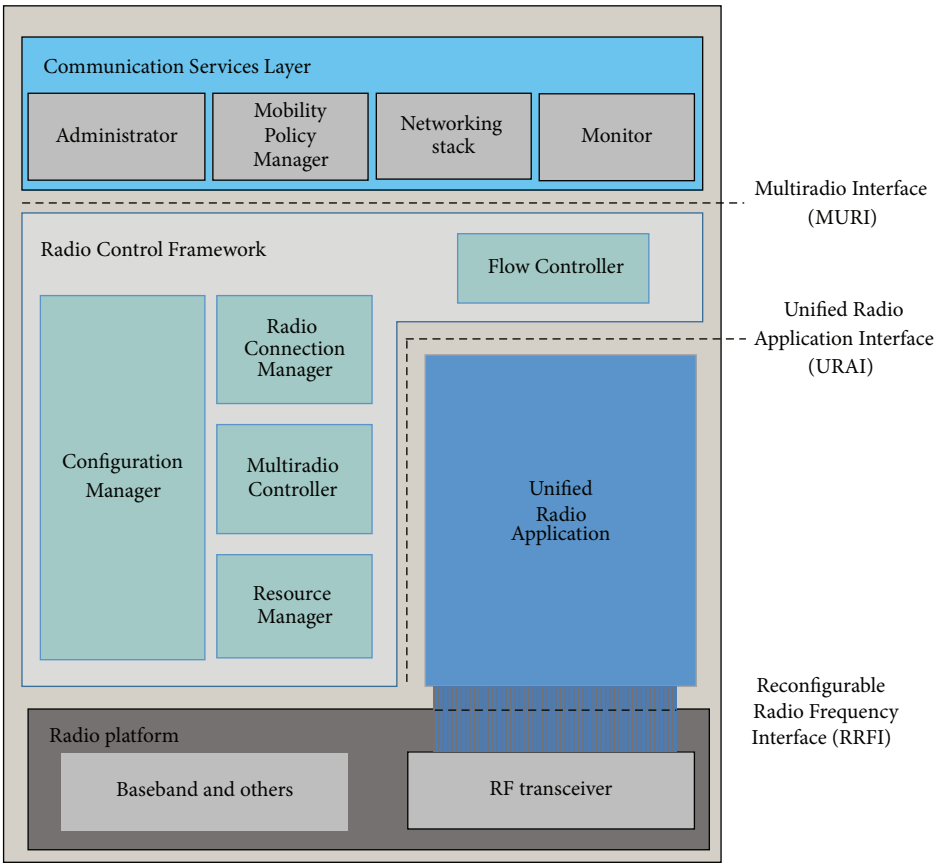

Figure 1: Reconfigurable MD architecture and related interfaces [13].

the flow of the signaling packets. The MRC entity schedules the requests for radio resources issued by concurrently executing URAs as well as detecting and managing the interoperability problems among the concurrently executed URAs. The RM entity manages the computational resources in order to share them among the simultaneously active URA. This guarantees their real-time execution.

The RA code, that is, the software that enforces generation of the transmit RF signals or the decoding of the received RF signals, becomes a URA once it is downloaded into a reconfigurable MD. Since all RAs exhibit common behavior from a reconfigurable MD perspective once they are downloaded in a reconfigurable MD, the downloaded RA code is called URA, which consists of functional blocks that exhibit the required modem functions of the corresponding RAT.

The radio platform shown in Figure 1 is part of the MD hardware that relates to the radio processing capability. It includes the programmable components, hardware accelerators, RF transceiver, and antenna(s).

2.2. Interfaces for Reconfigurable MD. As shown in Figure 1, there are three types of interfaces, the Multiradio Interface (MURI), Unified Radio Application Interface (URAI), and Reconfigurable RF Interface (RRFI), with which entities from the CSL, RCF, and radio platform can interact with one another.

The MURI interfaces each entity of the CSL and RCF. It provides three types of services: administrative services, access control services, and data flow services [14]. The URAI interfaces each entity of the RCF and URA. It provides five types of services: RA management services, user data flow services, multiradio control services, resource management services, and parameter administration services [17]. The RRFI interfaces the URA and the radio platform. It provides five types of services: spectrum control services, power control services, antenna management services, transmit (Tx)/receive (Rx) chain control services, and radio virtual machine protection services [15].

3. Proposed Procedures for LSA in Reconfigurable MD

In this section, we present an LSA procedure for reconfigurable MD in which the architecture is specified as the ETSI standard briefly summarized in the previous section. The procedure introduced in this section specifies how the entities in the CSL and RCF shown in Figure 1 interact with one another.

Figure 2 illustrates a conceptual view of realizing LSA, in which the basic scenario has been demonstrated by WG1 of TC-RRS of ETSI [9]. The National Regulation Authority (NRA) shown in Figure 2 manages the LSA Repository in such a way that it provides the LSA Repository information

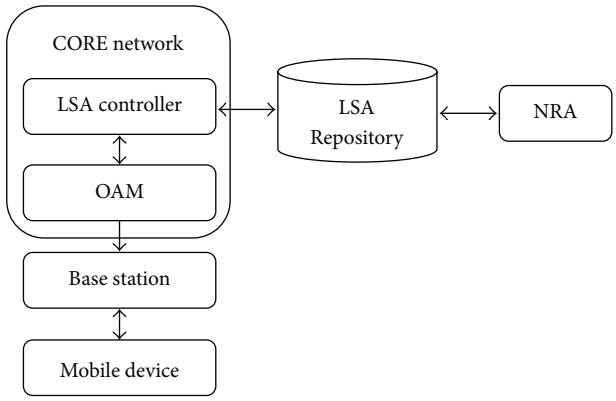

Figure 2: Conceptual view of realizing LSA.

about LSA license regarding the right of using the LSA band and receives a report regarding the use of LSA spectrum from the LSA Repository. The LSA Repository contains a database of spatial and temporal information regarding the spectrum use of the incumbent user. Based on the information provided from the LSA Repository, the LSA controller determines the availability of the spectrum that can be shared using LSA. In cases when the spectrum is available, the network management system, which is denoted as "Operation, Administration, and Maintenance (OAM)" in Figure 2, acknowledges the availability of the spectrum to the corresponding base station.

The use case of expanding the bandwidth using LSA has been released by WG1 of TC-RRS of ETSI in [9]. This is the basis of the LSA procedure introduced in this section. The use case can be summarized as follows. Let us first consider a case where a Mobile Network Operator (MNO) providing a Frequency Division Duplexing (FDD) LTE service wants to switch the spectral band from its own FDD LTE band to the LSA band at a specific time. Note that, as shown in [12], the LSA region is assumed to be supported with TDD LTE in the band at 2.3–2.4 GHz. Assuming the MNO has held the individual authorization for using the extra band at 2.3–2.4 GHz, the LSA controller shown in Figure 2 decides which base stations can be granted use of the extra spectral band for the required time period. Receiving the information regarding the availability of the extra spectral band from the LSA controller, the OAM shown in Figure 2 notifies the availability of the spectrum to those base stations which may use the extra spectral band at 2.3–2.4 GHz. In order to implement this use case, we propose a procedure for updating the configuration of MD with a new RA defined in a given LSA region, that is, TDD LTE in this use case.

Figure 3 illustrates the procedure of updating the configuration of MD with an arbitrary RA required for LSA. The procedure shown in Figure 3 can be summarized in the 17 steps shown as follows.

Step 1. In order to install a new URA, the the Administrator sends a *DownloadRAPReq* signal including the Radio Application Package (RAP) identification (ID) to the RadioApp Store.

Step 2. The Administrator receives a *DownloadRAPCnf* signal including the RAP ID and RAP from the RadioApp Store.

Step 3. Upon the download of RAP from the RadioApp Store, the Administrator sends an *InstallRAReq* signal including the RAP ID to the CM to request installation of the new RA.

Step 4. The CM first performs the URA code certification procedure in order to verify its compatibility, authentication, and so forth.

Step 5. The CM performs installation of URA and transfers an *InstallRACnf* signal including the URA ID to the Administrator.

Step 6. In order to deactivate the current URA, the MPM transfers the RCM *HardDeactivateReq* signal, which includes the RA ID.

Step 7. Upon a request from the RCM, the Radio Operating System (ROS) deactivates the designated URA.

Step 8. After the ROS completes hard deactivation of the URA, the RCM acknowledges completion of the deactivation procedure by sending a *HardDeactivateCnf* signal to the MPM.

Step 9. In order to create an instance of a new URA, the MPM transfers an *InstantiateRAReq* signal including the ID of the URA to be instantiated to the CM.

Step 10. The CM transfers an *RMParameterReq* signal and an *MRCParameterReq* signal including the ID of the URA in order to get the parameters needed for URA activation to the RM and MRC.

Step 11. The CM receives an *RMParameterCnf* signal including the ID of the URA and the radio resource parameters from the RM.

Step 12. The CM receives an *MRCParameterCnf* signal including the ID of the URA and computational resource parameters from the MRC.

Step 13. The CM transfers the URA ID and the received parameters for performing the URA instantiation to the ROS.

Step 14. After creating an instance, the CM transfers an *InstantiateRACnf* signal including the URA ID to the MPM.

Step 15. In order to activate the new URA, the MPM transfers an *ActivateReq* signal including the ID of the URA to the RCM.

Step 16. Upon request from the RCM, the ROS activates the designated URA.

Step 17. After the ROS completes activation of the URA, the RCM sends an *ActivateCnf* signal back to the MPM.

Note that Steps 3 and 5 utilize the administrative services of the MURI [14], Steps 6, 8, 9, 14, 15, and 17 make use of the

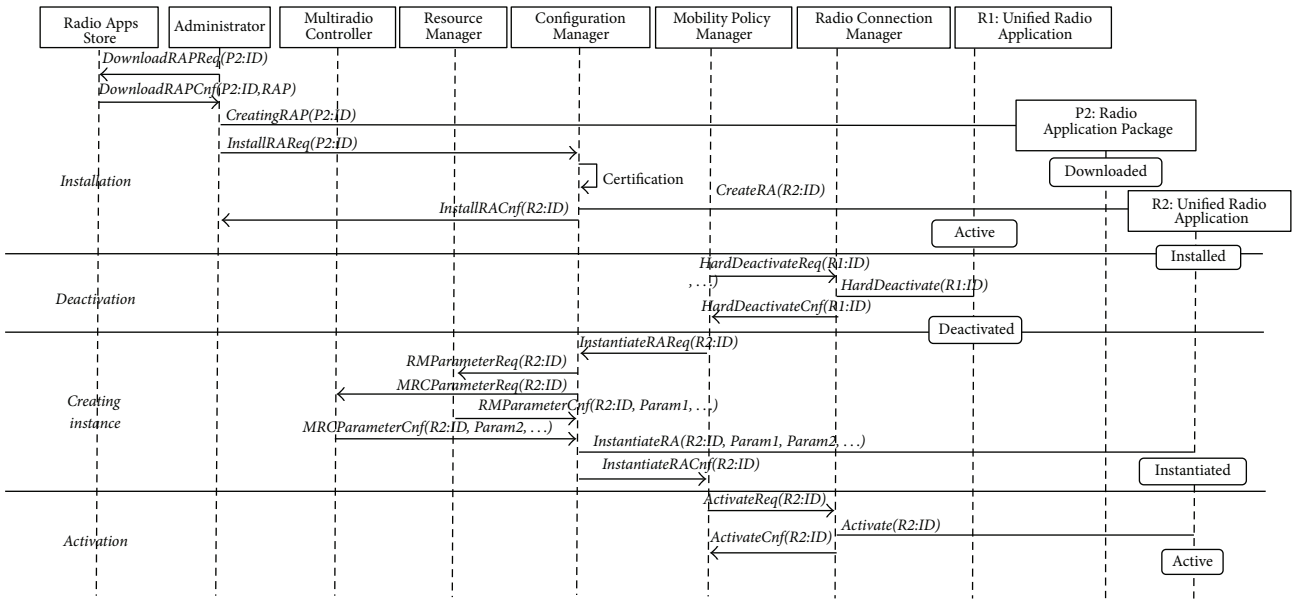

Figure 3: Procedure of MD reconfiguration for implementing LSA.

access control services of the MURI [14], Steps 7 and 16 utilize the radio application management services of URAI [17], and Steps 4 and 13 make use of the parameter administration services of URAI [17]. Steps 10, 11, and 12 are related to the interactions among the entities in the RCF, which are vendor-specific.

Through the procedure shown in Figure 3, the MD reconfiguration can be achieved by updating the present URA with a new one. Note that, in the use case presented by WG1 of TC-RRS of ETSI in [9], the present URA is FDD LTE, and the new one is TDD LTE. It is also noteworthy that the feasibility of the standard architecture and related interfaces can be verified from Figure 3 through the observation that the desired RA code is first downloaded from the RadioApp Store, then installed, instantiated, and activated in a given reconfigurable MD.

4. Implementation of a Reconfigurable MD for LSA

This section presents implementation of the prototype reconfiguration MD used as a test-bed for obtaining the experimental results of LSA introduced in Section 5. The implemented prototype system is compliant with the standard architecture of ETSI TC-RRS WG2 [13].

Figure 4(a) illustrates a reference model of the reconfigurable MD architecture introduced in [13]. According to the standard architecture of the reconfigurable MD defined by WG2 of TC-RRS of ETSI, operations supported by the Application Processor are based on non-real-time processing. The operations supported by the Radio Computer are based on real-time processing, while the dotted part in between these two parts shown in Figure 4(a) is either non-real-time or real-time depending upon the vendor's choice. This option means that the Operating System (OS) of the Application Processor must be a non-real-time OS such as Android or iOS, while that of the Radio Computer, which is referred to as ROS in Figure 4(a), has to be a real-time OS including RCF, as indicated in Figure 4(a). The Application Processor in Figure 4(a) includes the following components: (1) a driver that activates a hardware device, such as a camera or speaker, in the part of the Application Processor on a given MD and (2) a non-real-time OS for execution of the Administrator, MPM, networking stack, and Monitor [13], which are part of the CSL, as described previously. The Radio Computer includes the following components: (1) ROS for executing the functional blocks of the given RAs; (2) a radio platform driver, which is for the ROS to interact with the radio platform hardware; and (3) a radio platform, which typically consists of programmable hardware, dedicated hardware, RF transceiver, and antenna(s).

Figure 4(b) illustrates a block diagram of the reconfigurable MD prototype architecture that has been implemented as a test-bed based on the architecture shown in Figure 4(a). As shown in Figure 4(b), the Application Processor part of the test-bed consists of Ubuntu 12.04 [18] and CSL, while the Radio Computer part consists of a Linux kernel, RCF, radio platform driver, and radio platform. For the purpose of experimental tests, we have not adopted a real-time OS for the Radio Computer part because the primary purpose of the test-bed is to verify the feasibility of the standard architecture for the functionality of LSA-based spectrum sharing rather than the real-time functionality of the RA code execution. Furthermore, the test-bed system does not include all the entities of the CSL and the RCF defined in the ETSI standard. Specifically, in the test-bed system shown in Figure 4(b), CSL consists of an Administrator and MPM only, while RCF consists of CM, RCM, RM, and MRC only. Also, it can be observed from Figure 4(b) that the Linux kernel, which plays the role of ROS in the test-bed system, supports the execution of the functional blocks of a given RA code. The RA code prepared for our test-bed system consists of FDD LTE and

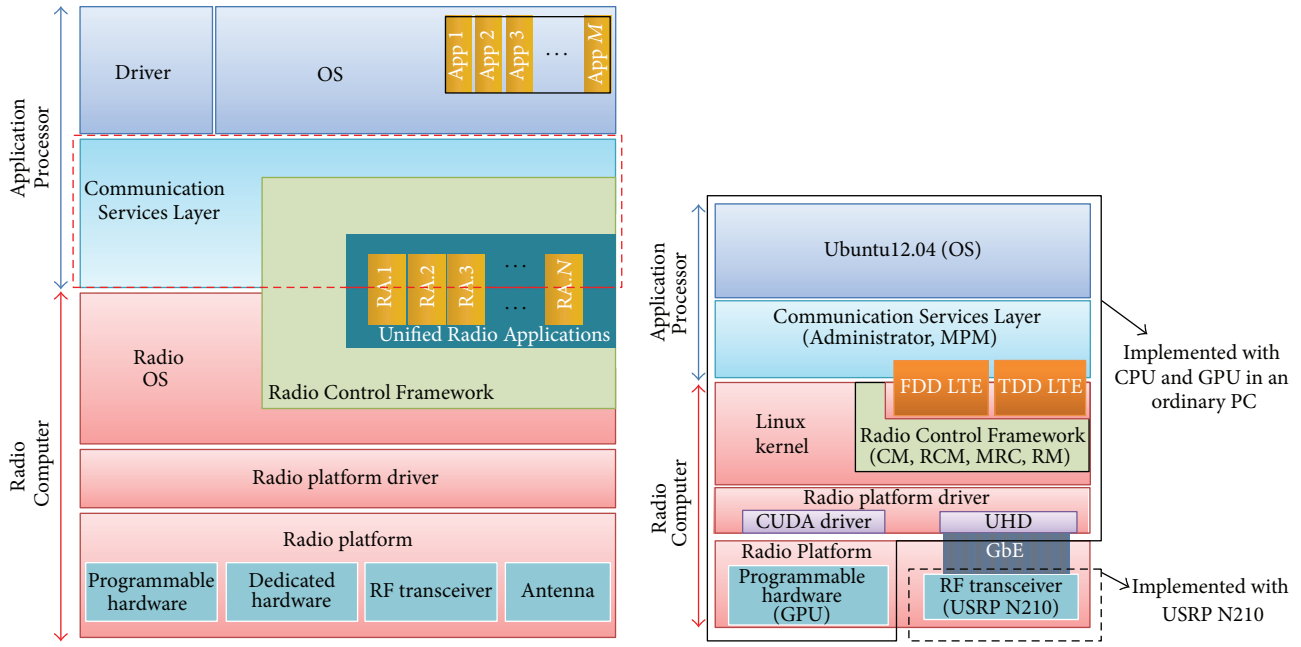

(a) Reference model of the ETSI-standard reconfigurable MD architecture [13]

(b) Implemented reconfigurable MD test-bed architecture

Figure 4: Block diagram of the reference model and implemented test-bed of a reconfigurable MD.

TDD LTE which are compliant with 3GPP Rel. 10 [19]. The RA code is executed on a GPU in radio platform of the test-bed. GPU in general, since it contains a great number of powerful threads, is appropriate for parallel computing. In order to utilize the number of threads efficiently, the RA code containing FDD LTE and TDD LTE has been implemented using Compute Unified Device Architecture (CUDA), that is, a C-based programming language provided by NVIDIA. The GPU adopted in our test-bed is NVIDIA's GeForce GTX Titan that is capable of 4,494 GFLOPS using 2,688 CUDA core processor cores [20]. In addition, the radio platform driver shown in Figure 4(b) includes the CUDA driver and the URSP Hardware Driver (UHD) through which the Linux kernel can access the radio platform consisting of a NVIDIA GeForce GTX Titan GPU and USRP N210 [21], respectively.

The key issue in RA code implementation is to maximize the degree of parallelization among the large number of threads in a given GPU. In fact, the parallelization can be considered in multiple layers, that is, among grids, blocks, and/or threads in a given GPU. Note that each grid contains multiple blocks and each block includes multiple threads. In order to maximize the degree of parallelization, each function block of the RA code should be partitioned into as many pieces as possible such that we can maximize the number of threads to be activated for executing a given task. For example, the procedure of channel estimation along the frequency axis [19], which is a function block needed in both FDD and TDD LTE, has been partitioned in our RA code implementation in such a way that a single grid containing 200 blocks each of which includes 6 threads in the NVIDIA GeForce GTX Titan GPU has been activated. It means that totally 1,200 threads are activated in parallel for the function block of the channel estimation along frequency axis. Similarly, for the function block of channel estimation along time axis [19], totally 8,400 threads, that is, 14 threads in each block and 600 blocks in a single grid, have been activated in parallel.

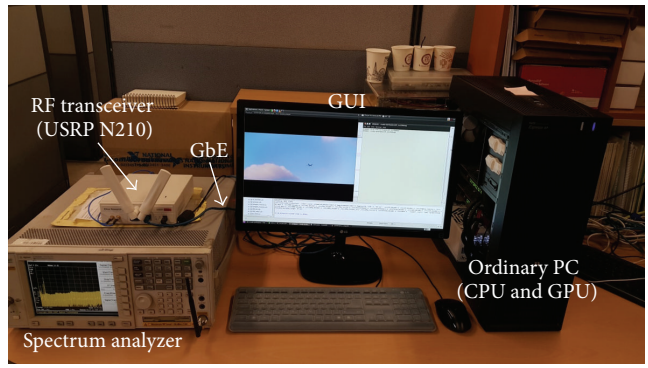

Figure 5: Photograph of the implemented reconfigurable MD test-bed.

Figure 5 illustrates a photograph of the implemented test-bed of the reconfigurable MD. The test-bed realizes the architectural model shown in Figure 4(b). As shown in Figure 5, the test-bed system consists of two parts, an ordinary Personal Computer (PC) and an RF transceiver. An ordinary PC, which provides a NVIDIA GeForce GTX Titan GPU and Central Processing Unit (CPU), was used to implement all the components of the reconfigurable MD shown in Figure 4(b) except for the RF transceiver, which has been separately implemented with USRP N210, as shown in Figure 5. In our

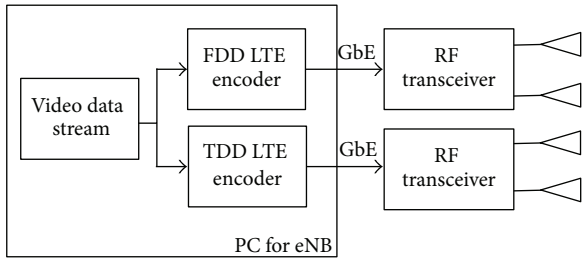

(a) Functional block diagram of eNB

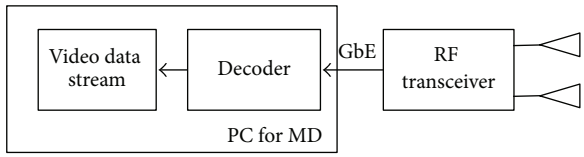

(b) Functional block diagram of MD

Figure 6: Functional block diagram of the test-bed system.

implementation, the RF transceiver is connected with the PC through a Giga-bit Ethernet (GbE), as shown in Figures 4(b) and 5. All the functional blocks in a given RA code are executed on the NVIDIA GeForce GTX Titan GPU board in the PC, while all the functionalities of the RF transceiver, including analog-to-digital and digital-to-analog conversions as well as frequency-up and frequency-down conversions, are performed in the USRP N210. Note that the lower part shown by a dotted line in Figure 4(b) corresponds to the RF transceiver implemented with USRP N210, while the other part shown by a solid line in Figure 4(b) corresponds to all the other parts of a reconfigurable MD implemented with the ordinary PC shown in Figure 5. Since an ordinary PC only provides a GPU and CPU, the implemented prototype system does not include Field Programmable Gate Arrays (FPGA) or Digital Signal Processors (DSP) in the part of the radio platform shown in Figure 4(b), while the GPU supports all the functional blocks required in the FDD LTE and TDD LTE that are needed in the LSA. The CPU in the PC was used to realize the functionalities of RCF as well as to control the GPU and USRP through the CUDA driver and UHD in the radio platform driver, respectively, as mentioned earlier. The Graphic User Interface (GUI) shown in Figure 5 provides monitoring of the video data stream, which is the result of decoding the received FDD or TDD LTE signals, as well as a set of environmental parameters such as data throughput and Bit Error Rate (BER). The spectrum analyzer shown in Figure 5 was used to observe the center frequency and bandwidth of the RF signals of FDD and TDD LTE.

5. Numerical Results

5.1. Experimental Tests. This subsection presents the experimental results of the LTE data throughput obtained from a test-bed consisting of an Evolved Node B (eNB) and MD operating in the signal environment of the use case considered in Section 3, that is, the use case of expanding bandwidth using LSA. In the experimental tests, we considered two types of MD for comparison purposes. One is a legacy MD of which the configuration is fixed with FDD LTE, and the other is capable of changing its configuration between FDD LTE and TDD LTE depending on the given signal environment. In general, a MD performs a horizontal handover; that is, it moves to an adjacent base station, when the Quality of Service (QoS) drops down to a preset threshold value. If the given QoS cannot be satisfied through a horizontal handover, a reconfigurable MD performs a vertical handover; that is, it changes the present radio application to another one that can bring about satisfactory QoS [12]. In this paper, the required QoS was set up with a preset level of LTE data throughput. Therefore, when the preset level of the LTE data throughput is not achieved through a horizontal handover, the MD checks the availability of the TDD LTE of the LSA band in order to perform a vertical handover from FDD LTE to TDD LTE. As we have implemented a single eNB for simplicity, however, the reconfigurable MD performs a vertical handover directly when the present LTE data throughput becomes lower than the threshold level. Consequently, whenever the QoS is not maintained, assuming the LSA band is available in the present region, a reconfigurable MD changes its configuration from FDD LTE to TDD LTE. As for the legacy MD, the configuration is always fixed with FDD LTE, whether or not the QoS is satisfied. In this subsection, we have summarized the LTE data throughput obtained from both the reconfigurable MD and legacy MD in a signal environment where the QoS and availability of the LSA band vary as a function of time. For the experimental tests introduced in this subsection, the MD prototype shown in Section 4 was used for the reconfigurable MD, while the dual mode eNB supporting FDD and TDD LTE shown in our previous work in [22] was used.

Figure 6 illustrates a functional block diagram of the dual mode eNB [22] that supports both FDD and TDD LTE and that of MD. Both eNB and MD were implemented with a PC including a GPU for base band signal processing and USRP N210, which plays the role of the RF transceiver. As shown in Figure 6(a), eNB encodes the video data stream in accordance with the data format of both FDD and TDD LTE. The encoded data are transferred to the RF transceiver of USRP N210 via GbE and radiated through the transmit antennas. For FDD LTE, the center frequency was set to 1.7 GHz, a licensed band, with its bandwidth being 10 MHz, while TDD LTE uses 2.35 GHz as its center frequency with its bandwidth being 15 MHz. For the experimental tests of LSA, eNB transmits the FDD LTE signals continually, while the TDD LTE signal is transmitted only for a preset period of time, which means eNB in our test-bed system transmits both FDD and TDD LTE signals only for a preset period of time, except for the FDD LTE signal, which is transmitted from eNB. Figure 6(b) illustrates a common functional block diagram for both reconfigurable MDs and legacy MDs. As shown in Figure 6(b), the RF signal transmitted from eNB is captured at the receive antenna of MD, and the frequency-down and analog-to-digital are converted at the RF transceiver of USRP N210. Then, the FDD and/or TDD LTE signal is decoded and retrieved into the video data stream.

Table 1: Scenario set up for experimental tests.

Time interval	QoS	LSA band
T_1: t_0~t_1	Satisfied	Not available
T_2: t_1~t_2	Not satisfied	Not available
T_3: t_2~t_3	Not satisfied	Available
T_4: t_3~t_4	Satisfied	Available
T_5: t_4~t_5	Satisfied	Not available

Table 2: System parameters.

System parameter	FDD LTE	TDD LTE
Communication standard	3GPP Rel. 10	
Channel coding	Turbo coding (coding rate = 1/2)	
Center frequency (GHz)	1.7	2.35
Transmission bandwidth (MHz)	10	15
Modulation scheme	16 QAM	64 QAM
UL/DL configuration	—	6
Special subframe configuration	—	1

Table 1 shows the scenario set up for the experimental tests in terms of QoS satisfaction and LSA band availability. Each time interval in Table 1 was set to 60 seconds. The experiment was performed for five time intervals starting at t_0 and ending at t_5. For example, during the first time interval, T_1, that is, from t_0 to t_1, the signal environment was set up in such a way that QoS was satisfied, and the LSA band is not available. The condition whether or not QoS is satisfied is determined, as mentioned earlier, depending on whether or not the data throughput at the receiving MD exceeds the preset threshold value. The value for the threshold has been arbitrarily set up to 10 Mbps. The signal environment where the QoS was satisfied was set up by allocating all the spectral resources of FDD LTE to the target MD. The other signal environment where QoS was not satisfied was implemented by allocating only a half of the entire spectral resources of FDD LTE to the target MD. For the availability of the LSA band, the LSA band becomes available only when the dual mode eNB transmits the video stream data in both FDD and TDD LTE. When eNB transmits the video stream data only in FDD LTE, the LSA band is not available. In our experiment, assuming that the LSA band is available for the time intervals of T_3 and T_4, the availability of the LSA band is set up for T_3 and T_4 as shown in Table 1, which means the procedure for the LSA controller to notify the availability of the LSA band to OAM has been omitted in our experiment. Note that since the MD normally operates in FDD LTE mode, the availability of the LSA band does not have to be checked as long as QoS with FDD LTE is satisfied. Consequently, if QoS with FDD LTE is not satisfied, the reconfigurable MD starts to set up its configuration with TDD LTE of the LSA band, while the conventional nonreconfigurable MD has to stay in FDD LTE mode with unsatisfactory data throughput.

Figure 7 shows an image of the experimental test for measuring the data throughput of the reconfigurable MD and legacy MD. The system parameters for FDD and TDD LTE were set up as shown in Table 2. Since the

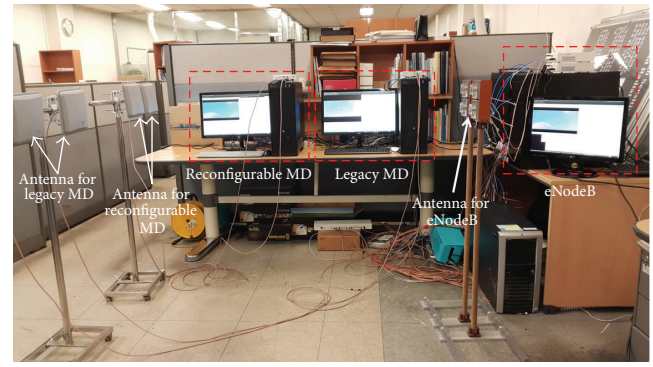

Figure 7: Photograph showing the experimental environment for comparing the received data throughputs of the reconfigurable MD and legacy MD.

Table 3: Average throughput with Key Performance Indicator (KPI) value for the reconfigurable MD.

MD	Time interval (Mbps)				
	T_1	T_2	T_3	T_4	T_5
Reconfigurable MD	14.88	7.32	14.39 (KPI = 1)	14.45	14.87 (KPI = 1)
Legacy MD	14.80	7.33	7.33	14.80	14.82

received data throughput for TDD LTE is determined by the uplink/downlink configuration type and the special subframe configuration type, the types in Table 2 were set up in such a way that the maximum throughput of FDD and TDD LTE becomes approximately the same.

Figure 8 illustrates the throughput values measured at the receiving MD. The data throughput shown in Figure 8 was obtained from the experimental environment shown in Figure 7 in which the eNB and MD use the system parameter values shown in Table 2 according to the experimental scenario shown in Table 1. Table 3 shows an average Rx throughput for each time interval together with Key Performance Indicator (KPI), which indicates whether or not the configuration of the reconfigurable MD has been correctly set up in accordance with a given signal environment. More specifically, KPI tells whether or not the configuration of the reconfigurable MD has been correctly changed from FDD/TDD LTE to TDD/FDD LTE during the time interval T_3/T_5. Therefore, KPI is set up to 1 or reset to 0 depending on whether the configuration of the reconfigurable MD is performed successfully or not. Consequently, throughput of the receiving MD would have become greater than 10 Mbps/14.5 Mbps during the time interval of T_3/T_5 if the configuration of the reconfigurable MD was successfully performed, that is, from FDD/TDD LTE to TDD/FDD LTE during the time interval of T_3/T_5. The solid line in Figure 8 corresponds to the performance of the reconfigurable MD, while the dotted line corresponds to the legacy MD. It can be observed from Figure 8 that, during the first time slot T_1, both the reconfigurable MD and legacy MD exhibit almost the same maximum throughputs, 14.88 M bits per second (bps) and 14.80 Mbps, respectively, with FDD LTE because the first time slot was set up for

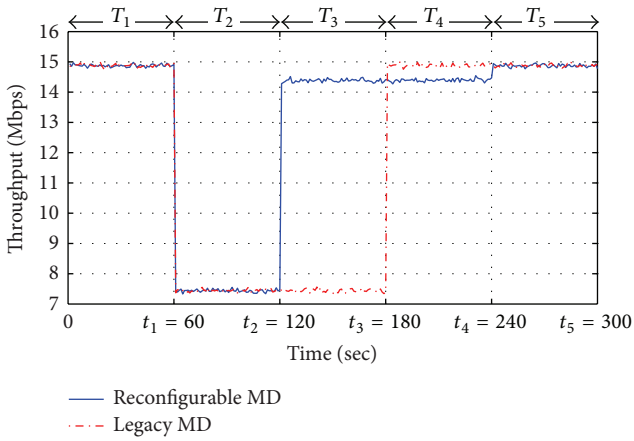

FIGURE 8: Throughput measured at the receiving MD according to the experimental scenario shown in Table 1.

QoS to be satisfied with FDD LTE. Note that, with the signal environment of QoS being satisfied, as mentioned earlier, it is implemented by allocating all of the spectral resources transmitting eNB to the target MD. Note that the maximum throughput of FDD LTE, 14.88 Mbps, can be calculated from the system parameters shown in Table 2 as 744,336 (number of 16 QAM symbols per frame) $*$ 0.5 (channel coding rate) $*$ 4 (number of bits per 16 QAM symbol)/10 ms (frame length). During the second time slot, T_2, the signal environment was set up for QoS not being satisfied and the LSA band not being available, as shown in Table 1. Setting the threshold value for determining whether or not QoS is satisfied to be 10 Mbps at the receiving MD, we have allocated only half of all the spectral resources of eNB to the target MD in order to implement the signal environment as QoS not being satisfied. It can be observed that, with half of all the spectral resources transmitting eNB, the maximum throughput is nearly 14.88/2 = 7.44 Mbps, which is far less than the threshold value of 10 Mbps. During T_2, eNB transmits data with only half of the entire spectral resources with which the throughput cannot exceed the threshold; therefore, QoS is not satisfied. Since the signal environment during T_2 does not provide the LSA band either, both the reconfigurable and legacy MDs cannot help staying in FDD LTE with nearly the same throughputs, 7.32 Mbps and 7.33 Mbps, respectively. During T_3, since eNB transmits the signal in both FDD and TDD LTE, meaning that the LSA band is now available, the reconfigurable MD can exploit the throughput of TDD LTE, 14.39 Mbps, by switching its configuration from FDD LTE to TDD LTE of the LSA band. The legacy MD, however, stays in FDD LTE with only a half throughput. Note that the maximum throughput of TDD LTE, that is, 14.5 Mbps, available with the system parameters shown in Table 2 can be calculated as 47,986 (number of 64 QAM symbols per frame) $*$ 0.5 (channel coding rate) $*$ 6 (number of bits per 64 QAM symbol)/10 ms (frame length). During T_4, as eNB transmits the signals of FDD LTE that satisfy the QoS requirement, the legacy MD can secure the maximum throughput comparable to the one obtained during T_1. Since the throughput is maintained above the threshold, the reconfigurable MD stays in TDD LTE. Since the throughput of TDD LTE has been arbitrarily set up a little bit lower than that of FDD LTE in our test-bed system, the throughput of the reconfigurable MD happens to be slightly lower than that of legacy MD during T_4. During T_5, as the LSA band is no longer available, the reconfigurable MD changes its configuration back to FDD LTE from TDD LTE with its throughput returning to the one obtained during T_1. Note that the lengths of the time intervals could be related to the possible interferences to/from primary/secondary users of the spectrum. In addition, since the transition in between the configuration changes takes about 5–10 ms in our test-bed, the lengths of T_3 and T_4 where the LSA band is available should not be too short for the MDs using the LSA band to exploit the benefit of LSA. But it should not be too long because, otherwise, the MDs occupying the LSA band could interfere with the primary users.

From our experimental tests performed in accordance with the preset scenario shown in Table 1, it is clear that, in order to fully utilize the benefits of the LSA band, the configuration of MD should be adjustable to the radio application used in the LSA band, which is set to TDD LTE in our experiments.

5.2. Computer Simulations. In the test-bed implemented for the experimental tests, the number of the reconfigurable MDs and that of legacy MDs were only 1 as shown in Figure 7. In this subsection, we introduce computer simulations performed for a scenario of multiple users in a given LSA band. The system parameters shown in Table 2, which were used for the experimental tests, have been adopted again in the simulations. The total number of users, which consists of the reconfigurable MDs as well as legacy MDs, is set to be 100 in the simulations. For simplicity but without loss of generality, we assume that the number of MDs that can be allowed using the LSA band is limited to 30 by the NRA shown in Figure 2 [5] in our simulations. Furthermore, the Rx throughput of each user has arbitrarily been set up with a random number between 30 Kbps and 300 Kbps where the threshold value that determines whether or not QoS is satisfied has been set up to 100 Kbps. Therefore, those MDs whose throughput is below the threshold, that is, 100 Kbps, are to apply for the LSA band by changing their configurations from FDD LTE to TDD LTE. Among those MDs, not more than 30 MDs are randomly selected for using the LSA band in our simulations. Consequently, the Rx throughput of each reconfigurable MD that has been allowed using the LSA band would be changed from a random number between 30 Kbps and 100 Kbps to another random number between 100 Kbps and 300 Kbps, if the reconfigurable MDs have been accepted to use the LSA band.

Figure 9 illustrates accumulated sum rates when the portion of the reconfigurable MDs is 0%, 10%, 50%, 70%, and 100% of the entire 100 users. As shown in Figure 9, since the LSA band is not available until the end of T_2, the accumulated sum rates for all the cases are quite comparable. As the LSA band becomes available during the time interval of T_3 and T_4, the sum rates increase more rapidly as the portion of the reconfigurable MDs is higher. Note that the

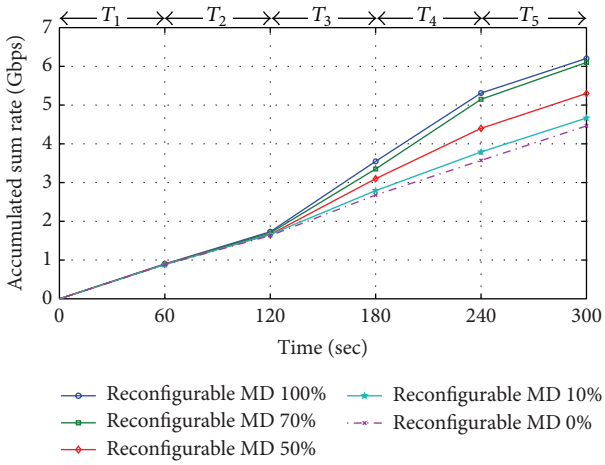

Figure 9: Accumulated sum rates.

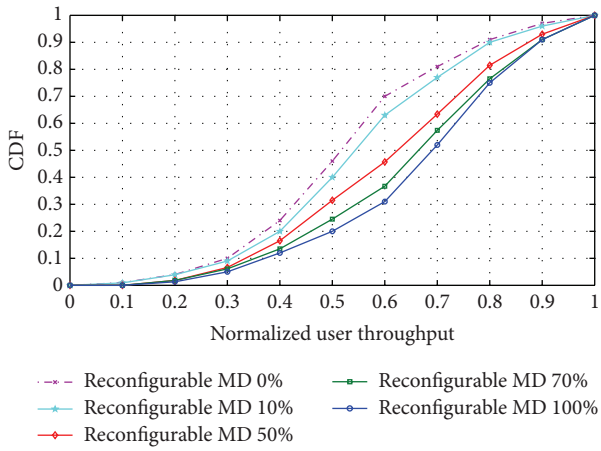

Figure 10: CDF according to the normalized user throughput.

number of the reconfigurable MDs whose throughputs are improved due to the LSA technology increases as the portion of the reconfigurable MDs is higher. From Figure 9, it can be observed that more number of reconfigurable MDs improves the accumulated sum rate more conspicuously.

Figure 10 illustrates Cumulative Distribution Function (CDF) according to the normalized user throughputs for the cases of the different reconfigurable MD portions, that is, 0%, 10%, 50%, 70%, and 100% of the entire 100 users. The normalized user throughput has been obtained by normalizing the throughput of each user with the maximum user throughput. As shown in Figure 10, when the entire user group consists of purely legacy MDs, for instance, the Rx throughput of nearly 70% of the entire users is less than 60% of that of the maximum user throughput. In contrast, when the entire user group consists of the reconfigurable MDs, only 30% of the entire user suffers from the low throughput, that is, 60% of that of the maximum user throughput. In other words, the other 70% of the entire users can enjoy the Rx throughput of higher than 60% of that of the maximum user throughput. From Figure 10, it can be concluded that more number of the reconfigurable MDs brings about more number of users satisfying the QoS.

6. Conclusion

In order to fully exploit the merits of LSA, the configuration of MD should be adjustable to the RA adopted in the LSA band. This paper shows the performance evaluation of reconfigurable MD in terms of system throughput in comparison to legacy MD in a preset test signal environment. For experimental tests, we implemented a prototype of reconfigurable MD with a system architecture that is compliant with the ETSI-standard reference architecture suggested by WG2 of ETSI TC-RRS [13]. The prototype MD has been implemented using NVIDIA GeForce GTX Titan GPU and USRP N210 as its modem and RF transceiver, respectively. In order to set up the configuration of MD in accordance with the radio application adopted in the LSA band, we also developed a systematic procedure for transferring control signals among the software entities defined in the reference architecture. The procedure shown in this paper is based on the use case of expanding bandwidth using LSA released by WG1 of TC-RRS of ETSI in [9]. Through the experimental tests performed with the prototype MD and computer simulations in a simple test environment, it has been verified that the reconfigurability of MD is a necessary condition for LSA technology to fully obtain its benefits.

Competing Interests

The authors declare that they have no competing interests.

Acknowledgments

This research was supported by the MSIP (Ministry of Science, ICT & Future Planning), Korea, under the ITRC (Information Technology Research Center) support program (IITP-2015- H8501-15-1006) supervised by the IITP (Institute for Information & Communications Technology Promotion).

References

[1] Cisco Visual Networking Index, *Global Mobile Data Traffic Forecast Update 2012–2017*, vol. 6, 2013, White Paper.

[2] E. Hossain and M. Hasan, "5G cellular: key enabling technologies and research challenges," *IEEE Instrumentation and Measurement Magazine*, vol. 18, no. 3, pp. 11–21, 2015.

[3] W. Roh, "5G mobile communications for a connected world and recent R&D results," in *Proceedings of the Smart Radio Symposium*, Seoul, Republic of Korea, June 2015.

[4] M. Matinmikko, H. Okkonen, M. Palola, S. Yrjölä, P. Ahokangas, and M. Mustonen, "Spectrum sharing using licensed shared access: the concept and its workflow for LTE-Advanced networks," *IEEE Wireless Communications*, vol. 21, no. 2, pp. 72–79, 2014.

[5] K. Jamshid et al., "Licensed shared access as complementary approach to meet spectrum demands: Benefits for next generation cellular systems," in *Proceedings of the ETSI Workshop on*

Reconfigurable Radio Systems, Cannes, France, December 2012.

[6] "Electronic Communications Committee (ECC) Report 205," Licensed Shared Access (LSA), 2014.

[7] M. Matinmikko, M. Palola, H. Saarnisaari et al., "Cognitive radio trial environment: first live authorized shared access-based spectrum-sharing demonstration," *IEEE Vehicular Technology Magazine*, vol. 8, no. 3, pp. 30–37, 2013.

[8] M. Mustonen, T. Chen, H. Saarnisaari, M. Matinmikko, S. Yrjölä, and M. Palola, "Cellular architecture enhancement for supporting the european licensed shared access concept," *IEEE Wireless Communications*, vol. 21, no. 3, pp. 37–43, 2014.

[9] ETSI TR 103.113, *Mobile Broadband Services in the 2300–2400 MHz Frequency Band under Licensed Shared Access Regime*, vol. 1.1.1, 2013.

[10] ETSI TS 103. 235, "System requirements for operation of Mobile Broadband Systems in the 2 300 MHz–2 400 MHz band under Licensed Shared Access (LSA)," V1.1.1, 2014.

[11] ETSI, "System architecture and high level procedures for operation of Licensed Shared Access (LSA) in the 2300 MHz–2400 MHz band," ETSI TS 103.235, 2015, v0.0.12.

[12] ETSI TS 136 101, *LTE; Evolved Universal Terrestrial Radio Access (E-UTRA); User Equipment (UE) Radio Transmission and Reception*, vol. v12.7.0, 2015.

[13] ETSI EN 303 095, *Reconfigurable Radio Systems (RRS); Radio Reconfiguration related Architecture for Mobile Devices*, vol. v1.2.1, 2014.

[14] ETSI TS 103 146-1, *Reconfigurable Radio Systems (RRS); Mobile Device Information Models and Protocols; Part 1: Multiradio Interface (MURI)*, vol. v1.1.1, 2013.

[15] ETSI TS 103 146-2, *Reconfigurable Radio Systems (RRS); Mobile Device Information Models and Protocols; Part 2: Reconfigurable Radio Frequency Interface (RRFI)*, vol. v1.1.1, 2015.

[16] M. Mueck, V. Ivanov, S. Choi et al., "Future of wireless communication: RadioApps and related security and radio computer framework," *IEEE Wireless Communications*, vol. 19, no. 4, pp. 9–16, 2012.

[17] ETSI, "Reconfigurable Radio Systems (RRS); multiradio interface for Software Defined Radio (SDR) mobile device architecture and services," ETSI TR 102.839, 2011, v1.1.1.

[18] http://www.ubuntu.com.

[19] ETSI TS 136 101, "*LTE; Evolved Universal Terrestrial Radio Access (E-UTRA); User Equipment (UE) radio transmission and reception (3GPP TS 36.101)*," v10.6.0, 2012.

[20] http://www.geforce.com/hardware/desktop-gpus/geforce-gtx-titan.

[21] http://www.ettus.com/product/details/UN210-KIT.

[22] C. Ahn, S. Bang, H. Kim et al., "Implementation of an SDR system using an MPI-based GPU cluster for WiMAX and LTE," *Analog Integrated Circuits and Signal Processing*, vol. 73, no. 2, pp. 569–582, 2012.

Hindawi Publishing Corporation
Mobile Information Systems
Volume 2016, Article ID 4313527, 12 pages
http://dx.doi.org/10.1155/2016/4313527

Research Article

Licensed Shared Access System Possibilities for Public Safety

Kalle Lähetkangas,[1] Harri Saarnisaari,[1] and Ari Hulkkonen[2]

[1]*Centre for Wireless Communications, University of Oulu, 90014 Oulu, Finland*
[2]*Bittium Wireless Ltd., Tutkijantie 7, 90570 Oulu, Finland*

Correspondence should be addressed to Kalle Lähetkangas; kallela@ee.oulu.fi

Received 11 March 2016; Accepted 30 May 2016

Academic Editor: Fernando Casadevall

We investigate the licensed shared access (LSA) concept based spectrum sharing ideas between public safety (PS) and commercial radio systems. While the concept of LSA has been well developed, it has not been thoroughly investigated from the public safety (PS) users' point of view, who have special requirements and also should benefit from the concept. Herein, we discuss the alternatives for spectrum sharing between PS and commercial systems. In particular, we proceed to develop robust solutions for LSA use cases where connections to the LSA system may fail. We simulate the proposed system with different failure models. The results show that the method offers reliable LSA spectrum sharing in various conditions assuming that the system parameters are set properly. The paper gives guidelines to set these parameters.

1. Introduction

The wireless operators should prepare for 1000 times growth in mobile data over the next 10 years [1, 2]. This growth is giving pressure for governmental spectrum users, which rarely utilize their spectrum, to free up their frequencies for commercial use. In the United States, 500 MHz of the spectrum from the federal and nonfederal applications is going to be freed completely or by spectrum sharing for commercial mobile radio systems by the year 2020 [3]. This may be the direction also in Europe. The main interest in the United States for spectrum sharing is the spectrum access system (SAS) [3]. For spectrum sharing in Europe, licensed shared access (LSA) [4–7] has gained interest, since the LSA systems can be made operator-specific. More specifically, the operators of every country can agree on their own spectrum utilization between the possible secondary users. LSA has been proposed as an option for sharing the spectrum with PS in [8].

This work extends our work in [9] and first gives an overview of how special applications such as public safety, shortly PS hereafter, and other governmental users fit into the possibilities of spectrum sharing with LSA and how to prepare for it. The PS has a wide range of different users and applications needing the spectrum. The users are, for example, first responders, police, firefighters, border control, and military, which are vital for the society. One of the critical issues in deploying commercial technology to these kinds of special applications is the ownership of the spectrum. For example, by the PS being an LSA licensee, it can obtain the legal right to utilize additional LSA spectrum resources when they are available. Note that the PS can also be an incumbent of other predetermined frequencies for guaranteed resources. While there are multiple choices for PS to utilize spectrum sharing, it is also a political decision how the spectrum will be shared. Spectrum sharing principles for public safety have been categorized in five different sharing models in [10] and the spectrum sharing has been extensively studied further in [11]. There is also ongoing work on use cases for synergies between commercial, military, and public safety domains in [12]. We examine sharing approaches in the means of owned spectral resources and their advantages and disadvantages. To our knowledge, this issue has not been considered previously although it may be one of those steps that are needed for the release of spectrum with LSA and for system development therein.

After the review of this novel topic, our second contribution is planning a more specific system where the PS is

an LSA licensee for LSA spectrum resources. Importantly, if the PS utilizes LSA spectrum resources, the PS requires the sharing process to be robust against connection problems. The fall-back measures for the LSA system are generally presented only on a high level [7] and they are still in the planning phase. While the LSA system has been implemented and demonstrated in the project [4], the trials have not yet included any connection breaks inside the LSA system. Our objective is to plan a system that can be tested in a live environment. More specifically, we design a highly robust LSA system to be implemented with current commercial technology and equipment. By robust it is meant that the proposed system is resilient to connection breaks in the LSA system that may be reality in real life due to electric breaks, and so forth, that is, in the cases where the PS services are often needed.

We validate our proposed spectrum reservation method via simulations. We study the duration of time intervals between connection checks for noticing connection breaks and the effect of doing the resource reservations a predetermined time before the incumbent transmissions. These are the main system design parameters and the aim is to give guidelines for selecting them properly.

The paper is organized as follows. In Section 2, we go through the different spectrum sharing possibilities with commercial domain and PS. In Section 3, we present a system model of an LSA system to be built in a live network for the PS and the key functionalities of the system components to overcome connection breaks. In Section 4, we present validating simulation results of the LSA system. We conclude the paper in Section 5.

2. Spectrum Sharing Possibilities

In this section, we provide an overview of alternatives for the spectrum sharing in the case of PS and a commercial system (CS). The truth is that the PS might not always use their full spectrum and it might remain available most of the time, at least locally. Examples are police patrolling where just a small voice service part of the spectrum needs to be reserved and military users that often, in peace time, need large part of the spectrum only in exercises and in special exercise areas. Naturally, in the case of increased threat they need it in patrolling in the cities, and so forth. The temporally and spatially available spectrum could be used for other purposes at those times unused by the PS assuming it will be released immediately back to the PS when needed. For example, the nonused spectrum can be used to speed up CS transmissions, for example, to ease rush hour data traffic; naturally, this is of interest in areas that have a high mobile traffic and that are not in isolated areas.

In addition, the PS may also need complementary or additional resources for its events and thus it would be beneficial for them to get spectrum from CSs. For example, when there is a large fire in a city, the demands of the PS users can grow dramatically especially if they would like to use new services like live video streaming, connections to data bases to collect information about the area, and social media to alarm people. In that case, the PS requires their full spectrum and possibly even more. With spectrum sharing, the additional spectrum can preferably be obtained from silent commercial devices. The target spectrum bands considered are any bands that can be exploited by the PS, for example, the bands of mobile operators and wireless camera and microphone systems.

In Figure 1, we plot different options for spectrum sharing in the means of owned spectral resources. The different options for allowing the other entity to use the spectrum are depicted with arrows. All the approaches can be grouped as follows. First, the sharing framework is designed so that the CS users are the LSA licensees. This way, incumbent is always allowed to use the spectrum and the CS obtains additional spectrum. Second, the CS is incumbent and complementary spectrum is given to the LSA licensee such as the PS. Third option is that all the users are using the CS. Note that these ideas can also be used in parallel in different situations and areas. We briefly list the above spectrum sharing system possibilities and their advantages and disadvantages as follows.

The PS Owns a Relatively Wide Spectrum (See Figure 1(a))

(1) The incumbent PS allows CS to use all its spectrum. In some areas, where the incumbent does not usually have activity, allowing is more or less naturally permanent. In cities, the incumbent activity can be more frequent and allowing happens on a faster time scale.

(2) The incumbent PS allows CS to use its free spectrum. The incumbent system might not need the entire spectrum but only parts of it. Thus, the remaining available spectrum can be utilized by the CS.

(+) The incumbent has all the control for spectrum utilization.

(+) The incumbent has a predictable quality for its applications.

(+) CS obtains additional spectrum.

(−) No guaranteed additional resources for CS.

(−) CS need devices that work using the spectrum of the incumbent.

CS or Other Applications Own the Majority of the Spectrum (See Figures 1(b) and 1(c))

(1) CS gives its available spectrum to the PS (Figure 1(c)).

(2) CS has the obligation to give enough spectrum to the other system using the spectrum during critical operations (Figures 1(b) and 1(c)).

(3) CS has the responsibility to give all its resources, including physical equipment, to PS during critical operations.

(4) Some spectrum can be given for CS by the other system but, as a tradeoff, they can be demanded to give their spectrum to the other system in highly critical situations.

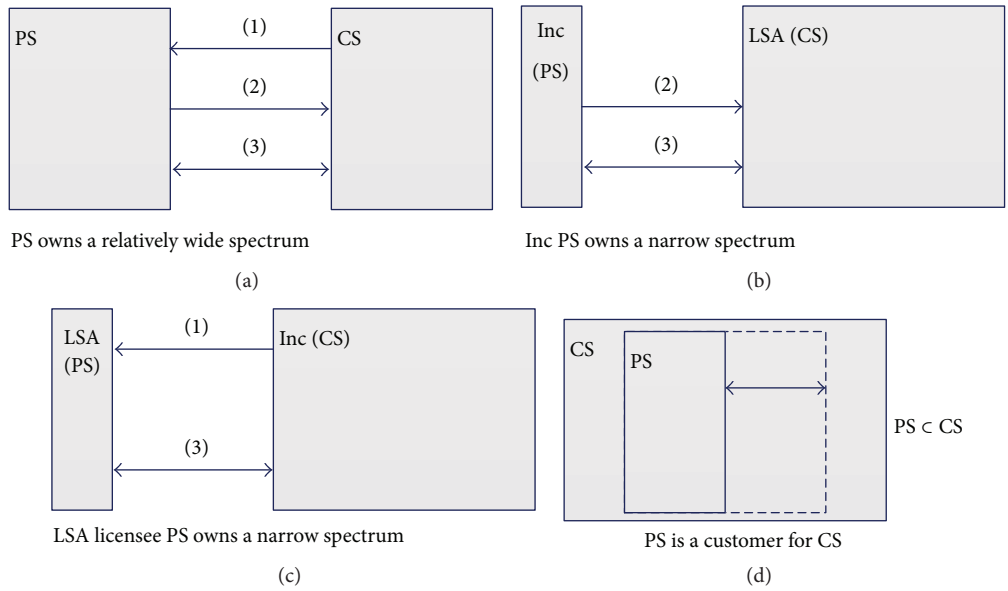

Figure 1: We have different options for spectrum sharing. We use Inc as an abbreviation for the incumbent of the system. (a) The PS owns sufficient number of spectra to support all of its requirements. (b) The incumbent PS has only the critical number of spectra and CS has a wide spectrum. (c) The PS is LSA licensee of CS. After the overview, we concentrate more specifically on this setting where CS allows spectrum use to PS. (d) The incumbent is a roaming user at the CS network. (1) CS allows spectrum use. (2) PS allows spectrum use. (3) CS is allowed to use the spectrum given that CS is obligated to give spectrum when needed.

(+) The LSA licensee obtains additional resources for its applications.

(−) If CS is obligated to give spectrum to the other user, the CS cannot have guaranteed resources.

CS Has a Complete System (See Figure 1(d); Users, Such as PS, Utilize the CS Network)

(1) All of the spectrum users, PS and CS, can be roaming users of the CS network.

(2) The PS can rent/obtain the CS network for their own use.

(+) The PS obtains instant coverage.

(+) The CS is constantly developing its network.

(−) The PS does not have complete control over the CS network.

(−) The system needs a priority protocol, if the incumbent users are PS users.

(−) There is no coverage or support for all the applications at every location. The PS still needs their own service in the areas where the CS network cannot support it.

(−) The PS has to trust CS and their security when being an CS user.

The current state of the affair is that the PS and CS have their own spectrum and they do not cooperate. Here, to obtain similar functionalities as the CS, the PS requires equal amount of spectrum as CS. The first step to this setting is cooperation, as illustrated in Figure 1(a). Naturally, sharing rules have to be agreed on; that is, CS, PS, or both allow their spectrum to be used by the other one. In the following subsections, we go through the options for spectrum sharing in more detail for LSA systems.

2.1. PS Is the Incumbent. In this subsection, we consider options for when the PS is the incumbent in an LSA system as, for example, in Figures 1(a) and 1(b). Here a part of the PS spectrum has been released for CS under the requirement that they must allow the incumbent PS to use that spectrum when and where needed. Obviously, this situation requires a political decision but it is listed here as an opportunity. It is discussed in the US that, in this scenario, the CS and other users can share the spectrum as secondary users [3]. Moreover, in the US, a wide bandwidth of spectrum will be released from governmental users to CSs in the upcoming years. Note that the majority of spectra can still be used by the PS during critical operations.

By being the incumbent, the PS has all the control to support its critical and noncritical applications with a predictable quality. Here the PS can build its network infrastructure and the management system for organizing its network and services. However, the PS might not build a nationwide network for itself. Moreover, the PS might not use its spectrum all the time. This leads to free spectrum which can be utilized by other applications. A possibility is to cooperate with a CS. The additional spectrum could be used as a complementary resource by the CS to unload its data traffic. There are multiple possibilities for cooperation.

First, the PS can allow the CS to use the spectrum at predetermined times and areas. This is applicable when the possible PS spectrum usage is known in advance. This is

the case, for example, when the PS has scheduled their operations. In these cases, the PS can have the spectrum for the reserved time and area, even if they are not using it. With this method, the spectrum is free at given times and the individual PS users do not need to worry about the CS transmitting at the same time. This is applicable, for example, in some of the military training scenarios and in border protection as the military is mostly using their spectrum in known areas during peace time.

As a second option, the PS can allow the CS to use the spectrum at all the times when the spectrum is free. This option needs a rapid method for the spectrum reservation. Here the PS should preferably notify the LSA repository a few moments before the transmission, so that the spectrum can be guaranteed to be free for the PS. Another possibility is for the PS to notify the LSA repository when the transmission begins. In this setting, the PS should accept possible interference from the LSA licensee in the beginning of its transmission. Moreover, in the scenarios above, the fall-back measures to handle connection breaks for guaranteeing the possible incumbent transmission should be expeditious.

Third, the PS can allow the CS to use the spectrum at the locations where the spectrum is not currently needed by the PS users. This option can be accomplished by tracking the PS users and by reserving the necessary spectrum for them at their locations. This is applicable for example, with the first responder units, whose locating is important also from the operational perspective.

Fourth, depending on the applications, the PS might not always need all of its frequencies. The PS can allow the CS to use the remaining free frequencies. Here the spectrum band can be divided into multiple smaller bands that can be accessed with the CS according to the need of the PS users.

Moreover, any combination of the above is also possible. In these systems, however, the spectrum is a complementary resource for the CS when the PS users are silent. To start building the system, the agreements between the incumbent PS and commercial LSA licensees can be first allowed in smaller areas. Then, if the CS is able to develop their applications in such a way that they do not cause intolerable interference to the PS operations, the agreements are easy to expand to wider areas.

The amount of gain obtained by the CS depends on the activity of the PS. For example, if the PS is silent most of the time, the CS obtains the spectrum most of the time. The greatest benefit for the PS by owning the spectrum is the control. It is possible for the PS to freely use the spectrum for its own applications. In addition, it is always possible to decline the spectrum use of the CS or other spectrum users. However, the resources owned by the PS might still not be enough to support all the PS operations. Moreover, the PS might not want to reserve a wide spectrum for its applications. Thus, it may be beneficial for the PS to also obtain additional resources and services from the CS when needed.

2.2. CS Is the Incumbent. In this subsection, we consider options for when the CS is the incumbent in an LSA system as shown in Figure 1(c). The CS has a wide spectrum and is giving spectrum resources to the PS, which only has a small portion of spectrum reserved, for example, to voice communication. Later in this work, we will concentrate only on this scenario in developing an LSA system for the PS. There are multiple possibilities for cooperation, which can all be implemented in parallel depending on the needs by the PS.

First, the resources can be shared with an LSA system. When the incumbent user comes to the area, PS will retreat or change its frequency. This suits the case when the PS is mostly using the spectrum in the area, where the CSs or other incumbent users remain silent. This is applicable if the PS uses spectrum mainly for noncritical applications, such as training, and has the authority to reserve the spectrum completely for itself during critical operations for obtaining spectrum. This is the use case, for example, in military and border control applications, where the PS would require spectrum for their communication during peace time. These PS operators can agree on multiple LSA agreements with multiple incumbents to obtain multiple spectrum bands. Then, they are able to legally utilize the band that is available. With PS being the LSA licensee, the PS users do not necessarily need to inform their location to the LSA repository, and the PS users are not tracked for spectrum information. This type of LSA sharing method brings security in some PS applications, where the location of PS operators should be kept as a secret. Another example of resource sharing like this is a high speed mobile network for the PS at sparsely populated training areas. This kind of high speed networks can also offer a backup mobile infrastructure, for example, in disaster areas and in rescue operations during electrical shortages when a commercial network of the CS is down.

Second, the CS can be obligated to give spectrum to the PS in areas that are not covered by the CS network. Thus, the PS can obtain spectrum for its own use here, that is, for training and for emergency use. This option is applicable in the long term only if the CS is not building its network in these areas, for example, if these areas give no financial benefit. Otherwise, there is no long-term guarantee of interference-free spectrum for the PS.

Third, the CS has the obligation to give required spectrum to the PS during critical operations. Here the PS can have the rights of the incumbent during critical operation. This is a viable option when the PS is mainly a minor user of the spectrum and critical operations happen rarely. The CS can build its network using a wide spectrum. Then, the spectrum is released when the PS users come to the area and need it. This option would require a backdoor for PS to be installed to CS equipment. For example, by using the backdoor, the PS could reserve spectrum or switch off related CS base stations with alarm signals or via central controller. In some PS cases, the spectrum can also be reserved in advance by the basis of the emergency calls, which usually happen via CS base stations and near the locations of the required PS needs.

2.3. PS Utilizes CS Network. One additional option on the above scenarios is the following. As shown in Figure 1, the PS users can be the roaming users of the CS network [13, 14].

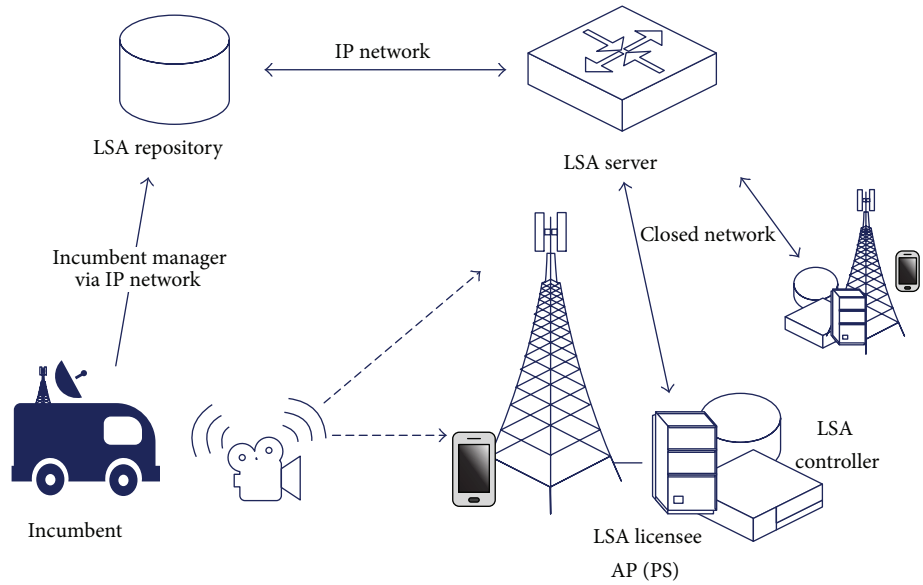

Figure 2: A wireless camera uses the spectrum with LSA licensee that has LSA controllers at every AP.

Here the entire spectrum is owned by CS and it is responsible for building the network. However, in order for the PS to be independent of CS networks, a backup system for the most critical applications and communication is still needed. Note also that this option is not spectrum sharing in the means of LSA, but is listed here as an opportunity.

When the PS users are roaming users at the CS network, they need priority over the CS users. Here the PS should obtain the highest priority for its critical applications. In addition, when the PS users are roaming users at the CS network, the CS operator needs to be able to support PS applications. The benefit of being a roaming user is the instant coverage of the CS network in densely built areas. Another benefit is that the CS develops its spectrum usage to meet the current requirements better because it is competing for users. However, the PS does not have full control over the network which reduces the security. Moreover, there needs to be solid encryption for the PS and the CS network should be built robustly.

3. System Model

Next we concentrate more specifically on developing the LSA system for the PS, which acts as an LSA licencee for accessible LSA spectrum resources as discussed in Section 2.2. The PS use case considered here is only for noncritical applications. The proposed resource allocation method builds on previous LSA work in [15, 16].

We consider an LSA system with an LSA repository, LSA controllers, an LSA licensee, and an incumbent user. These system elements and their connections are shown in Figure 2. The incumbent is the primary user of the LSA spectrum resources. We consider the incumbent to be, for example, employees of programme making and special events services, which are defined in [17, 18]. The LSA repository collects, maintains, and manages up-to-date data on spectrum use. The LSA licensee is a secondary user with a license to utilize the spectrum, when incumbent user is silent. The LSA licensee has multiple access points (APs) that utilize the resources. The LSA licensee has a network that connects the APs together. In contrast to [15] with one LSA controller, every AP of PS has its own distributed LSA controller. Thus, no single device is solely responsible for the spectrum allocations.

We also introduce an LSA server to the system. The LSA server is a mediator between the LSA repository and the LSA controllers. By using a mediator, the PS network can be kept closed from the IP network, which provides security. Here, the LSA server is the only device of the PS network that can be connected from the outside. The LSA server reports only the necessary network information from the LSA licensee network to the LSA repository.

The spectrum sharing between the users operates as follows. Incumbent user reserves the spectrum at least a predetermined time before using the spectrum, contrary to the on-demand operation mode for LSA spectrum resource reservation [6]. Thus, during a connection break the most recent information is still valid for the predetermined time. The incumbent reserves the resources by connecting the LSA repository with an incumbent manager. Then, the repository sends notification of the spectrum reservation to the LSA server. After the LSA server obtains spectrum reservation information, it forwards the information to the LSA controllers of affected APs. Finally, the LSA controllers compute the protection criteria of incumbent and control the spectrum usage of the APs.

In Figure 3, we present more precisely how to implement this system in a real Long-Term Evolution (LTE) network. We depict the components and their connections. Here LTE APs (eNodeBs) of PS utilize the spectrum as an LSA licensee. The PS has its own closed LTE network where the backhaul is

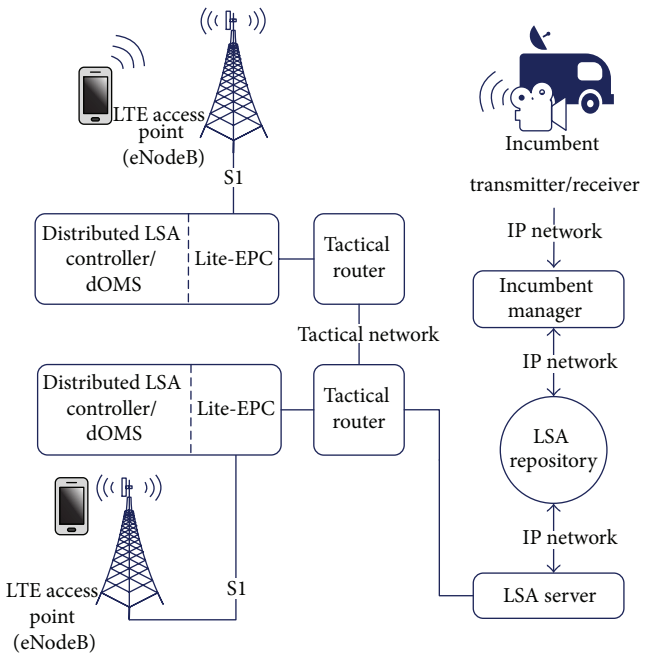

Figure 3: Two LTE access points in LSA licensee network.

built with tactical routers. In addition to wired links, these routers also support radio link connections [19]. They can also automatically reroute any given data from the source to the destination via alternative routes, given that the primary route fails. Every AP is connected to the closed network via a lite-EPC and a tactical router. The lite-EPCs provide LTE hot spots to the network and emulate the evolved packed core functionalities of an LTE network. The access points are connected with S1 interface to the lite-EPC. The computer with the lite-EPC works also as a distributed LSA controller. The LSA system components communicate with each other using http(s) with representational state transfer architechture. The data is formatted using JavaScript objects. We go through the main functions of the main components in the following subsections.

3.1. Incumbent via Incumbent Manager. Incumbents of our system use a http(s)-based incumbent manager to inform the repository of their spectrum access. The reservation message includes "starting" and "ending" time of the incumbents transmission, the reserved frequencies (center frequencies and bandwidths), the location, and the type of the usage. The reservation information is used to calculate the protection zone for incumbent.

The incumbent manager allows reserving the spectrum only for a predetermined time beforehand. More specifically, incumbent has to send a reservation message via incumbent manager to the LSA repository at least a predetermined time T_i before its transmission. This time can vary for different types of users. Additionally, the requirement for reservation of a predetermined time before the incumbent transmission can also be voluntary in some of the systems. Then, if the incumbent does not reserve the spectrum on time, it is obligated to possibly tolerate interference from the LSA licensee for the predetermined time, given that there are connection breaks.

3.2. LSA Repository. The LSA repository keeps a database of up-to-date information about incumbent spectrum reservations and about the conditions for utilizing the spectrum. The LSA repository forwards information about incumbent and its planned use of LSA spectrum resources to the LSA server, when the information becomes available. The information sent from the repository also includes the time when it is sent. The LSA repository can also reply to a request for the incumbent information. This reply includes the information that is new to the requesting device.

Connection checks to the LSA repository happen via heartbeat signals. The devices, which check the connection, request heartbeat signals periodically from the LSA repository. The LSA repository replies to a heartbeat request with a heartbeat signal. If there is no response, the connection is broken. Heartbeat response signals include the time when the heartbeat response signal is sent.

3.3. LSA Server. The LSA server acts as an LSA controller to the LSA repository. It has a strong firewall for separating the PS network from the IP network. After obtaining incumbent information from the LSA repository, the LSA server broadcasts this information to the distributed LSA controllers. The LSA server also saves incumbent information until the information expires. To obtain robustness for connection breaks to this setting, any tactical router could act as an LSA server, given that it has an Internet access and given that it has a programmable interface.

The LSA server sends heartbeat requests to the LSA repository between time intervals of T_{check}. The heartbeat responses are then forwarded to the LSA controllers. The LSA server notices a connection break to the LSA repository if there is no heartbeat signal within time T_{timeout} from the heartbeat request. When this kind of connection break occurs, the LSA server sends heartbeat failure signals to the lite-EPCs periodically between time intervals of T_{check}. These signals provide the LSA controllers information whether the connection break is external or internal.

The LSA server tries to reconnect to the LSA repository during a connection break. The LSA server requests up-to-date incumbent information from the LSA repository when becoming connected to it. The LSA server can also answer to a request for incumbent information and replies with the information that is new to the requesting device.

3.4. LSA Controller in Lite-EPC Computer. The LSA controllers control the spectrum utilization of the PS. They receive the incumbent information from the LSA server when it becomes available. Additionally, an LSA controller requests for up-to-date incumbent information from the LSA server when becoming connected to the PS network. All of the LSA controllers save the received incumbent information until it expires. The main task for an LSA controller is to calculate the protection zone for the incumbent using incumbent

information. The calculation is done similarly at every LSA controller using the same algorithms as in the centralized controller developed by the project [4]. However, a lite-EPC controls only the AP that is connected to it.

3.5. Distributed Operations Management System. We have depicted distributed operations management system as (dOMS) in Figure 3. The dOMS are distributed per AP and also work in the same computers as the lite-EPCs. They are responsible for sharing the spectrum between the other APs and include command tool for controlling the AP and the necessary commission plans with a site manager for validating the plans. Each of the individual dOMS sends command messages to their own APs for the frequency allocations and power levels. In other words, every unit of dOMS controls only their own AP but decides the spectrum sharing together with other units of dOMS.

The spectrum sharing between APs is done in dOMS that keep a list of APs in the vicinity. To share the LSA spectrum resources, the dOMS utilize signaling methods similar to coprimary spectrum sharing [20]. The difference to [20] is that the spectrum sharing is done between a single PS operator, without the need to compete with other operators. The signaling messages are sent inside the closed PS network.

The dOMS has the task to clear the spectrum, before incumbent utilizes the spectrum and when the spectrum reservation information becomes invalid due to a connection break. Recall that the sending times are included in all of the data originating from the LSA repository. The spectrum reservation information is valid for time T_i after a successful heartbeat signal, or any other data, is sent from the LSA repository.

Let T_{empty} be the time that it takes to empty the spectrum by the AP after a command from the dOMS. If no heartbeat signal or other data arrives from the LSA repository, the LSA spectrum resources are freed after time $T_i - T_{\text{empty}}$ from the sending time of the last successful data from the LSA repository. The spectrum can be emptied immediately or gradually by using graceful shutdown, which gradually lowers the power level of the APs. The dOMS can also order its AP to utilize some available backup frequency. Alternatively, any other fall-back measure [7] can be used.

4. Simulation Setup and Numerical Results

In this section, we present our simulation setup and results for our LSA system. We use simulations to validate the spectrum reservation method setup in the case of connection breaks inside the IP network. We assume that the closed PS network is built reliably. This means that there are no connection breaks inside the PS network. The incumbent is also assumed to utilize the LSA spectrum resources only after a successful reservation. This is a conventional method for incumbents, such as programme making and special events services, which are required to inform their spectrum utilization to a national telecommunications regulator. The connection breaks in the LSA system occurs in the IP network between the LSA repository and LSA controllers. We assume that the APs of PS with the same frequency are at a long distance from each other. We also assume that the APs, which are near each other, utilize different frequencies as usual. Thus, no dynamic spectrum sharing is simulated.

We use spectrum utilization and *valid spectrum knowledge* of the LSA licensee to measure the performance of the LSA system. The latter measure tells us the ratio of time that the spectrum reservation information is valid with respect to the total simulation time. For example, when the value of it is 0.5, the spectrum reservation information is valid for 50% of the time. Recall that the LSA licensee utilizes the free spectrum only when the spectrum knowledge is valid. Thus, the incumbent and the LSA licensee share the LSA resources perfectly only during this time. Therefore, the amount of valid spectrum knowledge reflects the LSA system performance. It also relates directly to the reliability of the LSA system, as the spectrum can be utilized by the LSA licensee during connection breaks if the spectrum knowledge is valid.

We show how our LSA system design parameters, T_{check} and T_i, affect the performance in different network scenarios with different incumbent activity levels. We simulate every scenario over 1000 iterations with different connection breaks and incumbents for average results. In every scenario, we draw the durations of the incumbent transmissions and connection breaks from Poisson distributions. We draw the number of incumbent transmissions and connection breaks from normal distributions, where the negative values are set to zero. The starting times of incumbent user transmissions and connection breaks are uniformly distributed. The rationale for using these simplifying distributions is to obtain first-level insights into our protocol behavior when using different design parameters in different scenarios. The total simulation time is 12 hours. The time to empty spectrum with an order from the dOMS, T_{empty}, is 30 seconds. The delay to transmit data from the LSA repository to the LSA controllers is three seconds when the connection is working.

We model the IP network connection breaks for different scenarios as follows. We model three types of network connections. They are *reliable*, *mediocre,* and *poor* and the parameters to simulate them are shown in Table 1. The last column, *Connection OK*, shows the quality of the connection, that is, the ratio of time that the connection is working between the LSA repository and LSA controllers with respect to the total simulation time. These ratios are also a point of reference for *valid spectrum knowledge* in the currently available LSA systems. More specifically, in the current LSA systems, the spectrum is shared perfectly only when the connection is working. The rationale for simulating low connection reliabilities comes from the fact that the PS should remain functional when the commercial IP networks have serious connection problems.

Similarly, we model the incumbent activity for three types of incumbents. The incumbent types are *rare*, *occasional,* and *active* and the parameters to simulate them are shown in Table 2. The last column, *spectrum utilization*, shows the ratio of time that the incumbent utilizes the spectrum with respect to the total simulation time.

Table 1: The parameters for simulating the connection quality.

	Mean # of connection breaks	Variance	Mean duration of a connection break	Connection OK
Reliable	0	2	5 min	0.99
Mediocre	7	2	20 min	0.73
Poor	15	2	60 min	0.29

Table 2: The parameters for simulating the incumbent activity.

	Mean # of transmissions	Variance	Mean transmission time	Spectrum utilization
Rare	0	2	40 min	0.06
Occasional	5	2	40 min	0.26
Active	12	2	40 min	0.50

In the next simulations, we study the LSA system performance with respect to T_{check}. Recall that the value of T_{check} is the time between heartbeat signal requests.

In Figure 4, the incumbent notifies about itself 15 minutes before its transmission; that is, $T_i = 15$ min. From Figure 4, we observe that the spectrum knowledge for *reliable*, *mediocre,* and *poor* internet qualities is higher than 99%, 73%, and 29%, which are the corresponding percentages of times for internet connection working. Thus, the spectrum can be utilized by the LSA licensee even during some of the connection breaks with our reservation method. Moreover, we see that the quality of the internet connection is important, when the incumbent informs about its spectrum utilization on a short notice.

From Figure 4, we also see that the spectrum knowledge by the LSA licensee is higher when T_{check} is low, that is, when the connection to the LSA repository is checked more often. This is because then it is more likely to get an answer from the repository for validating the connection. Therefore, with an unreliable internet connection, the value of T_{check} should be as low as possible to have the most valid spectrum knowledge. However, from the figure we also see that it is more important to have a good internet connection than to make the value of T_{check} as low as possible.

In Figure 5, the incumbent notifies about itself 60 minutes before its transmission; that is, $T_i = 60$ min. When comparing this figure to Figure 4, we see that the spectrum knowledge is overall better for every type of internet quality for a greater value of T_i. We also can see that setting T_i large is more important in terms of spectrum knowledge than to set T_{check} low. Moreover, we observe that the spectrum is known for over 50% of the time when the internet quality is *poor*, that is, when the internet connection is working 29% of the time. Therefore, the T_i should be large if the internet quality is low. From Figure 5, we see that the *mediocre* internet quality is allowable in this setting; that is, the spectrum can be utilized 100% of the time, when the T_{check} is below 3 minutes. Thus, given that the internet connection to the PS network can be mediocre, the PS should utilize frequencies of incumbents which are able to report their frequencies reliably in advance. Moreover, if the internet connection is poor, the PS requires either additional methods for utilizing all of the free spectrum

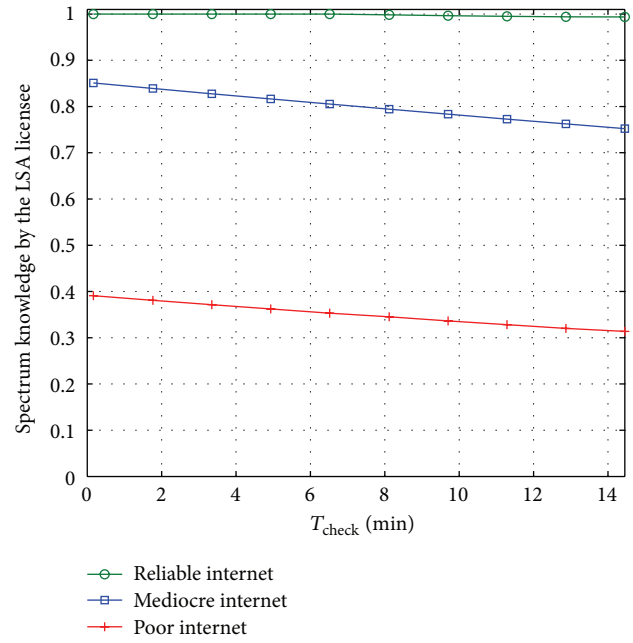

Figure 4: The spectrum knowledge of the channel as a function of T_{check} while $T_i = 15$ min with different qualities of internet connection. The incumbent is *rare*; that is, it utilizes the channel approximately 6% of the time.

or an incumbent that reports its spectrum utilization even earlier.

In the next simulations, we study the LSA system performance with respect to T_i, with different types of incumbents and internet qualities. Recall that the value of T_i indicates the predetermined time before which the incumbent is required to send its spectrum reservation to the LSA repository.

In Figure 6, the incumbent is *rare* and the T_{check} is set to be 15 minutes. From Figure 6, we see a rise of the spectrum knowledge as a function of T_i. This implies that when the internet quality is poor, the incumbent should reserve the spectrum as early as possible. This is applicable for incumbents that know their spectrum needs beforehand or rarely change their frequency allocations and have a static

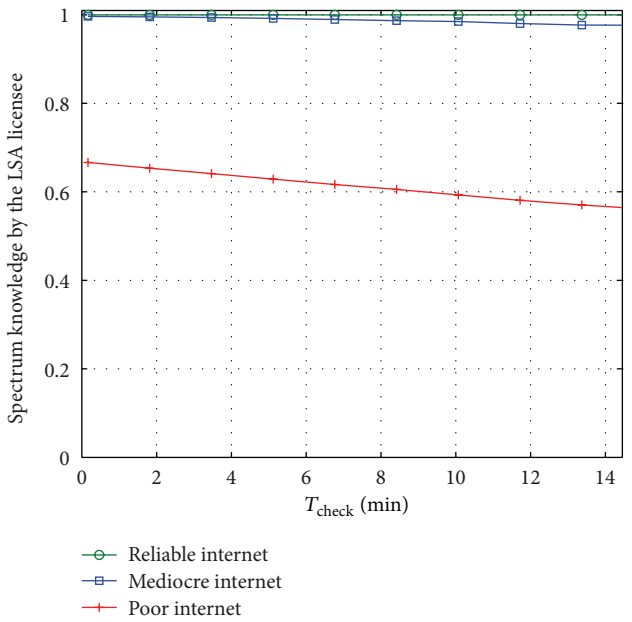

FIGURE 5: The spectrum knowledge of the channel as a function of T_{check} while $T_i = 60$ min. The incumbent is *rare*.

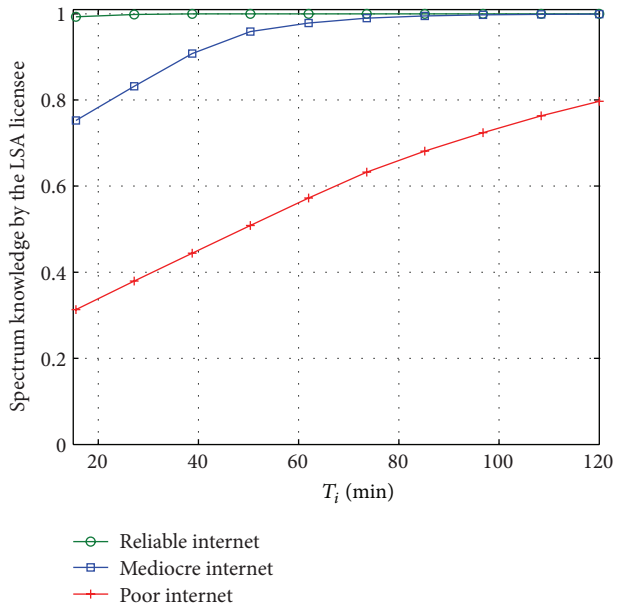

FIGURE 6: The spectrum knowledge of the channel as a function of T_i while $T_{\text{check}} = 15$ min. The incumbent is *rare*.

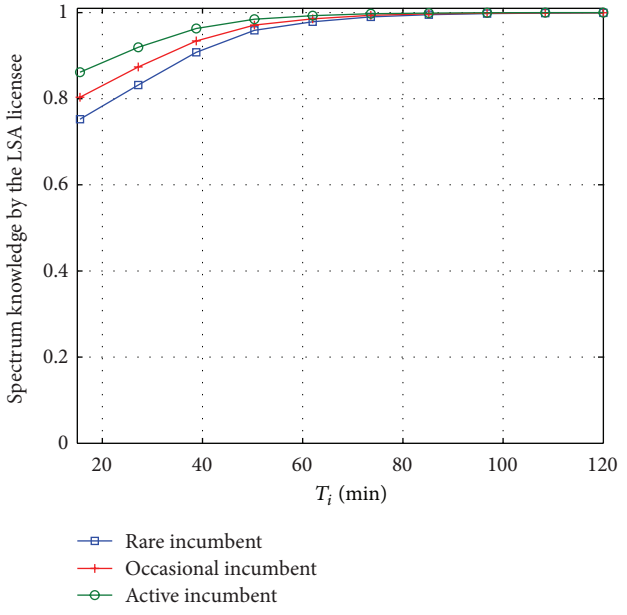

FIGURE 7: The spectrum knowledge of the channel as a function of T_i while $T_{\text{check}} = 15$ min with different incumbent activity levels. The internet connection is *mediocre*.

operation. An example of this kind of incumbent is an organizer of programme making special events.

In Figure 7, we study how different activity levels of the incumbent affect the LSA system performance. We observe from the results that the spectrum knowledge is higher when the incumbent is more active. This is because then the incumbent reserves the spectrum more often, and the reservations include the spectrum knowledge. However, if the incumbent is very active, it might be hard for all incumbent applications to report the plans at a predetermined time before utilizing the spectrum. Thus, the PS with a poor internet connection should utilize different methods, such as sensing, to obtain the LSA resources with an active incumbent.

In Figure 8, we plot the spectrum utilization of the LSA licensee. In this figure, we compare the spectrum utilization by the LSA licensee by using two measures. First, we plot the utilized spectrum resources divided by *all the resources*. Second, we plot the utilized spectrum resources divided by the *available resources*, that is, the LSA resources that are available at the times when the incumbent does not transmit. From the figure, we see that the LSA licensee can utilize the spectrum less often when the incumbent is more active, while the available spectrum for the LSA licensee is utilized relatively better. Therefore, as natural, it is always preferable for the LSA licensee that the incumbent does not transmit. Moreover, the overall spectrum is utilized more effectively when there are more incumbents.

In Figure 9, we study the spectrum utilization of the complete LSA system. This is the utilization of the spectrum by either the LSA licensee or the incumbent. We plot the utilized spectrum resources divided by the total spectrum resources. We see that the spectrum utilization is inline with the spectrum knowledge by the LSA licensee shown in Figure 7. The spectrum is utilized approximately 100% of the time when the T_i is over 80. We can see that the proposed LSA system with *mediocre* internet connection to the LSA licensee is ideal for sharing the spectrum with incumbents, such as mobile operators, if they can reliably estimate their spectrum needs 80 minutes beforehand.

In Figure 10, we plot the utilized spectrum resources divided by the total spectrum resources for different values of T_{check} with an *occasional* incumbent and *mediocre* internet. Note that the value of T_{check} affects only spectrum utilization

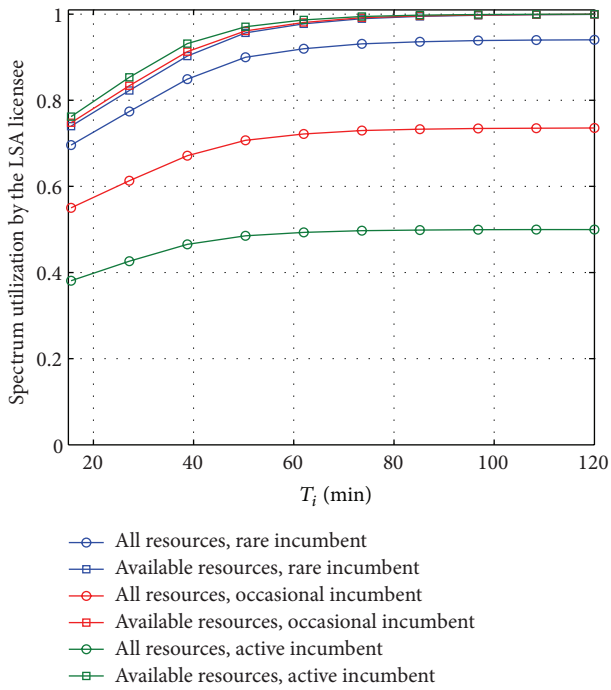

FIGURE 8: LSA resource utilization by the LSA licensee as a function of T_i while $T_{\text{check}} = 15$ min in a *mediocre* channel.

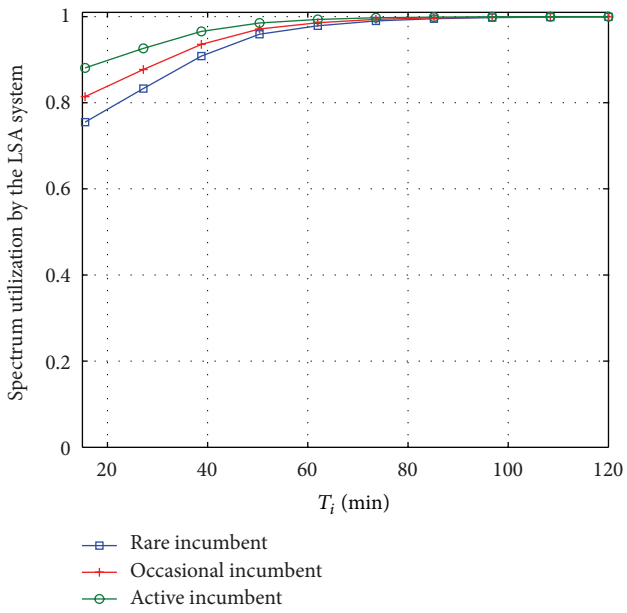

FIGURE 9: LSA resource utilization by the LSA system as a function of T_i while $T_{\text{check}} = 15$ min in a *mediocre* channel.

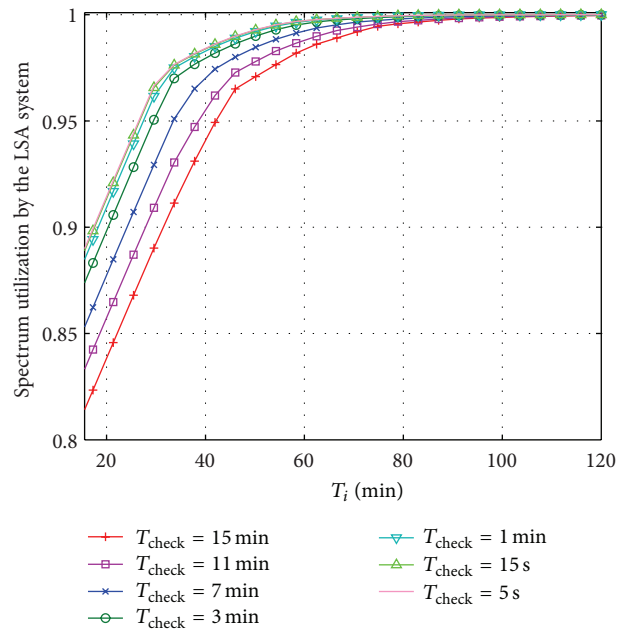

FIGURE 10: LSA spectrum resource utilization as a function of T_i with *occasional* incumbent in a *mediocre* channel.

of the LSA licensee. Thus, from Figure 10, we notice that the LSA licensee receives more resources with smaller values of T_{check}. This is because the LSA licensee knows more valid spectrum information when it checks the connection more often. However, the amount of valid spectrum information does not grow significantly, when the T_{check} becomes smaller than 15 seconds. From the figure, we also see that the valid information does not vary significantly for different values of T_{check} if the T_i is over 80 minutes. Thus, the value of T_{check} can be set adaptively according to the value of T_i, that is, according to the predetermined time before which the incumbent sends its spectrum reservation to the LSA repository.

5. Conclusion

We gave an overview of spectrum sharing possibilities between PS and CS since there may be a possibility to find more spectrum for their users in the future. While there are multiple choices for PS to utilize spectrum sharing, it is also a political decision how the spectrum will be shared. Therefore, PS should be ready for every scenario. If PS owns the spectrum, it can rent the free spectrum to CS via an LSA/SAS system. Another option for providing high quality PS performance is the following. We reserve only a small portion of the spectrum for voice service to PS. We let CS networks utilize the remaining spectrum with the condition that CS is obligated to release spectrum to PS when needed for critical applications. We gave multiple options to automatically reserve CS resources for PS use. In addition, the PS can be a roaming user at CS network. Furthermore, PS can be an LSA licensee of the incumbent CS.

Moreover, if LSA sharing arrangement is used, there needs to be a reliable method for spectrum allocation to PS during connection breaks. We developed a specific LSA system for robustness to overcome short-term connection breaks. In this system, the PS is the LSA licensee and the CS is the incumbent, which can be, for example, when the PS requires additional resources with LSA. In our system, the incumbent reserves the spectrum for a predetermined

time beforehand and is not transmitting during this predetermined time. We validated the reservation system and studied how to select suitable durations for the predetermined times and for time intervals between connection checks. The time intervals between connection checks can be selected adaptively based on the network quality and on the time before which the incumbent sends its spectrum reservations. The simulations show that the proposed system is able to reduce the impact of possible connection breaks inside the LSA system.

However, this method is not alone sufficient for utilizing all the LSA spectrum resources during all connection breaks. There might be a long connection break and no possibility for an internet connection. In addition, the incumbent might not always have an internet connection but can still utilize the spectrum. Therefore, if the PS is an LSA licensee and requires available LSA spectrum resources, it needs to develop other methods to guarantee its own error-free transmission and incumbent protection.

To protect the incumbent without internet connection, there can be additional signals that tell about a connection break and that the incumbent is using the spectrum, such as errors accumulating to the LSA licensees, human intervention at the base stations, local reservation signals with separate control channels, and sensing methods. In the upcoming work, we will develop the LSA system to coexist with the already available sensing methods and enable spectrum sharing and utilization also during major connection breaks.

Competing Interests

The authors declare that there is no conflict of interests regarding the publication of this paper.

Acknowledgments

The authors would like to acknowledge CORE++ project consortium: VTT, University of Oulu, Centria University of Applied Sciences, Turku University of Applied Sciences, Nokia, PehuTec, Bittium, Anite, Finnish Defence Forces, FICORA, and Tekes.

References

[1] Cisco, "Cisco visual networking index: global mobile data traffic forecast update, 2015–2020," Cisco White Paper, 2014, http://www.cisco.com/c/en/us/solutions/collateral/service-provider/visual-networking-index-vni/mobile-white-paper-c11-520862.pdf.

[2] "The 1000x mobile data challenge," Qualcomm Presentation, 2013, http://www.qualcomm.com/media/documents/files/1000x-mobile-data-challenge.pdf.

[3] The White House, "Realizing the full potential of government-held spectrum to spur economic growth," Presidents Council of Advisors on Science and Technology, 2012, https://www.whitehouse.gov/sites/default/files/microsites/ostp/pcast_spectrum_report_final_july_20_2012.pdf.

[4] Core++ project web page, June 2016, http://core.willab.fi.

[5] The Electronic Communications Committee, "Licensed shared access (LSA)," ECC Report 205, The Electronic Communications Committee, Copenhagen, Denmark, 2014, http://www.erodocdb.dk/Docs/doc98/official/pdf/ECCREP205.PDF.

[6] ETSI, "Reconfigurable radio systems (RRS); System requirements for operation of mobile broadband systems in the 2300 MHz—2 400 MHz band under licensed shared access (LSA)," ETSI TS 103 154 V1.1.1, October 2014, http://www.etsi.org/deliver/etsi_ts/103200_103299/103235/01.01.01_60/ts_103235v010101p.pdf.

[7] ETSI, "Reconfigurable radio systems (RRS); system architecture and high level procedures for operation of licensed shared access (LSA) in the 2 300 MHz–2 400 MHz band," ETSI TS 103 235 V1.1.1, October 2015, http://www.etsi.org/deliver/etsi_ts/103200_103299/103235/01.01.01_60/ts_103235v010101p.pdf.

[8] ETSI, "Reconfigurable radio systems (RRS); use cases for spectrum and network usage among public safety, commercial and military domains," Article ID 102900, ETSI TR 102 970 V1.1.1, 2013, http://www.etsi.org/deliver/etsi_tr/102900_102999/102970/01.01.01_60/tr_102970v010101p.pdf.

[9] K. Lähetkangas, H. Saarnisaari, and A. Hulkkonen, "Licensed shared access system development for public safety," in *Proceedings of the European Wireless Conference*, Oulu, Finland, May 2016.

[10] R. Ferrús, O. Sallent, G. Baldini, and L. Goratti, "Public safety communications: enhancement through cognitive radio and spectrum sharing principles," *IEEE Vehicular Technology Magazine*, vol. 7, no. 2, pp. 54–61, 2012.

[11] R. Ferrús and O. Sallent, *Mobile Broadband Communications for Public Safety: The Road Ahead Through LTE Technology*, John Wiley & Sons, New York, NY, USA, 2015.

[12] ETSI, "Reconfigurable radio systems (RRS); Feasibility study on inter-domains synergies; synergies between civil security, military and commercial domains," ETSI TR 103 217, June 2016, https://portal.etsi.org/webapp/workProgram/Report_WorkItem.asp?wki_id=43285.

[13] "Ukkoverkot commercial service," June 2016, http://www.ukkoverkot.fi/.

[14] R. Hallahan and J. M. Peha, "Enabling public safety priority use of commercial wireless networks," *Homeland Security Affairs*, vol. 9, article 13, 2013, http://www.hsaj.org/articles/250.

[15] M. Palola, T. Rautio, M. Matinmikko et al., "Licensed Shared Access (LSA) trial demonstration using real LTE network," in *Proceedings of the 9th International Conference on Cognitive Radio Oriented Wireless Networks (CROWNCOM '14)*, pp. 498–502, June 2014.

[16] M. Palola, M. Matinmikko, J. Prokkola et al., "Live field trial of Licensed Shared Access (LSA) concept using LTE network in 2.3 GHz band," in *Proceedings of the IEEE International Symposium on Dynamic Spectrum Access Networks (DYSPAN '14)*, pp. 38–47, McLean, Va, USA, April 2014.

[17] Electronic Communications Committee, "Broadband wireless systems usage in 2300–2400 MHz," ECC Report 172, 2012, http://www.erodocdb.dk/docs/doc98/official/pdf/ECCRep172.pdf.

[18] European Radiocommunications Committee, "Handbook on radio equipment and systems videolinks for ENG/OB use," ERC Report 38, 1995, http://www.erodocdb.dk/docs/doc98/official/pdf/REP038.pdf.

[19] Elektrobit, "Enhancing the link network performance with EB tactical wireless IP network (TAC WIN)," EB Defense Newsletter, December 2014, http://www.bittium.com/file.php?fid=785.

[20] M. Jokinen, M. Mäkeläinen, and T. Hänninen, "Demo: co-primary spectrum sharing with inter-operator D2D trial," in *Proceedings of the 20th Annual International Conference on Mobile Computing and Networking*, pp. 291–294, September 2014.

Hindawi Publishing Corporation
Mobile Information Systems
Volume 2016, Article ID 7480460, 13 pages
http://dx.doi.org/10.1155/2016/7480460

Research Article

PSUN: An OFDM-Pulsed Radar Coexistence Technique with Application to 3.5 GHz LTE

Seungmo Kim, Junsung Choi, and Carl Dietrich

Bradley Department of Electrical and Computer Engineering, Virginia Tech, Blacksburg, VA 24060, USA

Correspondence should be addressed to Seungmo Kim; seungmo@vt.edu

Received 3 March 2016; Accepted 3 May 2016

Academic Editor: Miguel López-Benítez

This paper proposes Precoded SUbcarrier Nulling (PSUN), an orthogonal frequency-division multiplexing (OFDM) transmission strategy for a wireless communications system that needs to coexist with federal military radars generating pulsed signals in the 3.5 GHz band. This paper considers existence of Environmental Sensing Capability (ESC), a sensing functionality of the 3.5 GHz band coexistence architecture, which is one of the latest suggestions among stakeholders discussing the 3.5 GHz band. Hence, this paper considers impacts of imperfect sensing for a precise analysis. Imperfect sensing occurs due to either a sensing error by an ESC or a parameter change by a radar. This paper provides a framework that analyzes performance of an OFDM system applying PSUN with imperfect sensing. Our results show that PSUN is still effective in suppressing ICI caused by radar interference even with imperfect pulse prediction. As an example application, PSUN enables LTE downlink to support various use cases of 5G in the 3.5 GHz band.

1. Introduction

In 2010, the US National Telecommunications and Information Administration (NTIA) Fast Track Report [1] identified the 3550–3650 MHz band to be potentially suitable for commercial broadband use. The NTIA identified it as one of the candidate bands, in response to the president's initiative [2] to identify 500 megahertz of spectrum for commercial wireless broadband. In 2012, the Federal Communications Commission (FCC) released a Notice of Proposed Rulemaking (NPRM) [3] where they proposed creation of the Citizens Broadband Radio Service (CBRS). The FCC voted to approve the suggestions developed through two NPRMs [3, 4] and adopted rules for managing 150 megahertz in the 3550–3700 MHz band (the 3.5 GHz band) in a report and order [5].

The FCC proposes structuring the CBRS according to a *three-tiered* shared access model comprised of Incumbent Access (IA), Priority Access (PA), and General Authorized Access (GAA). IA includes federal military radars and fixed satellite service, which are protected from PA and GAA. PA operations are protected from GAA operations. Priority Access License (PAL), three-year authorization to use a 10-megahertz channel in a single census tract, will be assigned in up to 70 megahertz of the 3550–3650 MHz portion of the band. GAA use will be allowed throughout the 150-megahertz band. GAA users will receive no protection from interference of other CBRS users. There exist *spectrum access systems (SASs)* incorporating a dynamic database and interference mitigation techniques. A SAS collects pulse parameters of the incumbent radars and provides them with the coexisting CBRS devices. In many cases, a SAS may not be able to provide such information directly to the CBRS users due to security concerns related to military radar systems. Then, a SAS provides such information in an indirect manner, for example, query responses to the CBRS users.

The NTIA recommends addition of Environmental Sensing Capability (ESC), a component for *sensing capability* [6]. The NTIA's review of the public record indicates that many stakeholders proposed employing sensing techniques to augment capability of a SAS. The inputs from the ESC can be used by the SAS to direct the PA and GAA tier users to another channel or, if necessary, to cease transmissions to avoid potential harmful interference to federal radar systems.

In addition, the FCC recommends in [3, 4] the CBRS system to be a small-cell system where each transmitter can keep its transmitting power low. The most popular examples

of small-cell systems so far in practice are Wireless Fidelity (Wi-Fi) and the 3rd Generation Partnership Project (3GPP) Long-Term Evolution (LTE). To the best of our knowledge, it is more challenging to design a small-cell system based on LTE (than Wi-Fi) because as a "cellular" system it tends to have higher requirements, for example, higher mobility with lower latency. Therefore, we set LTE as our model system for the CBRS in the 3.5 GHz band. Contributions of this paper are summarized as follows.

(1) This paper proposes Precoded SUbcarrier Nulling (PSUN), an OFDM transmission strategy that effectively suppresses pulsed interference from a radar. By applying PSUN at a transmitter (Tx) and pulse blanking (PB) at a receiver (Rx), an LTE system can mitigate intercarrier interference (ICI) caused by pulsed interference from coexisting radars. It is noteworthy that this paper suggests a coexistence method *without modifying the incumbent radars' operations*.

(2) This paper provides an analysis framework for OFDM-pulsed radar coexistence. To the best of our knowledge, this paper is the first work that considers existence of ESC in the coexistence problem, which reflects uniqueness of the problem that it is managed by both means of database and spectrum sensing. Furthermore, the framework takes into account the impacts of *imperfect prediction of radar interference*.

(3) This paper suggests use cases of the fifth-generation (5G) mobile networks that LTE downlink can support by using the 3.5 GHz band, based on the analyses and results that this paper provides.

2. Related Work

In [7], a novel radar waveform that minimizes a radar's in-band interference on a coexisting communications system is proposed. This approach assumes that a radar has full knowledge of the interference channel and modifies its own signal vectors in such a way that they fall into the null space of the channel matrix between the radar and the coexisting communications system. In [8], the coexistence scenario of [7] is extended to more than one interference channel. Our work is distinguished from [7, 8] because it proposes a strategy that requires *no change of the incumbent radar system*. It is a meaningful contribution considering the widely acknowledged concern about national security and cost of changing the incumbent system.

In [9, 10], opportunistic spectrum sharing between an incumbent radar and a secondary cellular system is studied. The work specifies applications that are feasible in such a coexistence scenario. It is found that noninteractive video on demand, peer-to-peer file sharing, file transfers, automatic meter reading, and web browsing are feasible, while real-time transfers of small files and VoIP are not. In [11], it is suggested that the secondary communication system utilizes information of the incumbent radar that is provided by a database. In [12], impacts of interference from shipborne radars to LTE systems are studied. An eNodeB's signal-to-interference-plus-noise ratio (SINR) plummets when hit by radar pulses, but an LTE system is able to recover during the time between radar pulses. Average throughput of user equipment (UE) drops under radar interference. The authors concluded that the UE throughput loss in the uplink direction is tolerable even with a radar deployed only 50 kilometers away from the LTE system. In [13], the study in [12] is extended. The authors studied impacts of shipborne radars that operate in the same channel and are located in the vicinity of a 3.5 GHz macrocell and outdoor small-cell LTE systems. With such additional consideration of out-of-band effects of shipborne radars, the authors still conclude that both macrocell and outdoor small-cell LTE systems can operate inside current exclusion zones. In [14], on the other hand, it is concluded that LTE systems are unable to cope well with narrowband bursty interference on the downlink. Our work is distinguished from [9–14] because this paper studies *how to actually cancel radar interference*, while only feasibility of coexistence was discussed in the prior studies.

In addition, this paper provides *a generalized analytical framework*. This paper takes into consideration a comprehensive interplay among multiple variables regarding the military radars' operations, such as the number of radars, pulse parameters, antenna sidelobes, and out-of-band emissions, which will be discussed in Section 3. Moreover, impacts of imperfect prediction of radar interference are measured by appropriate probabilities which will be explained in Section 5.

Note that this paper is an extension of our previous study that was published in [15]. The extension is twofold: (i) we change the performance metric from bit error rate to maximum data rate to more fairly reflect the impact of PSUN on an OFDM system performance; (ii) we use 3.5 GHz LTE as a near-term example that serves to illustrate how the technique could be applied to operation of future 5G systems in bands shared with pulsed radars.

3. Coexistence Model

This paper discusses the performance of an LTE small-cell system that coexists with multiple military radars that rotate and generate pulsed signals. Note that this paper focuses on the *downlink* of an LTE system where an eNodeB acts as a Tx and a UE becomes an Rx.

Also, this paper assumes that there is no impact of fading from mobility nor multipath since the ICI that is caused by radar interference has far more significant impacts than Doppler shift and delay spread. Therefore, we assume that the only two channel impairments are *radar interference* and *additive white Gaussian nose (AWGN)*. In other words, an OFDM symbol goes through an AWGN channel when the LTE system is not interfered by the radar. There is a period of time when the radar beam does not point at the LTE system since a radar rotates; during this time, an LTE system is assumed to experience an AWGN channel. It should be noted that hence the simulation results that are presented in Section 6 do not take fading into consideration.

3.1. Characterization of a Military Radar. It is very important to note that a 3.5 GHz band coexistence problem is more challenging than what is often acknowledged. This paper

Table 1: Parameters for antenna horizontal sidelobe analysis.

Parameter	Remark
θ_{beam}	Angle of a radar antenna's horizontal beam with main lobe and sidelobes that cause interference on an LTE system
θ_{pass}	Angle that a radar antenna's horizontal beam passes through an LTE cell
θ_{intf}	The total angle that a radar antenna's horizontal beam interferes with an LTE cell
d	Distance between a radar and an LTE cell
r_c	Diameter of an LTE cell
T_{rot}	Radar rotation time

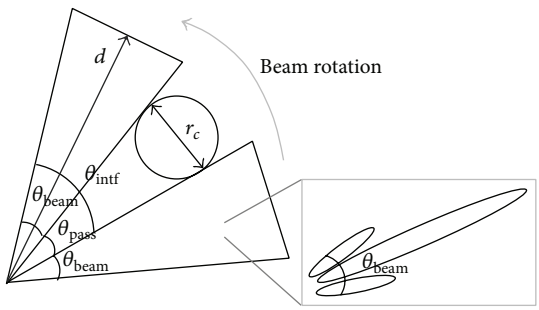

Figure 1: Impact of antenna horizontal sidelobes.

considers two aspects that increase the impact of a pulsed radar's interference on an LTE cell: a radar's antenna sidelobes and out-of-band emissions. These analogous spatial and frequency domain effects are serious due to the *extreme difference in transmitting power between radar and LTE*.

3.1.1. Antenna Sidelobes. Following the FCC's guideline in designing a CBRS system coexisting with military radars [3–5], a sufficiently large spatial separation must be guaranteed between a federal military radar and an LTE system to guarantee a low level of interference from an LTE eNodeB (Tx) to the radar. In spite of this large distance from a radar, an LTE UE (Rx) cannot avoid radar interference with a very high level due to the much higher transmitting power of a radar. The power of a radar's signal received at an LTE Rx is so high that even sidelobes cause significant interference to the communications system. This is interpreted as *a greater value of horizontal angle of a radar's beam* that actually causes interference on a coexisting LTE system. Figure 1 illustrates such an impact of a radar antenna's horizontal sidelobes. It describes that the angle of a radar beam, θ_{beam}, contains not only its main lobe but also the sidelobes. The value of θ_{beam} differs according to type of radar. For instance, the antenna pattern of a radar analyzed in [1] has cosine pattern with sidelobes that are 14.4 dB lower than the main lobe.

Now we formulate such a coexistence model in which an LTE system is interfered by a radar that rotates and transmits pulses. Table 1 describes parameters used in the analysis, including those shown in Figure 1. Suppose that a radar rotates counterclockwise and an LTE system is within interference range of the radar's signal. The angle of rotation during which the radar's beam passes through a cell of an LTE system is given by

$$\theta_{\text{pass}} = \frac{360^\circ \cdot r_c}{2\pi d}. \tag{1}$$

As illustrated in Figure 1, the total angle through which the radar beam interferes with a cell of an LTE system can be written as

$$\theta_{\text{intf}} = \theta_{\text{beam}} + \theta_{\text{pass}}. \tag{2}$$

Note that θ_{beam} differs according to type of radar, while θ_{pass} is determined by d and r_c. Then the total interference time is defined as the time period when a cell of an LTE system is interfered by a radar within a beam rotation, which is obtained by

$$T_{\text{intf}} = \frac{\theta_{\text{intf}}}{360} \cdot T_{\text{rot}}. \tag{3}$$

Such an impact of a radar's antenna horizontal sidelobes is evidenced in Figure 5 of [16]. The report describes an observed case in which a wireless communication system receives energy from an SPN-43 shipborne radar at a level that is approximately 30 dB higher than the noise floor, even when the main lobe of the radar antenna is towards the direction opposite to a cell of the wireless communications system. This implies that sidelobes of a radar beam can have a significant impact on operation of a coexisting wireless communications system.

3.1.2. Out-of-Band Emission. Due to extremely high peak transmitting power of a radar, out-of-band emission from a radar operating in a neighboring channel also has a significant impact on a coexisting LTE system. Radars themselves are separated among different channels to avoid interfering with each other. This spectral separation is enough to protect radars from interference due to other radars but is insufficient to protect a wireless communications system that operates with a much lower transmitting power.

Figure 2 illustrates a simulation result of a radar's out-of-band interference on an LTE system. We simulated an LTE system operating at 3.5 GHz and a radar generating pulses at 3.5, 3.55, and 3.6 GHz. The transmitting powers of a radar and an LTE eNodeB are assumed to be 83 dBm and 23 dBm, respectively. The distance between an LTE eNodeB and a UE is 100 meters, while the radar is assumed to be separated by distance of 100 kilometers. Also, the radar's pulse repetition time (PRT) and duty cycle are 1 msec and 10%, respectively. A radar has an extremely large bandwidth due to its pulsed nature. Since transmitting power of a radar is too much higher than that of wireless communications Tx, it is still higher than an LTE eNodeB's signal at a UE, even with a 50 MHz or 100 MHz offset. This implies that we must take into account interference caused by radars' out-of-band emissions when we analyze coexistence between a pulsed radar and a wireless communications system. As mentioned earlier, a

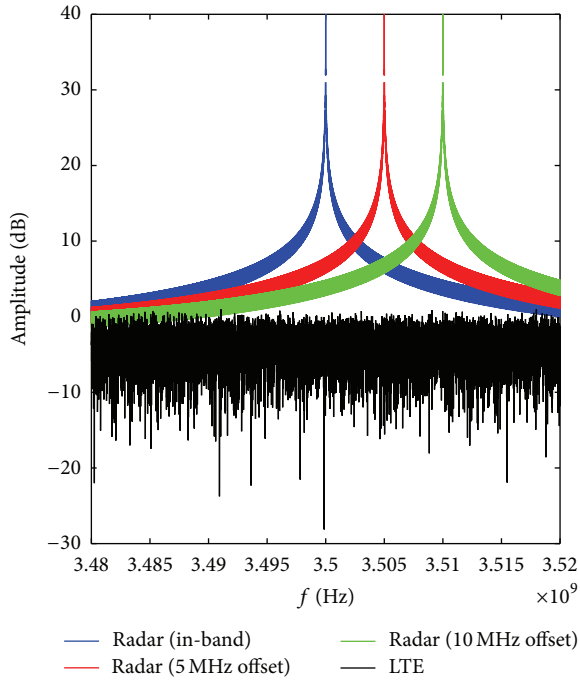

Figure 2: Impact of out-of-band emissions.

radar's out-of-band transmission does not cause significant interference to another radar in an adjacent band because transmitting powers of the radars are similar. However, to an LTE system, an out-of-band radar emission causes significant interference due to a significant difference in transmitting power between an LTE eNodeB and a radar.

Regarding the simulation setting discussed above, it is noteworthy to elaborate the rationale behind selection of the value of *path loss exponent* that equals 2. In the geography of the coexistence model, the lengths are significantly different between the two main parts: (i) between a radar and an LTE system and (ii) between an eNodeB and a UE in an LTE system. The idea is that the former part is much longer in distance and thus more affected by the path loss. In the former part of a coexistence geography, the path loss becomes the dominant channel impairment due to the long distance (e.g., tens of kilometers). On the other hand, in the latter part, radar interference becomes the main channel impairment since the path loss does not influence the performance due to short-distance propagation. As mentioned earlier, in a LTE-radar coexistence scenario, the former part is much longer in length than the latter part. Therefore, when selecting a value of the path loss exponent, it is the former part that we should consider more significantly than the latter part. Since the former part is very likely composed of a long line-of-sight path, it is approximated as 2 to give a conservative estimate, e.g., one that is less favorable to the LTE link.

Such interference from out-of-band radars can be interpreted as a greater number of radars that cause interference since radars operating in neighboring channels also cause interference to an OFDM system. Hence, there are additional bursts of interference from the out-of-band radars within an in-band radar's rotation period. It is likely that the radars have different values of T_{rot}, duty cycle, and PRT, which makes the task of an LTE system to track interfering pulses more difficult. In this paper we reflect the impact of out-of-band interference due to radars on lower and upper adjacent frequencies in such a way that there occurs a *threefold increase* in the number of OFDM symbols that are hit by a radar pulse. Therefore, *the total length of time that a radar interferes with an LTE cell within a radar rotation* T'_{intf}, can be given by $T'_{\text{intf}} \leq 3T_{\text{intf}}$. Note that $T'_{\text{intf}} = 3T_{\text{intf}}$ is true when there is no overlap in time among pulses generated by the three radars.

Table 2: Computation of the total interference time T'_{intf}.

θ_{beam} (deg)	θ_{intf} (deg)	T_{intf} (msec)	T'_{intf} (msec)
5	10.7	59.6	178.8
10	15.7	87.4	262.2
30	35.7	198.5	595.5

Table 2 demonstrates T'_{intf} according to different values of θ_{beam}, assuming that $T'_{\text{intf}} = 3T_{\text{intf}}$. We set θ_{beam} to 5, 10, and 30 degrees. Let us apply $T'_{\text{intf}} = 595.5$ msec to the current LTE standard as an example. Within a radar rotation time $T_{\text{rot}} = 2$ sec, 2000 LTE subframes can be transmitted. Since 14 OFDM symbols are transmitted in a subframe, 28000 OFDM symbols can be transmitted. As a result, $(595.5/2000) \times 28000 \approx 8337$ out of 28000 OFDM symbols are hit within a rotation of a radar.

3.2. Generalized Expression of Radar Interference. In the 3.5 GHz Band, radars report their operating parameters (i.e., pulse parameters and position) to a SAS, and an ESC also senses and sends the parameters to a SAS. Based on such a coexistence model, *the frequency of pulse interference within a certain time* can be quantified for use in analysis. There are four factors affecting the frequency: (i) the number of radars, (ii) PRT of a radar, (iii) level of interference from antenna sidelobes of a radar, and (iv) level of interference caused by out-of-band radars. However, it is extremely difficult for an ESC to keep track of all the four factors since military radars keep changing their parameters and the radars' parameters are even classified in many cases, as explained in an army's regulation document [22]. To this end, this paper generalizes the frequency of pulse occurrence by defining a quantity called *the probability of pulsed interference*, ρ. It is defined to be the probability that an OFDM system experiences a pulsed interference within a certain period of time. In this way, the quantity ρ generalizes the impacts of all of the four factors described above.

Note that this paper adopts the LTE standard's parameters for simulating a CBRS system as will be demonstrated in Section 6, and the scope of defining ρ is 1 msec, the length of a subframe defined in the LTE standard. If $\rho = 0$ during a simulation of 1000 subframes, none of the subframes are hit by a radar pulse. If $\rho = 1$, on the other hand, every subframe experiences radar interference during the simulation. Note that this analytical framework can be extended to any other type of OFDM communication without loss of generality. In other words, the definition of ρ can be set within any specified

Table 3: Existing ICI self-cancellation (ISC) schemes and the proposed subcarrier nulling ($L = 2$).

ICI self-cancellation (ISC) scheme	Subcarrier allocation
Data conversion [17]	$X'(k) = X(k), X'(k+1) = -X(k)$, where k is the subcarrier index
Symmetric data conversion	$X'(k) = X(k), X'(N-k-1) = -X(k)$, where N is the FFT size
Weighted data conversion [18]	$X'(k) = X(k), X'(k+1) = -\mu X(k)$, where μ is a real number in $[0, 1]$
Plural weighted data conversion [19]	$X'(k) = X(k), X'(k+1) = -e^{-j\pi/2}X(k)$
Data conjugate	$X'(k) = X(k), X'(k+1) = -X^*(k)$
Data rotated and conjugate [20]	$X'(k) = X(k), X'(k+1) = -e^{-j\pi/2}X^*(k)$
PSUN	$X'(k) = X(k), X'(k+1) = 0$

time period that can be measured by the number of OFDM symbols.

4. Precoded SUbcarrier Nulling (PSUN)

4.1. Proposition of PSUN. Pulse blanking (PB) is known to be one of the most effective techniques for suppressing pulsed interference [23–25]. Unfortunately, PB still leaves a significant level of ICI. In PB, time domain samples of the received signal affected by pulsed interference are set to zero. The technique deteriorates performance of an OFDM system by affecting not only the interfered samples but also the desired samples. This problem occurs due to the fact that (inverse) Fourier transform provides a time-frequency mapping in such a way that every frequency/time sample contributes to generating a time/frequency symbol. In an OFDM system, PB takes place in the time domain whereas the data symbols are mapped to the subcarriers in the frequency domain. An OFDM Rx blanks only several samples that are radar-interfered in the time domain. However, such a partial change leads to corruption of all the samples in the frequency domain due to characteristic of the Fourier transform, which still causes ICI. This paper focuses on suppression of such ICI that remains after applying PB at an OFDM Rx.

This paper suggests that the negative impact of PB can be considered a form of time-selective fading. Channel coding is usually applied in combination with interleaving and diversity to mitigate performance degradation due to fading [26]. In OFDM systems, the main means of combating time-selective fading are block interleaving and antenna diversity. However, our results indicate that neither method can effectively mitigate ICI caused by PB. Interleaving is ineffective because PB does not result in bursty errors due to the one-to-all mapping characteristic of the Fourier transform. Antenna diversity is also not effective against the ICI caused by PB because an entire LTE cell is likely to be hit at once by a radar's beam. A multiple-antenna technology can bring no benefit when the signals received by all the antennas are interfered with simultaneously.

ICI self-cancellation (ISC) is an aggressive means of combating ICI. It cancels ICI by allocating precoded $L-1$ redundant subcarriers between data subcarriers, which results in a $1/L$ data rate. Based on the work of Zhao and Haggman [17], several ISC schemes have been proposed [18–20]. Some of the existing ISC schemes are summarized in Table 3, assuming $L = 2$. Note that $X(\cdot)$ and $X'(\cdot)$ indicate the original transmitted data symbol and the symbol after ISC precoding, respectively.

We discovered that the most effective way of reducing ICI induced by PB is *to insert null subcarriers*, instead of allocating any other types of redundant subcarriers. The rationale is illustrated in Figure 3. It is an example that is simplified to clearly demonstrate the impact of location of PB on the level of ICI. Figure 3(a) represents an example signal at Tx while Figures 3(b) and 3(c) show *two different locations of PB* at Rx. The example signal contains three among 64 subcarriers around the center (28th, 30th, and 32nd) that are set to 1 while all the others are set to 0. Note that the transmitted signal in Figure 3(a) shows the real part of the original complex signal. It is observed from Figure 3 that the location of PB has a very significant impact on the level of ICI caused by PB. Comparing Figures 3(b) and 3(c), *the ICI becomes more severe as higher-amplitude samples are blanked*. In other words, the ICI level can be reduced as the time domain fluctuation gets flatter. It is straightforward that the simplest way of keeping time domain amplitudes low is to reduce the number of subcarriers. An OFDM Rx can suppress ICI remaining after PB better when a Tx has allocated *null subcarriers* instead of other types of redundancy, since use of null subcarriers reduces the number of high-energy bins in the time domain.

For this reason, an OFDM Tx employing PSUN *precodes an OFDM symbol by inserting null tones between data tones so that the ICI after PB at its Rx can be suppressed*. This makes PSUN a type of ISC, as listed in Table 3. Various manners of inserting null tones for different purposes have been studied in the literature [27–29]. In this work, PSUN allocates the null tones in such a way that the radar interference is minimized. Figure 4 shows that PSUN outperforms the other ISC schemes. Note that for the weighted data conversion scheme the value of μ becomes $1/2$. The reason for PSUN's higher performance is that PSUN yields smaller variation of an OFDM symbol in the time domain because it transmits a smaller number of subcarriers.

4.2. The Transmission Protocol of PSUN. Let r denote the coding rate of PSUN. With the coding rate of $r = 1/L$, PSUN inserts $L-1$ null tones between data tones. Figure 5 illustrates how PSUN inserts null tones in an exemplar OFDM symbol, with QPSK and the FFT size of 32. Figure 5(a) demonstrates an OFDM symbol without PSUN. Figures 5(b) and 5(c) show

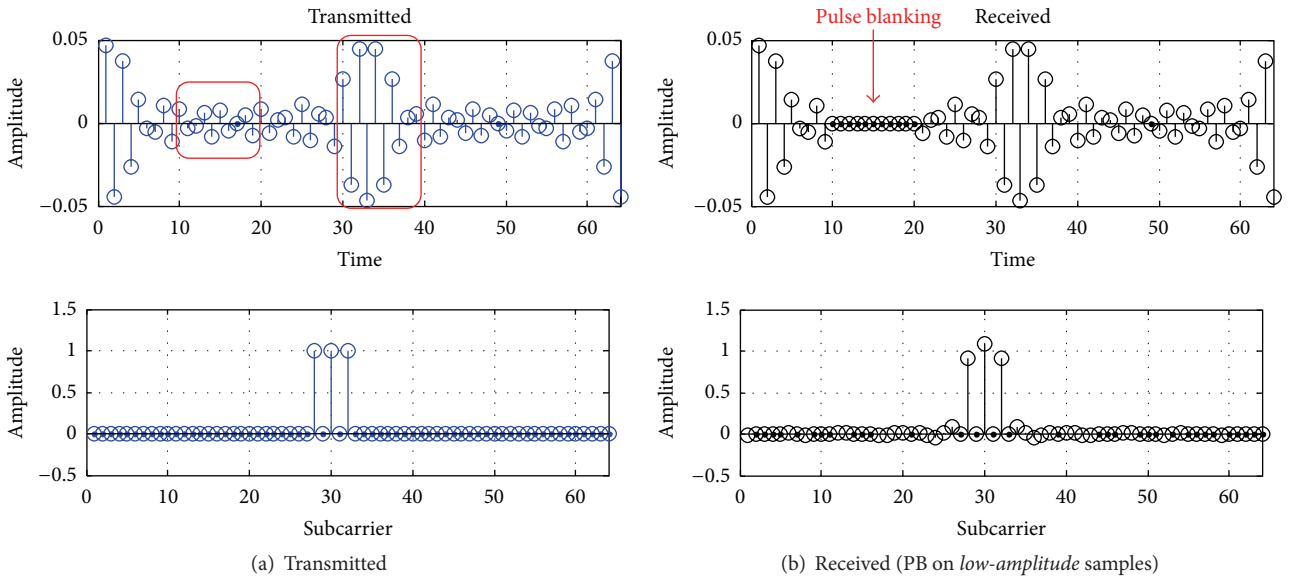

(a) Transmitted

(b) Received (PB on *low-amplitude* samples)

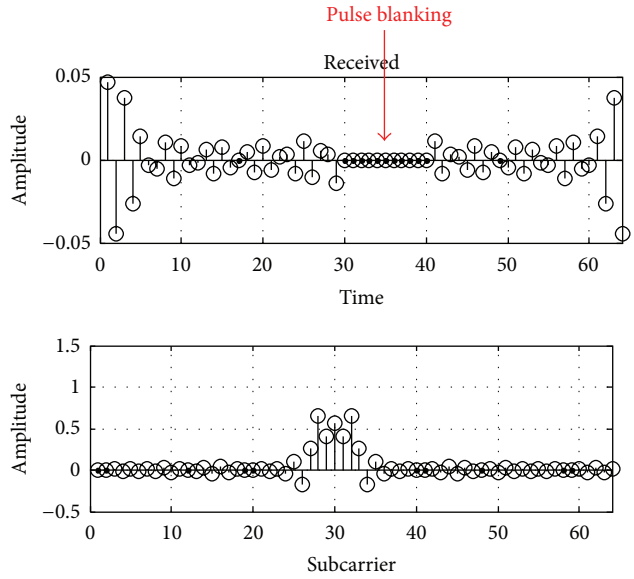

(c) Received (PB on *high-amplitude* samples)

FIGURE 3: Dependency of ICI on the location of PB.

examples of precoding the OFDM symbol using PSUN with r equal to 1/2 and 1/4, respectively. PSUN extracts the first half/fourth of the data tones from the original OFDM symbol given in Figure 5(a). Note that this method of taking $1/L$ of its original data is only an example. PSUN can do it in various other ways; another example is to extract a data tone in every L subcarrier. Then PSUN inserts null tones (marked with red squares) between the data tones, which leads to the mapping illustrated in Figures 5(b) and 5(c).

This is where PSUN sacrifices data rate by $1/r$ within an OFDM symbol. To minimize such loss of data rate, an OFDM Tx performs two important operations when adopting PSUN. First, it *localizes OFDM symbols to be hit a priori and allocates null tones in the symbols only*. The a priori knowledge about radar pulse parameters is provided by a SAS but sensed by an ESC beforehand. Figure 6 shows a subframe in which an OFDM symbol is expected to be hit by a radar pulse. Only that symbol is precoded with the null subcarriers at Tx before transmission. Second, within the OFDM symbol to be radar-interfered, an OFDM Tx *disables channel coding and shifts the saved redundancy to PSUN*. This assumes that, for an OFDM symbol to be radar-interfered, the pulsed interference is more severe than AWGN. This protects the symbol from radar interference, while keeping the total number of transmitted bits the same. Multiple OFDM symbols can be hit simultaneously because an interference pulse can be either shorter or longer than an OFDM symbol. In this case, the OFDM symbols are all precoded. All the other symbols that are not precoded are transmitted with channel coding and full data tones.

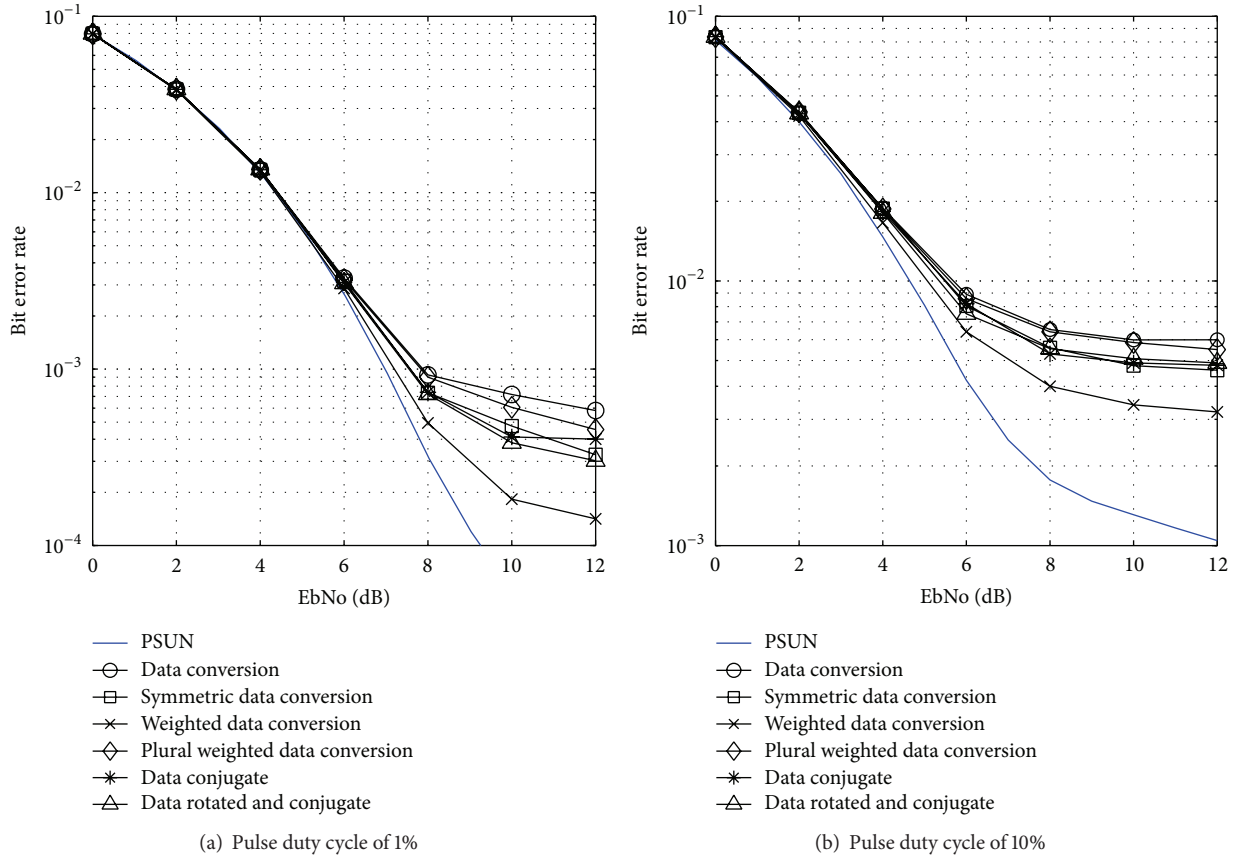

(a) Pulse duty cycle of 1%

(b) Pulse duty cycle of 10%

Figure 4: Comparison of PSUN to other ISC schemes (QPSK, 1024-FFT).

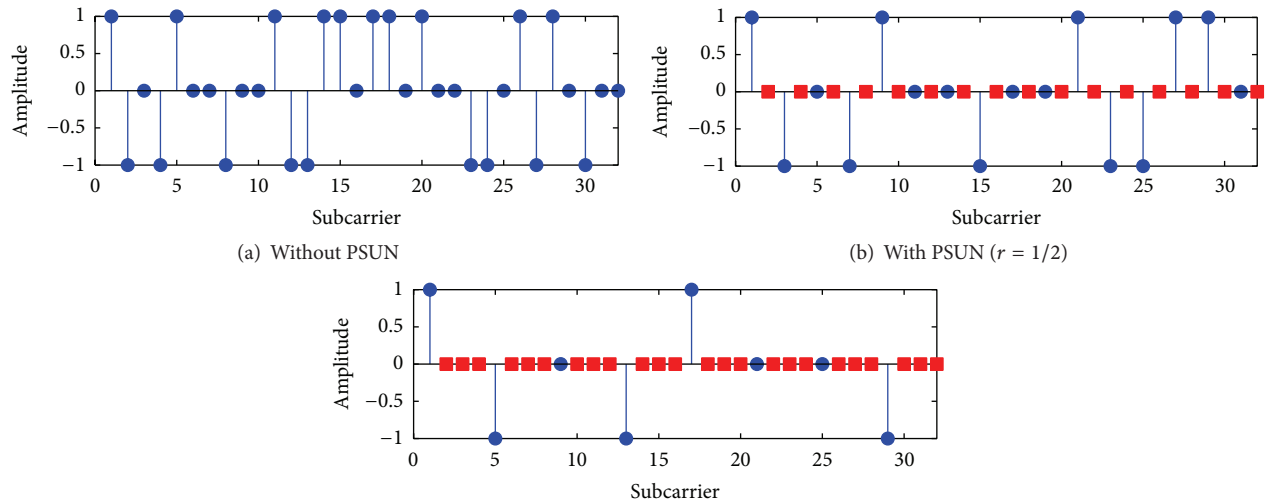

(a) Without PSUN

(b) With PSUN ($r = 1/2$)

(c) With PSUN ($r = 1/4$)

Figure 5: An OFDM symbol applying PSUN (QPSK, 32-FFT).

Figure 6 illustrates PSUN from such a macroscopic standpoint. An OFDM Tx employing PSUN reduces loss of data rate by *selecting certain OFDM symbols to insert null subcarriers*. According to the FCC's suggestion, a priori knowledge of interference from incumbent radars is available at an LTE eNodeB. Radars report their operating parameters (i.e., pulse parameters and position) to a SAS, and an ESC also senses the parameters and sends them to a SAS.

Taking LTE as an example of a CBRS system, there are 14 OFDM symbols in a subframe. Figure 5 showed only

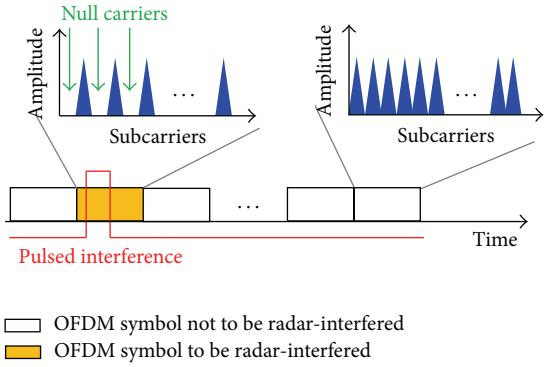

FIGURE 6: Transmission protocol of PSUN ($r = 1/2$).

one OFDM symbol that is expected to be hit by a radar pulse. In Figure 6, an OFDM symbol to be radar-interfered is highlighted by orange color. However, there are 13 other OFDM symbols that are not radar-interfered. An OFDM Tx applying PSUN does not precode these OFDM symbols for two reasons: (i) they undergo AWGN channels against which channel coding achieves better protection than PSUN; (ii) thus, as explained earlier, unnecessary loss of data rate can be avoided by not applying redundancy in subcarriers.

It is possible that two or more consecutive OFDM symbols can be interfered by the same pulse because an interference pulse can be either shorter or longer than an OFDM symbol depending on the pulse's duty cycle. In such a case, all of the OFDM symbols that are expected to be radar-interfered are precoded.

5. Imperfect Pulse Prediction

We discovered that three types of imperfect pulse prediction are possible in a 3.5 GHz band coexistence framework: (i) false prediction; (ii) missed prediction; and (iii) mislocation. *False alarm* and *missed detection* are defined as an ESC's inaccurate claim of presence/absence of an interfering radar pulse, given that a pulse is in fact absent/present. *Mislocation* is a unique type of imperfect pulse prediction that we suggest in this paper. It occurs when an ESC accurately predicts the location of a pulse interference in terms of *subframe* but being inaccurate in terms of *symbol* within a subframe. More specifically, it is called a mislocation when an ESC predicts that an OFDM symbol within a subframe will be hit by a radar pulse and in fact the interference actually occurs at the predicted subframe but at a different OFDM symbol.

Let us interpret actual impacts of the three types of imperfect pulse prediction. Recall that channel coding and PSUN are countermeasures against AWGN and pulsed interference, respectively. A *false alarm* is interpreted as a situation where an OFDM symbol that is not to be radar-interfered is predicted to be radar-interfered and thus precoded with PSUN. Therefore, in the OFDM symbol, redundant bits for channel coding are removed and null subcarriers are allocated instead which is a weaker protection than channel coding against AWGN, but in fact the symbol is not hit by a radar pulse but goes through an AWGN channel. On the other hand, when a *missed detection* occurs, an OFDM symbol to be radar-interfered is not predicted to be radar-interfered and thus not precoded with PSUN. Thus the OFDM symbol is protected with channel coding instead which is a weaker protection than PSUN against pulsed interference. Overall, although in the opposite way, either a false alarm or missed detection deteriorates performance of an OFDM system that applies PSUN. Most interestingly, a *mislocation* has the impact of a false alarm and missed detection within a single subframe. Recall that a false alarm unnecessarily precodes an OFDM symbol that will undergo AWGN with PSUN, while missed detection does not precode a symbol that will be hit by a radar pulse. Let us assume that an ESC has predicted an OFDM symbol named "A" to be hit by a radar pulse and hence has precoded it. A mislocation occurs when in fact another OFDM symbol called "B" has actually been hit. The problem is that OFDM symbol "B" has not been precoded with null subcarriers since the ESC has predicted it not to be hit by a radar pulse but to go through an AWGN channel. Therefore, a mislocation results in two OFDM symbols that are incorrectly precoded within a single subframe. OFDM symbol "A" has been protected against a radar pulse but has actually undergone an AWGN, while "B" has been believed to experience an AWGN and thus has not been precoded but in fact has gone through a radar interference. To interpret this situation, a false alarm has occurred at OFDM symbol "A" whereas missed detection has happened at "B." This is how a mislocation causes a false alarm and missed detection at the same time within one subframe.

Major causes of the above imperfect pulse prediction are twofold. Firstly, an ESC can cause sensing errors. Secondly, an ESC can lose track of radars' pulse parameters. The former affects false alarm and missed detection, while the latter impacts all of the three types of imperfect pulse prediction.

5.1. Sensing Error by an ESC. Typically for a protocol requiring spectrum sensing, either a matched filter or an energy detector can be used [30, 31]. This paper assumes that an ESC, a device with sensing capability, uses an energy detector. Assuming that an interference signal from a radar and noise are both modeled as white Gaussian processes, the problem of sensing a radar's pulsed interference signal by an ESC can be given by the following hypotheses test:

$$\begin{aligned} H_0&: Y \sim \mathcal{N}\left(0, \sigma_0^2\right), \\ H_1&: Y \sim \mathcal{N}\left(0, \sigma_0^2 + \sigma_1^2\right), \end{aligned} \tag{4}$$

where

Y is an observation sample;

σ_0^2 is power of noise;

σ_1^2 is power of an interference signal.

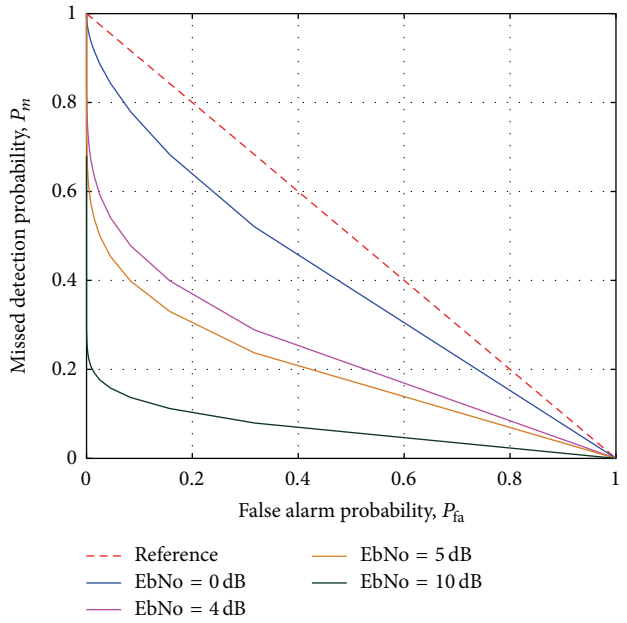

Figure 7: ROCs of the energy detector at an ESC.

Since an ESC adopts an energy detector, based on the Neyman-Pearson detection theory, the probability of false alarm, P_{fa}, and missed detection, P_m, are defined by

$$P_{\text{fa}} \triangleq \Pr\left(H_1 \mid H_0\right) = 1 - \Gamma\left(\frac{1}{2}, \frac{\eta_{\text{se}}}{2\sigma_0^2}\right),$$
$$P_m \triangleq \Pr\left(H_0 \mid H_1\right) = 1 - \Gamma\left(\frac{1}{2}, \frac{\eta_{\text{se}}}{2\left(\sigma_0^2 + \sigma_1^2\right)}\right), \tag{5}$$

where η_{se} denotes the sensing error threshold and the incomplete gamma function is given by

$$\Gamma(t, z) = \frac{1}{\Gamma(t)} \int_0^x t^{t-1} e^{-x} dx. \tag{6}$$

A receiver operating characteristic (ROC) curve is used for an analysis of interplay between P_{fa} and P_m. Figure 7 shows ROCs of (5) according to the energy per bit to noise power spectral density ratio (EbNo). An increase in the sensing threshold for given signal and noise power values moves the operating point toward the upper direction along one of the curves in the figure. At a high EbNo regime both P_m and P_{fa} can maintain low values, even if the sensing threshold changes much. This is not the case for low EbNo.

5.2. Loss of Track of Radars' Operating Information. It is difficult to track a radar's pulsed signals for the following two reasons. Firstly, the pulse information might not be fully available to the SAS. There has been strong opposition from military stakeholders to provide information to the database about radars' position or other information that could make them more prone to be affected by enemy jammers. Secondly, a radar may change its pulse parameters and position for various purposes, such as higher security or avoidance of interference among radars. According to a recent extensive survey paper [32], most radar systems have fixed position and operating parameters. However, airborne and shipborne radars may not have preplanned routes and, therefore, an error region has to be defined for such cases. In this case, there occurs a time during which an ESC loses track of a radar's pulse parameters. An ESC requires some time to sense a radar's parameter changes, during which it cannot avoid providing outdated information to a SAS.

We suggest that an ESC's losing track of radars' operating information must be understood more seriously than an ESC's sensing errors. The reason is that it is more likely and can cause any of the three types of imperfect pulse prediction but is more difficult to study since it is not a characteristic of an ESC but that of a radar which is an independent variable in this paper. Therefore, this paper provides a framework for analyzing this loss of track. Values of the false alarm, missed detection, and mislocation probabilities, P_{fa}, P_m, and P_{ml}, over the interval of [0,1] are considered, so that the analysis can be generalized over any case in which an ESC loses track of radars' operating parameters.

6. Performance Evaluation

6.1. Simulation Setup. The discussion in [9, 10] can be interpreted that the CBRS system coexisting with the pulse radar utilizes spectrum more efficiently in the downlink than in the uplink, in terms of the data rate per megahertz. Hence, spectrum sharing with radar would be more appropriate for applications that require greater capacity in the downlink than the uplink, which is a typical characteristic of many applications. Therefore, this paper assesses the performance of the downlink of an LTE system by measuring *the number of bits per second that an LTE UE successfully receives*. The number of *transmitted* bits differs according to the modulation scheme. (In this paper's simulations 16-QAM and 64-QAM were evaluated.) We analyze the metric as functions of six variables that are chosen to represent three different aspects of coexistence between an LTE Rx and military radars as follows. (i) EbNo represents impact of AWGN; (ii) pulse duty cycle and ρ represent characteristics of interference by a radar; (iii) P_{fa}, P_m, and P_{ml} represent impacts of imperfect pulse prediction. Each variable gauges different levels of channel impairment, that is, AWGN or radar interference. It differentiates the bit error rates which again directly determines the number of *received* bits.

Table 4 summarizes the simulation parameters for LTE and radar. We leverage LTE physical-layer simulations which are 3GPP compliant [33]. The FFT size is set to 1024 but the results based on this parameter can hold for other values of FFT size. The reason is that PB is a channel impairment that occurs in time domain, and LTE is always synchronized in time regardless of FFT size. Coding rates of channel coding and PSUN are kept identical to be $r = 1/2$, for ease of demonstrating the impacts of shifting redundancy from channel coding to subcarrier nulling. The only two channel impairments that are considered in this paper are AWGN and radar interference; as a result no typical fading effects are considered. Hence the simulations do not accurately follow

Table 4: Simulation parameters.

Parameter	Value
LTE	
FFT size	1024
Subcarrier spacing	15 kHz
Sampling frequency	15.36 MHz
OFDM symbol time	66.7 μs
Subframe length	1 ms
CP length	5.2 μs (1st)/4.69 μs (the following 6)
OFDM symbols/subframe	14
Modulation	16-QAM, 64-QAM
Channel coding	(133,171) convolutional code ($r = 1/2$)
PSUN	$r = 1/2$
Radar	
Pulse repetition time	1 ms
Rotation rate	30 rpm

the modulation and coding scheme (MCS) that are associated with channel quality indicator (CQI). *In order for LTE to operate in the 3.5 GHz band, a new set of MCS and CQI must be matched.* Radar pulse repetition time is set identical to an LTE subframe duration (1 msec) for accuracy of computation. Each simulation is conducted through 10^6 subframes.

To elaborate the discussion about a new set of MCS and CQI, we claim that it will be necessary because the 3.5 GHz environment is a totally different one from the previous spectrum bands in which LTE systems have been operating. In addition to all the mobility and multipath impacts, design of an LTE system at the 3.5 GHz band needs to consider pulsed interference generated by radars. However, this exceeds the scope of this paper and will be discussed in our future work. In other words, the results that are discussed in this paper do not have any impact from the new set of MCS and CQI.

6.2. Results

6.2.1. EbNo. Figure 8(a) shows the number of received bits per second versus EbNo with 16-QAM and 64-QAM. Recall that an OFDM Tx employing PSUN disables channel coding but puts the redundancy saved from no channel coding to null subcarriers between data subcarriers instead. In low EbNo region, AWGN is the predominating channel impairment that outweighs radar interference, which results in lower effectiveness of PSUN. In other words, outperformance of PSUN over the case without PSUN gets increased as EbNo gets higher. In that way, radar interference becomes prevailing which leads to greater performance advantage of PSUN. Moreover, such advantage of PSUN gets greater with higher modulation order.

6.2.2. Pulse Parameters of the Radar. Figure 8(b) demonstrates the number of received bits per second versus the duty cycle of a radar pulse. We generalized the values of pulse duty cycle for wider generality of this work, although many of the pulsed radars deployed in practice use relatively small values of duty cycle, for example, 0.1–10%. It is straightforward that higher pulse duty cycle yields greater outperformance of PSUN over the case without PSUN. Also, similar to the results with EbNo above, performance advantage gets greater as the modulation order becomes higher.

Figure 8(c) illustrates the number of received bits per second versus the probability that an OFDM symbol is hit by a radar pulse, ρ. When $\rho = 0$, the performance must be the same between the cases with and without PSUN since PSUN does not allocate null subcarriers when no OFDM symbol is radar-interfered. As explained in Section 3.2, a greater value of ρ yields a smaller number of received bits per second. Similar to the discussion of pulse duty cycle in Figure 8(b), a greater value of ρ indicates a more severe situation of radar interference. Due to this, it still holds true that outperformance of PSUN increases as ρ becomes greater. The performance curve drops faster in 64-QAM than 16-QAM, which implies that higher-order modulation is more sensitive to radar interference. Nevertheless, performance advantage of PSUN gets greater as the modulation order gets higher.

6.2.3. Pulse Prediction Errors. So far we have seen the performances assuming *perfect pulse prediction*. The results shown through Figures 8(d) and 8(f) depict how the performance of an OFDM system is deteriorated with *imperfect pulse prediction*. Figure 8(d) shows the number of received bits per second versus the probability of false alarm, P_{fa}. It is straightforward that higher P_{fa} decreases the number of received bits per second of an OFDM system employing PSUN, while the case without PSUN stays unrelated to the level of P_{fa}. The reason is that, with a false alarm, an OFDM symbol is protected by PSUN instead of channel coding, but in fact it undergoes an AWGN channel where channel coding is more effective protection than PSUN.

Figure 8(e) shows the number of received bits per second versus the probability of missed detection, P_m. As explained earlier in Section 5, at an OFDM Tx applying PSUN, missed detection is translated as a situation where an OFDM symbol is not predicted to be radar-interfered and hence not precoded with PSUN but in fact hit by a radar pulse. In other words, the particular symbol is equipped with channel coding instead of PSUN and hence contributes to degradation of performance. The performance degradation of OFDM Rx without PSUN is shown by the gap at zero P_m. As P_m increases, the performance of PSUN gets closer to the case without PSUN. The performance advantage of PSUN increases as the modulation order gets higher.

Figure 8(f) shows the number of received bits per second versus the probability of pulse mislocation, P_{ml}. A mislocation refers to a wrong location of to-be-interfered OFDM symbol within a subframe. Recall that, with a mislocation, a false alarm and missed detection occur at the same time within a subframe. This is why performance propensity according to P_{ml} from Figure 8(f) is nearly linear while the ones according to P_{fa} and P_m are logarithmic and exponential, respectively, as observed from Figures 8(d) and 8(e).

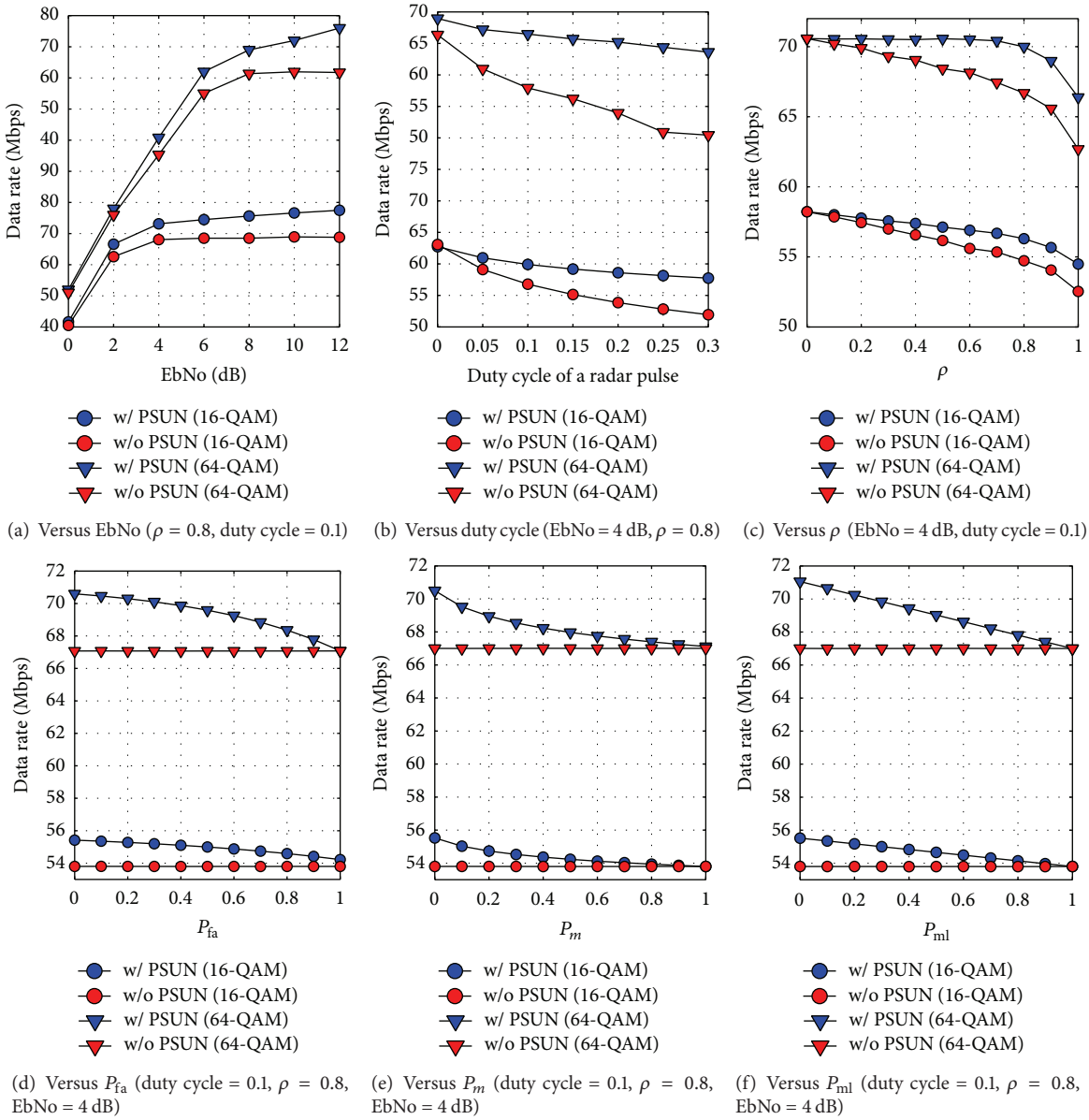

(a) Versus EbNo (ρ = 0.8, duty cycle = 0.1)

(b) Versus duty cycle (EbNo = 4 dB, ρ = 0.8)

(c) Versus ρ (EbNo = 4 dB, duty cycle = 0.1)

(d) Versus P_{fa} (duty cycle = 0.1, ρ = 0.8, EbNo = 4 dB)

(e) Versus P_m (duty cycle = 0.1, ρ = 0.8, EbNo = 4 dB)

(f) Versus P_{ml} (duty cycle = 0.1, ρ = 0.8, EbNo = 4 dB)

Figure 8: Data rate versus EbNo, the duty cycle of a radar pulse, ρ, P_{fa}, P_m, and P_{ml}.

7. Feasibility of 5G Applications Using 3.5 GHz LTE with PSUN

Fifth-generation (5G) mobile networks will operate in a highly heterogeneous environment characterized by the existence of multiple types of access technologies over multiple chunks of spectrum bands. In other words, enabling 5G use cases and business models requires the allocation of additional spectrum for mobile broadband and needs to be supported by flexible spectrum management capabilities. Based on the analyses and results of this paper, we suggest that the 3.5 GHz band can be a usable additional spectrum for enabling LTE to support several functionalities of 5G technologies.

We refer to a white paper [21] issued by the Next Generation Mobile Networks (NGMN), a mobile telecommunications association of mobile operators, vendors, manufacturers, and research institutes, for understanding the representative example use cases of 5G and the corresponding requirement of data rate for each use case. A consistent user experience with respect to throughput needs a minimum data rate guaranteed everywhere. The data rate requirement of a use case is set as the minimum user experienced data rate required for the user to have a quality experience of the targeted use case. The use cases are summarized in Table 5.

According to our results, LTE with PSUN can fulfill the *downlink* requirements of several use cases which are listed under the category of "candidates for LTE with PSUN" in

Table 5: Data rate requirements for use cases of 5G [21].

Use case	Data rate requirement (downlink/uplink)
Candidates for LTE with PSUN	
Massive low-cost/long-range/low-power M2M	1–100 kbps
Resilience and traffic surge	0.1–1 Mbps/0.1–1 Mbps
Ultrahigh reliability & ultralow latency	50 kbps to 10 Mbps/a few kbps to 10 Mbps
Ultrahigh availability & reliability	10 Mbps/10 Mbps
Airplanes connectivity	15 Mbps/7.5 Mbps
Broadband access in a crowd	25 Mbps/50 Mbps
50+ Mbps everywhere	50 Mbps/25 Mbps
Ultralow latency	50 Mbps/25 Mbps
Others	
Broadband like services	Up to 200 Mbps/modest (e.g., 500 kbps)
Ultralow-cost broadband access	300 Mbps/50 Mbps
Mobile broadband in vehicles	300 Mbps/50 Mbps
Broadband access in dense areas	300 Mbps/50 Mbps
Indoor ultrahigh broadband access	1 Gbps/500 Mbps

Table 5. While most of the requirements of the selected use cases are set to be 50 Mbps, our results (Figures 8(a) through 8(f)) indicate that LTE with PSUN is capable of supporting data rates that are higher than 50 Mbps and 40 Mbps with 64-QAM and 16-QAM, respectively. For example, observing Figure 8(a), the required EbNo values for achieving the data rate of 50 Mbps are 0 and 1 dB for 64-QAM and 16-QAM, respectively.

It is discussed in [9, 10] that although average data rate is roughly the same for all file sizes, because of interruptions as a radar rotates, average received data rate for smaller files may vary depending on when the transmission begins relative to the radar's rotation cycle. This effect does not occur during transmission of larger files that span one or more rotation periods of the radar. The authors suggested several appropriate applications that can tolerate interruptions from a pulsed radar, video on demand, peer-to-peer file sharing, and automatic meter reading, or applications that transfer large enough files so the fluctuations are not noticeable, such as song transfers. Among these applications, a white paper that analyzed the mobile traffic pattern of 2015 [34] finds a direction that LTE with PSUN can target in the 3.5 GHz band. It says that *mobile video traffic* accounted for 55% of total mobile data traffic in 2015. Mobile video traffic now accounts for more than half of all mobile data traffic. It will be very promising if LTE with PSUN can support video traffic in the 3.5 GHz band while coexisting with military radar.

8. Conclusion

This paper proposes PSUN, an OFDM transmission scheme enabling an LTE system to coexist with federal military radars in the 3.5 GHz band. The scheme is comprised of PB at an Rx and precoding of null subcarriers at Tx of an OFDM system. To maximize data rate, OFDM Tx employing PSUN (i) localizes OFDM symbols to be radar-interfered a priori and (ii) shifts redundancy from channel coding to subcarriers in the OFDM symbols. This paper considers existence of sensing functionality in the 3.5 GHz band coexistence architecture and hence impacts of imperfect sensing which can occur due to a sensing error by ESC and parameter changes by a radar. Results show that PSUN is still effective in suppressing ICI remaining after PB even with imperfect pulse prediction and as a result enables an LTE system to support various use cases of 5G that require the data rate lower than 50 Mbps in the downlink and relatively larger file size such as video streaming.

Disclosure

This work was presented, in part, in the 2nd IEEE WCNC International Workshop on Smart Spectrum Technologies (IWSS 2016), Doha, Qatar, on 3 April 2016.

Competing Interests

The authors declare that they have no competing interests.

References

[1] NTIA, *An Assessment of the Near-Term Viability of Accommodating Wireless Broadband Systems in the 1675–1710 MHz, 1755–1780 MHz, 3500–3650 MHz, 4200–4220 MHz and 4380–4400 MHz Bands*, NTIA, 2010.

[2] Memorandum for the Heads of Executive Departments and Agencies, *Unleashing the Wireless Broadband Revolution*, 2010.

[3] FCC 12-148, "Amendment of the commision's rules with regard to commercial operations in the 3550–3650 MHz band," Notice of Proposed Rulemaking in GN Docket 12-354, 2012.

[4] FCC 14-49, "Amendment of the commission's rules with regard to commercial operations in the 3550–3650 MHz band," Further Notice of Proposed Rulemaking in GN Docket 12-354, 2015.

[5] FCC 15-47, "Amendment of the commissions rules with regard to commercial operations in the 3550–3650 MHz band," Report and Order and Second Further Notice of Proposed Rulemaking in GN Docket 12-354, 2015.

[6] NTIA, "Response to commercial operations in the 3550–3650 MHz band," GN Docket 12-354, 2015.

[7] S. Sodagari, A. Khawar, T. C. Clancy, and R. McGwier, "A projection based approach for radar and telecommunication systems coexistence," in *Proceedings of the IEEE Global Communications Conference (GLOBECOM '12)*, pp. 5010–5014, Anaheim, Calif, USA, December 2012.

[8] A. Khawar, A. Abdel-Hadi, and T. C. Clancy, "Spectrum sharing between S-band radar and LTE cellular system: a spatial approach," in *Proceedings of the IEEE International Symposium on Dynamic Spectrum Access Networks (DYSPAN '14)*, pp. 7–14, McLean, Va, USA, April 2014.

[9] R. Saruthirathanaworakun, J. M. Peha, and L. M. Correia, "Opportunistic sharing between rotating radar and cellular," *IEEE Journal on Selected Areas in Communications*, vol. 30, no. 10, pp. 1900–1910, 2012.

[10] R. Saruthirathanaworakun, J. M. Peha, and L. M. Correia, "Gray-space spectrum sharing between multiple rotating radars and cellular network hotspots," in *Proceedings of the IEEE 77th Vehicular Technology Conference (VTC '13)*, June 2013.

[11] F. Paisana, J. P. Miranda, N. Marchetti, and L. A. DaSilva, "Database-aided sensing for radar bands," in *Proceedings of the IEEE International Symposium on Dynamic Spectrum Access Networks (DYSPAN '14)*, pp. 1–6, McLean, Va, USA, April 2014.

[12] M. Ghorbanzadeh, E. Visotsky, P. Moorut, W. Yang, and C. Clancy, "Radar in-band interference effects on macrocell LTE uplink deployments in the U.S. 3.5 GHz band," in *Proceedings of the International Conference on Computing, Networking and Communications (ICNC '15)*, pp. 248–254, Garden Grove, Calif, USA, February 2015.

[13] M. Ghorbanzadeh, E. Visotsky, P. Moorut, W. Yang, and C. Clancy, "Radar inband and out-of-band interference into LTE macro and small cell uplinks in the 3.5 GHz band," in *Proceedings of the IEEE Wireless Communications and Networking Conference (WCNC '15)*, pp. 1829–1834, March 2015.

[14] H.-A. Safavi-Naeini, C. Ghosh, E. Visotsky, R. Ratasuk, and S. Roy, "Impact and mitigation of narrow-band radar interference in down-link LTE," in *Proceedings of the IEEE International Conference on Communications (ICC '15)*, pp. 2644–2649, London, UK, June 2015.

[15] S. Kim, J. Choi, and C. Dietrich, "Coexistence between OFDM and pulsed radars in the 3.5 GHz band with imperfect sensing," in *Proceedings of the IEEE Wireless Communications and Networking Conference*, Doha, Qatar, April 2016.

[16] M. Cotton and R. Dalke, "Spectrum occupancy measurements of the 3550–3650 Megahertz maritime radar band near San Diego, California," NTIA Report TR-14-500, 2014.

[17] Y. Zhao and S.-G. Haggman, "Sensitivity to Doppler shift and carrier frequency errors in OFDM systems-the consequences and solutions," in *Proceedings of the IEEE 46th Vehicular Technology Conference*, vol. 3, pp. 1564–1568, Atlanta, Ga, USA, May 1996.

[18] Y. Fu and C. Ko, "A new ICI self-cancellation scheme for OFDM systems based on a generalized signal mapper," in *Proceedings of the 5th International Symposium on Wireless Personal Multimedia Communications*, vol. 3, pp. 995–999, IEEE, 2002.

[19] Y.-H. Peng, Y.-C. Kuo, G.-R. Lee, and J.-H. Wen, "Performance analysis of a new ICI-self-cancellation-scheme in OFDM systems," *IEEE Transactions on Consumer Electronics*, vol. 53, no. 4, pp. 1333–1338, 2007.

[20] Q. Shi, Y. Fang, and M. Wang, "A novel ICI self-cancellation scheme for OFDM systems," in *Proceedings of the 5th International Conference on Wireless Communications, Networking and Mobile Computing (WiCOM '09)*, pp. 1–4, IEEE, Beijing, China, September 2009.

[21] The Next Generation Mobile Networks, *NGMN 5G White Paper*, The Next Generation Mobile Networks Ltd., Frankfurt, Germany, 2015.

[22] Operations and SignalSecurity, Army Regulation 530-1, 2005.

[23] S. Brandes, *Suppression of Mutual Interference in OFDM Based Overlay Systems*, Universitat Fridericiana Karlsruhe, Karlsruhe, Germany, 2009.

[24] S. Brandes, U. Epple, and M. Schnell, "Compensation of the impact of interference mitigation by pulse blanking in OFDM systems," in *Proceedings of the IEEE Global Telecommunications Conference (GLOBECOM '09)*, pp. 1–6, Honolulu, Hawaii, USA, December 2009.

[25] U. Epple, D. Shutin, and M. Schnell, "Mitigation of impulsive frequency-selective interference in OFDM based systems," *IEEE Wireless Communications Letters*, vol. 1, no. 5, pp. 484–487, 2012.

[26] A. Goldsmith, *Wireless Communications*, Cambridge University, Cambridge, UK, 2005.

[27] S. Ahmed and M. Kawai, "Dynamic null-data subcarrier switching for OFDM PAPR reduction with low computational overhead," *Electronics Letters*, vol. 48, no. 9, pp. 498–499, 2012.

[28] M. Ghogho, A. Swami, and G. B. Giannakis, "Optimized null-subcarrier selection for CFO estimation in OFDM over frequency-selective fading channels," in *Proceedings of the IEEE Global Telecommunicatins Conference (GLOBECOM '01)*, pp. 202–206, San Antonio, Tex, USA, November 2001.

[29] B. Wang, P.-H. Ho, and C.-H. Lin, "OFDM PAPR reduction by shifting null subcarriers among data subcarriers," *IEEE Communications Letters*, vol. 16, no. 9, pp. 1377–1379, 2012.

[30] H. V. Poor, *An Introduction to Signal Detection and Estimation*, Springer, New York, NY, USA, 2nd edition, 1994.

[31] J. W. Chong, D. K. Sung, and Y. Sung, "Cross-layer performance analysis for CSMA/CA protocols: impact of imperfect sensing," *IEEE Transactions on Vehicular Technology*, vol. 59, no. 3, pp. 1100–1108, 2010.

[32] F. Paisana, N. Marchetti, and L. A. Dasilva, "Radar, TV and cellular bands: which spectrum access techniques for which bands?" *IEEE Communications Surveys and Tutorials*, vol. 16, no. 3, pp. 1193–1220, 2014.

[33] 3GPP, "Further advancements for EUTRA physical layer aspects, release 9," 3GPP TR 36.814 V9.0.0 (2010-03), 2010.

[34] Cisco, "Cisco visual networking index: global mobile data traffic forecast update," White Paper 20152020, 2016.